TO MY FAMILY and EDA

IN-SITU FT-IR SPECTROSCOPIC INVESTIGATION of NO_x + CH_4 SURFACE REACTIONS on PALLADIUM PROMOTED WO_3/TiO_2-ZrO_2 MIXED OXIDES

A THESIS

SUBMITTED TO THE DEPARTMENT OF CHEMISTRY

THE INSTITUTE OF ENGINEERING AND SCIENCES OF BILKENT UNIVERSITY

IN PARTIAL FULFILLMENT OF THE REQUIREMENTS

FOR THE DEGREE

OF

MASTER OF SCIENCE

By

ANIL AĞIRAL

JUNE 2005

I certify that I have read this thesis and in my opinion it is fully adequate, in scope and in quality, as a thesis of the degree of Master of Science

_____

Assoc. Prof. Margarita Kantcheva (Supervisor)

I certify that I have read this thesis and in my opinion it is fully adequate, in scope and in quality, as a thesis of the degree of Master of Science

_____

Assoc. Prof. Ömer Dağ

I certify that I have read this thesis and in my opinion it is fully adequate, in scope and in quality, as a thesis of the degree of Master of Science

_____

Assoc. Prof. Gürkan Karakaş

I certify that I have read this thesis and in my opinion it is fully adequate, in scope and in quality, as a thesis of the degree of Master of Science

Assoc. Prof. Ahmet Oral

I certify that I have read this thesis and in my opinion it is fully adequate, in scope and in quality, as a thesis of the degree of Master of Science

Assist. Prof. Dönüş Tuncel

Approved for the Institute of Engineering and Sciences

Prof. Dr. Mehmet Baray
Director of Institute of Engineering and Sciences

ABSTRACT

IN-SITU FT-IR SPECTROSCOPIC INVESTIGATION of $NO_x + CH_4$ SURFACE REACTIONS on PALLADIUM PROMOTED WO_3/TiO_2-ZrO_2 MIXED OXIDES

ANIL AĞIRAL

M.Sc. in Chemistry

Supervisor: Assoc. Prof. Margarita Kantcheva

June 2005

The interaction of methane at various temperatures with NO_x species formed by room temperature adsorption of NO/O_2 mixture on tungstated zirconia-titania (25 wt % of WO_3, denoted as WZT) and palladium(II)-promoted (1.5 wt % of Pd) zirconia-titania (1.5Pd/ZT) and tungstated zirconia-titania (1.5Pd/WZT) is investigated using in situ FTIR spectroscopy.

The structure and surface properties of ZT, WZT, 1.5Pd/ZT and 1.5Pd/WZT are studied by XRD, DR-UV-Vis spectroscopy and FT-IR spectroscopy of adsorbed CO and NO. Zirconia-titania was prepared by a homogenous coprecipitation of urea at 70°C. Formation of crystalline $ZrTiO_4$ compound at calcination temperature of 600°C is observed. Based on the data of XRD and DR-UV-Vis spectra, very good mixing of oxides has been achieved with high surface area (118 m^2/g) and small crystallite size (4.4 nm). The WZT sample has paratungstate type polytungstate species forming intermediate WO_x surface domains which give rise to strong Brønsted acidity. Pd-containing samples were prepared impregnating the ZT and WZT samples with $Pd(NO_3)_2.2H_2O$ solution. The WZT support can stabilize isolated Pd^{2+} ions coordinated to surface oxygen atoms.

The spectrum of CO adsorbed on the ZT sample reveals the presence of coordinatively unsaturated (cus) Zr^{4+} and Ti^{4+} sites. Their amount decreases considerably after the modification of the sample with WO_3. The adsorption of CO and NO on the 1.5Pd/ZT and 1.5Pd/WZT samples indicates the presence of palladium ions in two different environments.

The adsorption of NO at room temperature on the samples studied involves process of disproportionation of NO on surface oxide ions leading to formation of adsorbed anionic nitrosyl, NO^-, and NO_2.

The addition of molecular oxygen to the NO causes its oxidation to NO_2/N_2O_4. These gases adsorb molecularly over the surface and undergo self-ionization and disproportionation with the participation of surface hydroxyl groups. Introduction of WO_x species and Pd^{2+} ions to the zirconia-titania mixed oxide hinders the processes of NO_2/N_2O_4 self-ionization and disproportionation by elimination of the necessary active sites.

NO_x species formed at room temperature on the WZT and 1.5Pd/ZT samples suppress the oxidation of the methane, whereas in the case of the 1.5Pd/WZT catalyst the surface nitrates initiate the formation of nitromethane. Mechanism for the reduction of NO over the 1.5Pd/WZT catalyst is proposed, which involves a step of thermal decomposition of the nitromethane to adsorbed NO and partially oxidized hydrocarbons (methoxy and/or formate species) through the intermediacy of cis-methyl nitrite. The reduction of the adsorbed NO by the partially oxidized hydrocarbons leads to the products of the CH_4-SCR, molecular nitrogen and carbon oxides. Under in situ conditions, nitromethane and cis-methyl nitrite are stabilized on the surface of the 1.5Pd/WZT catalyst, whereas the adsorption of the authentic reagent results in adsorbed nitromethane and its trans isomer. It is concluded that nitromethane formed in situ and authentic nitromethane follow different decomposition routes.

Keywords: In situ FT-IR; Pd promoted zirconia-titania; Tungstated zirconia titania; Mixed oxides; Reactivity of stable surface NO_x compounds; NO_x; Selective catalytic reduction by methane; Mechanism; Nitromethane; Methyl nitrite.

ÖZET

PALADYUM DEPOLANMIŞ WO_3/TiO_2-ZrO_2 KARIŞIM OKSİT KATALİZÖRÜNÜN YÜZEYİNDE GERÇEKLEŞEN $NO_X + CH_4$ REAKSİYONLARININ IN-SITU FT-IR SPEKTROSKOPİSİ ile İNCELENMESİ

ANIL AĞIRAL

Kimya Bölümü Yüksek Lisans

Tez Yöneticisi: Doç. Dr. Margarita Kantcheva

Haziran 2005

Oda sıcaklığında tungstenlenmiş zirkonyum oksit-titanyum oksit (ağırlıkça 25 % WO_3, WZT olarak kısaltıldı), paladyum depolanmış zirkonyum oksit-titanyum oksit (ağırlıkça 1.5 % Pd, 1.5Pd/ZT) ve paladyum depolanmış tungstenlenmiş zirkonyum oksit-titanyum oksit (1.5Pd/WZT) katalizörleri yüzeyinde NO ve O_2'in ortak adsorpsiyonu ile oluşan NO_x komplekslerinin değişik sıcaklıklarda metan ile etkileşimi in situ FTIR spektroskopisi ile incelendi.

ZT, WZT, 1.5Pd/ZT and 1.5Pd/WZT numunelerinin yapısal ve yüzey özellikleri XRD, DR-UV-Vis ile CO ve NO'in adsorpsiyonunun FTIR spektroskopisi yöntemleriyle incelendiler. Zirkonyum oksit-titanyum oksit 70^oC'de üre çözeltisinin içinde ortak çökelme yöntemiyle hazırlandı. 600^oC'de fırınlama işleminden sonra $ZrTiO_4$ kristal fazının oluşumu gözlendi. XRD ve DR-UV-Vis spektroskopisi verileri ışığında, oksitlerin çok iyi karışarak yüksek yüzey alanı ($118 m^2/g$) ve küçük kristal boyutu (4.4 nm) elde edildi. WZT numunesi paratungsten tipinde yüksek Brønsted asiditesine sahip orta yoğunlukta tungsten grupları oluşturur. ZT ve WZT numunelerine $Pd(NO_3)_2.2H_2O$ çözeltisi sulu ekleme yöntemiyle eklenerek paladyumlu numuneler hazırlandı. WZT numunesinin Pd^{2+} iyonlarını yalnız başlarına yüzeydeki oksijen atomlarına bağlayarak kararlı hale getirebildiği görüldü.

ZT numunesine CO adsorpsiyonu koordinasyona açık Zr^{4+} ve Ti^{4+} iyonlarının varlığını gösterdi. Bu iyonların yoğunluğu numuneye WO_3 eklenmesiyle azaldı. 1.5Pd/ZT ve 1.5Pd/WZT numunelerine CO ve NO adsorpsiyonu koordinasyona açık iki çeşit Pd^{2+} iyonları olduğunu gösterdi.

Oda sıcaklığında NO'in numunelere adsorpsiyonu sonucu bu molekül yüzeydeki oksijen iyonları tarafından bozunarak anyonik nitrozil, NO^- ve NO_2'i oluşturdu.

NO, oksijen tarafından oksitlenerek NO_2/N_2O_4 ikilisini oluşturur. Bu gazlar yüzeye molekül düzeyinde bağlanarak hidroksil gruplarının da katkısıyla iyonlaşarak bozunmaya başladılar. WO_x gruplarının ve Pd^{2+} iyonlarının zirkonyum oksit-titanyum oksit numunesine eklenmeleri yüzeydeki aktif bölümlerin kaybolması sonucu NO_2/N_2O_4 ikilisinin bozunma derecelerini karışım oksite nazaran azalttı.

Oda sıcaklığında oluşan NO_x kompleksleri metanın oksidasyonunu WZT ve 1.5Pd/ZT numunelerinde azaltmasına karşılık, 1.5Pd/WZT katalizörü yüzeyinde nitrometanın oluşmasını başlatır. 1.5Pd/WZT katalizörü yüzeyinde NO'in indirgenme mekanizması önerildi. Bu mekanizma nitrometanın cis-metil nitrit üzerinden NO'e ve kısmi yükseltgenmiş hidrokarbonlara (metoksi ve/veya format iyonlarına) termal bozunmasını içermektedir. Yüzeye bağlanmış NO'in kısmi yükseltgenmiş hidrokarbonlarla indirgenmesi sonucu seçici katalitik indirgenme ürünleri olan moleküler nitrojen ve karbon oksitler oluştu. Seçici katalitik indirgenme reaksiyonu koşullarında (in-situ) oluşan nitrometan ve cis-metil nitrit yüzeye daha kararlı bağlanırken, nitrometanın yalnız başına adsorpsiyonu adsorbe olmuş nitrometan ve onun trans izomerinin varlığını gösterdi.

Anahtar Kelimeler: In situ FT-IR; Pd depolanmış zirkonyum oksit-titanyum oksit; Tungstenlenmiş zirkonyum oksit-titanyum oksit; Karışım oksitler; Kararlı NO_x bileşiklerinin reaktivitesi; NO_x; Metan ile seçici katalitik indirgenme; Mekanizma; Nitrometan; Metil nitrit.

ACKNOWLEDGMENT

I would like to express my sincere thanks and gratitude to my supervisor, Assoc. Prof. Margarita Kantcheva for all her guidance and encouragement she has offered me throughout the period of this research.

I would like to thank all present and former members of Bilkent University Department of Chemistry for their support and help.

I would like to express my gratitude to my love Eda Süer for her support and love.

TABLE OF CONTENTS

LIST OF TABLES

LIST OF FIGURES

1. INTRODUCTION

1.1. An environmental problem: NO_x emission

Flame combustion of fossil fuels leads to reaction between carbon containing constituents of the fuel and the oxygen of the air

$$C_mH_n + (m + n/4)O_2 \leftrightarrow (m)CO_2 + (n/2)H_2O \quad (1)$$

Carbon dioxide and water are the main products of this reaction but emission of unburned hydrocarbons and intermediate oxidation products like alcohols, aldehydes and carbon monoxide are formed as side products due to incomplete combustion.

During flame combustion, temperature reaches 1700 K and at this temperature, formation of nitrogen oxides from air constituents nitrogen and oxygen is thermodynamically favored according to the reaction [1]

$$N_2 + O_2 \leftrightarrow 2NO \quad (2)$$

NO is a well known atmospheric pollutant and it reacts with photochemical pollutants like carbonyl containing molecules, alcohol radicals, ozone, organic hydroperoxides and peroxyacyl nitrates to generate more nitrogen oxides and organic nitrates [2]. NO_2 which is an oxidation product of NO, contributes to acid rain and urban smog; the reaction involving ozone depletes the ozone layer [3] and unburned hydrocarbons in polluted air interact in the photolytic cycle of NO to generate ground level ozone [4].

NO_x emission sources are internal combustion engines, industrial boilers, power plants, waste incinerators, gasifiers, engines and gas turbines or from decomposition of a large number of organic products by light or micro-organisms [2]. According to report of US Department of Energy [5], annual world production of NO_x is over 30 million metric tons (mmt) of which 21 mmt is produced in the USA and 95 % comes from vehicles and power sources.

In vehicle engines, the emission of carbon monoxide , hydrocarbons (HC) and nitrogen oxides depends on the engine air-to-fuel ratio (A/F), defined as

$$A/F = \frac{\text{Mass of air consumed by the engine}}{\text{Mass of fuel consumed by the engine}} \quad (3)$$

When there is just enough air for complete combustion of all hydrocarbons in the fuel, A/F is 14.7 . If A/F ratio is below 14.7 (rich conditions), incomplete fuel combustion occurs under excess fuel conditions. The exhaust gas includes more reducing gases (CO, HC) than oxidizing gases (O_2, NO_x). When A/F is higher than 14.7 (lean conditions), exhaust gas will contain more oxidizing reactants than reducing reactants [1]. The graph below shows the dependence on air-fuel ratio in a schematic manner.

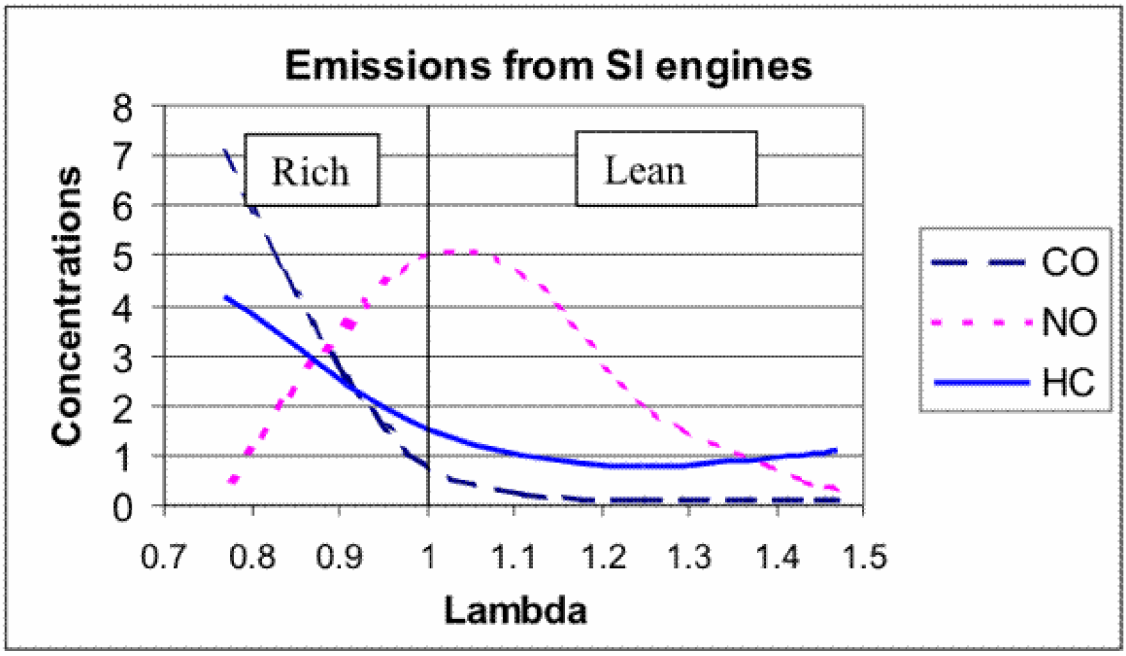

Figure 1. Production of NO, CO and HCs over a wide range of air to fuel ratios [6].

$$\text{Lambda} = \frac{\text{Actual engine A/F}}{\text{Stoichiometric engine A/F}} \qquad (4)$$

Various reactions occur for the removal of CO, hydrocarbon and nitrogen oxide in engine-out exhaust gas. These are:

(1) Reactions with oxygen

$$C_mH_n + (m + 0.25n)O_2 \leftrightarrow mCO_2 + 0.5nH_2O \qquad (5)$$

$$CO + 0.5O_2 \leftrightarrow CO_2 \qquad (6)$$

$$H_2 + 0.5O_2 \leftrightarrow H_2O \qquad (7)$$

(2) Reactions with NO

$$CO + NO \leftrightarrow 0.5N_2 + CO_2 \qquad (8)$$

$$NO + H_2 \leftrightarrow 0.5N_2 + H_2O \quad (9)$$

$$C_mH_n + 2(m + 0.25n)NO \leftrightarrow 1(m + 0.25n)N_2 + 0.5nH_2O + mCO_2 \quad (10)$$

Emission control systems should promote these reactions in order to remove carbon monoxide, hydrocarbons and nitrogen oxides from engine-out exhaust gas.

It is important to remove NO_x emission from stationary sources such as industrial boilers, power plants, incinerators and gas turbines. In the next section, the catalytic approach for the control of nitrogen compounds to avoid emissions of NO_x will be given for mobile and stationary sources.

1.2. Catalytic Emission Control

For vehicle engines, three-way catalyst (TWC) system can promote the reactions (5-10) for the removal of carbon monoxide, hydrocarbons and nitrogen oxides. Several exhaust gas components, HC, CO and NO_x, are reduced simultaneously if the combustion can be controlled at stoichiometric conditions. The TWC converter uses two different types of catalysts, a reduction catalyst and an oxidation catalyst. Both types consist of a ceramic structure coated with a metal catalyst, usually platinum, rhodium and/or palladium. Figure 2 shows a schematic picture of dual-bed emission control which maintains high conversion efficiency for the three exhaust gas constituents.

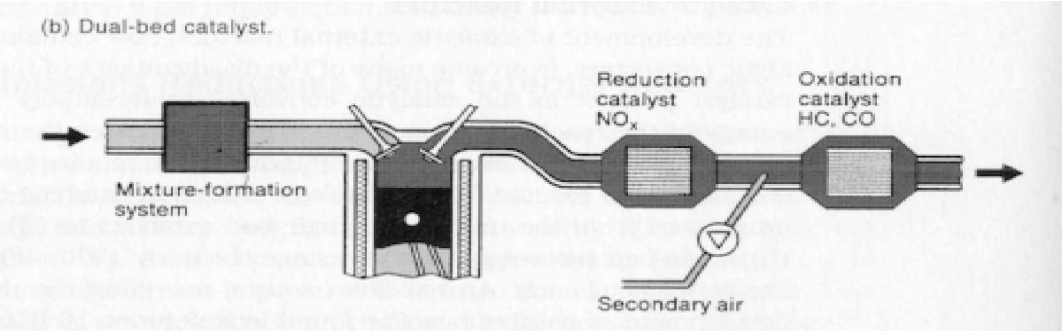

Figure 2. Dual-bed emission control [7].

Whereas the TWC technology is accepted for limiting the emission of carbon monoxide and hydrocarbons, it is inefficient to remove NO_x for the lean-burn and diesel engines. Possibility to lower engine-out emission of NO_x using exhaust gas recirculation systems is omitted because in this case emission of particulate matter can be increased.

Selective catalytic reduction (SCR) process is one solution to reduce NO_x emission by catalyst after treatment. In this process ammonia or a substance that forms ammonia in situ is used as a reducing agent, however, this technology can not be applied to passenger cars.

According to thermodynamics, in the exhaust gas composition NO is unstable with respect to N_2 and O_2 and at typical engine operating conditions direct decomposition of NO,

$$NO \leftrightarrow 0.5N_2 + 0.5O_2 \quad (11)$$

additionally, SCR by hydrocarbons,

$$(6m+2)NO + 2C_mH_{2m+2} \leftrightarrow (3m+1)N_2 + 2mCO_2 + (2m+2)H_2O \quad (12)$$

are thermodynamically feasible [1, 8, 9]. Up to now, no heterogenous catalyst has been found to catalyze direct decomposition of NO. SCR with hydrocarbons gave promising results to promote the reaction (12).

The selective catalytic reduction (SCR) of NO with ammonia has been extensively studied as a catalytic technology for NO_x elimination from stationary sources [2]. The SCR process is based on the reaction between NO_x and NH_3, injected into the flue gas stream, to produce water and nitrogen. The SCR catalyst is designed to promote the selective low temperature (300^oC-400^oC) reaction of NO_x and ammonia (NH_3), converting to nitrogen and water vapor via the following reactions (10)

$$4NO + 4NH_3 + O_2 \rightarrow 4N_2 + 6H_2O \quad (13)$$

$$2NO_2 + 4NH_3 + O_2 \rightarrow 3N_2 + 6H_2O \quad (14)$$

The SCR technology uses ammonia injection into the process stream prior to this catalytic reaction. When molecules of NO_x, ammonia and oxygen simultaneously contact the "catalytic site", the SCR reaction takes place converting NO_x and ammonia to nitrogen and water vapor. As this is an exothermic reaction, a small amount of heat is released to the stream, thereby increasing the temperature of the stream. Catalytic tests performed with various oxide catalysts for the selective reduction of NO with ammonia indicated that vanadia supported catalysts are the most active and selective giving excellent results.

Figure 3 shows a typical SCR system for the abatement of NO_x. First the SCR catalyst bed is heated to operating temperature and gaseous or liquid ammonia is injected into the flue gas stream then ammonia is adsorbed onto the catalyst surface. Finally ammonia on the catalyst surface reacts with NO_x in the presence of oxygen to form water and molecular nitrogen according to reactions (13, 14).

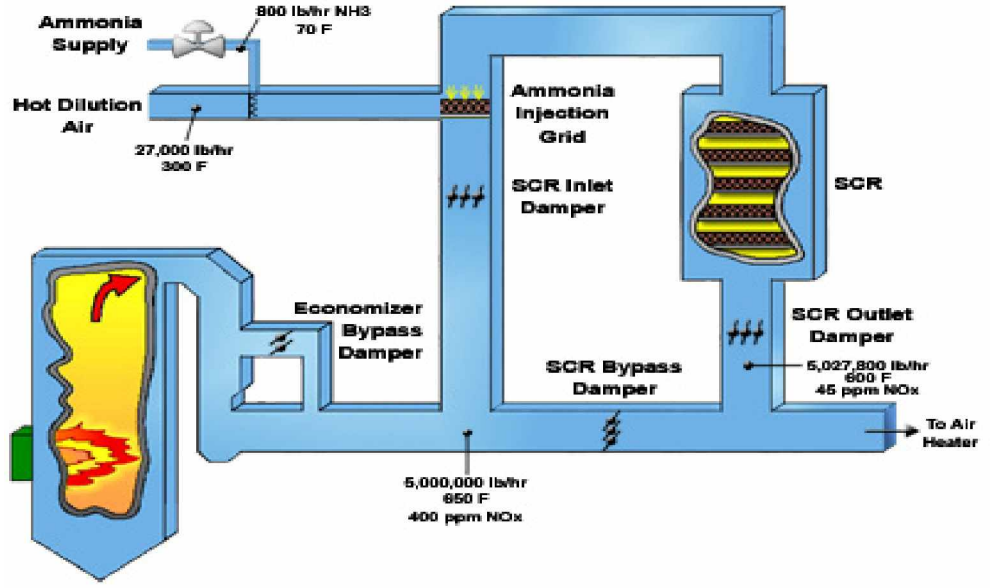

Figure 3. Typical SCR system with operating data [11].

The SCR of nitrogen oxides with ammonia is a wide-spread technology but it has some disadvantages. The amount of ammonia injected into the NO_x stream is a critical operating parameter. The required ratio of ammonia to NO_x should be stoichiometric. The ratio of ammonia to NO_x must be maintained to assure high levels of NO_x reduction, while also assuring that too much ammonia is not present. Ammonia that is not reacted will slip through the SCR catalyst bed and exhaust to atmosphere and this can create a new environmental problem [12].

N_2O is formed as a product of the SCR reaction [13], even though it is a strong greenhouse gas and contributes to the depletion of the stratospheric ozone layer. At present there is no legislation concerning N_2O concentration limits, although this is expected to change in the near future.

There are also technical problems arising from catalyst plugging by fine particle dust, catalyst poisoning by SO_2, conversion of SO_2 to SO_3, formation of ammonium bisulfate and the deposition of ammonium bisulfate on the catalyst at temperatures below 270°C. All these factors lead to catalyst deactivation [14].

Recently, much attention has been directed to the selective catalytic reduction (SCR) of NO using hydrocarbons as reductants in the presence of excessive oxygen. Research in this area has been focused on the SCR of NO with methane due to the fact that methane is the main component of natural gas and exists in most combustion exhausts [15]. The overall reaction for the CH_4-SCR technique is [16]

$$CH_4 + 2NO + O_2 \rightarrow N_2 + CO_2 + 2H_2O \qquad (15)$$

The reaction of NO_x with CH_4 removes both of environmental pollutants which cause greenhouse effect. Another advantage is that CH_4 is cheaper than ammonia and its transportation is much safer because methane sources are in close proximity to the stationary sources. For the usefulness in practical applications, methane should be shown to have reduction efficiencies similar to those of ammonia.

1.3. SCR of NO_x with Methane

The reaction of SCR of nitrogen oxides by hydrocarbons was discovered independently by Iwamoto et al. [17, 18] and Held et al. [19, 20]. Different kinds of solid catalysts like simple and mixed metal oxides, zeolites and platinum group metals were tested.

Li and Armor [16] used metal exchanged zeolites for NO reduction with methane in the presence of excess oxygen. The catalysts they used were ZSM-5 and zeolite Y exchanged with Co^{2+}, Cu^{2+}, Fe^{2+}, Cr^{3+} and Na^{+}. They reported that Na^{+} exchanged ZSM-5 (Na-ZSM-5) is inactive whereas the activity increases in the order Cr < Fe < Cu < Co and selectivity of CH_4 over a Co-ZSM-5 catalyst decreases with increasing concentration of oxygen in the feed. Cu-ZSM-5, that is a unique catalyst for the direct nitric oxide decomposition, is found to be a poor catalyst for nitric oxide reduction by methane in the presence of excess of oxygen. The apparent reaction order of NO and CH_4 over Co-ZSM-5 catalyst were 0.44 and 0.56, respectively.

Co-ZSM-5 is very active for removal of NO at 723 K [21]. Yokoyama and Misono [22] proposed that Ce-exchanged ZSM-5 was more active than Cu-ZSM-5 at 573 K. Li and Armor [23] concluded from their studies that Ga-containing H-ZSM-5 has comparable activity with Co-ZSM-5 and gallium catalysts are more selective than cobalt catalysts when water is absent in the feed. Activity is decreased by the water vapor in the feed more, as compared to Co-ZSM-5.

Nishizaka and Misono [24] studied the reduction of methane over H-ZSM-5 catalyst as a function of temperature for four metal containing catalyst. The sequence of increasing activity is Pd > Ru > Pt > Cu. They observed a conversion of about 70% for NO and 65% for CH_4 at 723 K for Pd/H-ZSM-5 and Pd-Ce/H-ZSM-5.

For the practical implementation of metal zeolite catalysts for NO reduction, catalyst durability is very important. However, steam which is unavoidably present in combustion gases irreversibly deactivates zeolite catalysts above a certain temperature [25-27]. Deactivation is due to dealumination of zeolite and this results the loss of ion-exchange capacity which causes an

irreversible change in activity and selectivity. In addition to water vapor, SO_2 in the feed stream shows a moderate poisoning effect.

In conclusion, zeolite based catalysts have serious drawbacks due to their diminished activity by wet conditions. Due to these problems, studies on metal-loaded oxide catalysts have found renewed interest

A number of different metal oxides have been shown to exhibit activity in the catalytic reduction of NO_x with methane [2, 9]. A few of them selectively reduce NO_x in the presence of excess oxygen. These materials are alkaline earth and rare-earth oxides [28-30] (e.g. Li/MgO and Sr/La_2O_3), Group IIIB [31] and supported transition metal oxides [32-35]. Comparing to zeolitic systems, these catalysts have better thermal stability, higher water resistivity and lower activity.

In recent years, Pd catalysts have been found to be highly selective in the presence of excess oxygen (i.e. $[O_2]/[CH_4] > 2$). Several authors [24, 36, 37, 38] have shown that when Pd is supported on acidic materials it can be active for the selective reduction of NO with CH_4. When Pd catalysts are tested under SCR with CH_4, their performance could vary from inactive to active but unselective, passing through highly selective. This performance depends on the metal loading and support acidity [36, 39]. Pd particles are transformed into PdO clusters which are very active for methane combustion. High selectivity of low-loading Pd catalysts supported on acidic materials is ascribed to the stabilization of the Pd^{2+} ions [40].

1.4. Reaction Mechanism of SCR of NO_x by Methane in Excess O_2

Since methane is one of the most difficult hydrocarbons to be activated, high temperature and reactive catalytic systems are needed to be utilized as a reductant in the SCR of NO. Selectivity and catalytic activity depend on priority of NO_x to O_2 for the reaction with methane. Over H-ZSM-5 containing Co, Mn, Ga, In and Pd catalysts [16, 41-49], CH_4 selectively reacts with NO_x instead of being completely combusted with O_2. It is shown that NO_2 formation on the catalyst surfaces is a necessary step in the SCR and formation of active NO_x species need the presence of O_2 [50-53]. These facts are supported by the lower rate of NO/CH_4 reaction and a similar rate of NO_2/CH_4 reaction as compared with the $NO/O_2/CH_4$ reaction. It is assumed that the formation of various surface NO_x species and their reactivity with CH_4 may have direct relationship with the catalytic activity and selectivity in the CH_4-SCR of NO_x. The NO_x groups interact with methane to form a new adsorbed intermediate containing C, N and O atoms. In subsequent steps, this intermediate reacts with $NO + O_2$ or NO_2, and N_2 is formed [54].

Lobree et al. [55] investigated the interactions of adsorbed NO and NO_2 with CH_4 over Pd-H-ZSM-5 by in-situ infrared spectroscopy together with temperature programmed desorption (TPD) and reaction (TPR) spectroscopy. They observed that above 650 K adsorbed nitrosyl species ($Z^-H^+[Pd(OH)(NO)]^+Z^-$) react with CH_4 to produce CH_2NO (or its isomer CHNOH) with the release of water. The CH_2NO formed, decomposes producing water and leaving behind CN (neutral) which further reacts with NO to form N_2 and CO. The reaction with O_2 produce NO and CO. They compared the activities of H-ZSM-5 and Pd-HZSM-5 for NO reduction by CH_4 in the presence of O_2 and concluded that acidity of Pd^{2+} cations is higher than that of Brønsted acid protons and they are the principal active component.

Shimizu et al. [56] studied active site structure and reaction mechanism for CH_4-SCR on Pd-H-Mordenite. Combined with kinetic results, they proposed that during CH_4-SCR reaction, the Pd^{2+}-NO complex is present as the main Pd species and adsorbed NO on Pd^{2+} is reduced by CH_4 derived reactive species (CH_x) to form NH_4^+ on highly acidic sites. Then NH_4^+ reacts with NO adsorbed on Pd^{2+} and NO_2 species formed by NO and O_2 resulting in N_2 formation.

Watson and Ozkan [57] studied Pd catalysts supported on titania for the SCR of NO by CH_4. They found that Pd^0 sites are essential for dissociative adsorption of methane. Under in-situ conditions, NH_3 is observed to form as molecularly adsorbed species on Lewis acid sites which are believed to act as a reducing agent for the adsorbed NO. It is mentioned that direct interaction of nitro/nitroso species with surface CH_x remains a possibility.

An analysis of published data on the CH_4-SCR mechanism indicates that nitric oxide is oxidized to nitrogen dioxide and/or surface nitrite/nitrate complexes which are selectively reduced by methane to molecular nitrogen through the possible formation of organic nitro compounds. These organic nitro compounds are shown to be very reactive. They transform into molecular nitrogen under the action of oxygen due to intermediate formation of ammonia, which is a very efficient reducing agent. Cowan et. al. [58] showed that the rate determining step for CH_4-SCR is hydrogen abstraction, whose site is adsorbed NO_2 formed by oxidation of NO. Initial steps are

$$2NO + O_2 \rightarrow 2NO_2 \qquad [16]$$

$$CH_4 + NO_{2(ads)} \rightarrow CH_3\cdot + HONO \qquad [17]$$

In the next step, methyl radicals combines directly with adsorbed NO_2 yielding CH_3NO_2, nitromethane. Above 220^{o}C decomposition of nitromethane gives NH_3 which can react to give nitrogen.

Xie et. al. [30, 59] observed the formation of gas phase methyl radicals which reacts with NO to form nitrosomethane on their CH_4-SCR active Sr/La_2O_3 and Ba-doped MgO catalysts.

1.5. Metal Oxide Supports for CH_4-SCR Catalysts

The performance of CH_4-SCR catalysts has been found to strongly depend on the acidity of the support. Zeolitic materials exhibit strong Lewis and Brønsted acidity. Transition and non-transition metals loaded on zeolites have been shown to exhibit activity for the SCR of NO_x with methane in excess oxygen. Li and Armor [50] found that the most active catalysts for NO_x removal by CH_4 in oxygen excess were based on cobalt supported on several zeolites, such as Co-ferrierite and Co-ZSM-5. However, water vapour and SO_2 can act as poisons on the catalyst surface and decrease the activity. Use of non-zeolitic solid acid supports is an alternative approach to durable performance for CH_4-SCR in moist streams. Among metal oxide supports, Al_2O_3, ZrO_2 and TiO_2 have taken interest.

γ-Al_2O_3 is widely used as support in catalysis. It has large surface area, thermal stability and low cost, however it has low acidity and this limits its application in CH_4-SCR. Pd/γ-Al_2O_3 exhibits very low activity in CH_4-SCR but high acivity in combustion of methane [24, 60]. Li et al. [61] demonstrated that sulfation of γ-Al_2O_3 generates strong acid sites which is essential for the reduction of NO with methane over Pd catalyst and sulfated γ-Al_2O_3 is promising to act as a support for Pd catalyst. ZrO_2 is of great interest on account of its surface acidity. Zhao et al. [62] showed that monoclinic zirconia has Lewis and Brønsted acid sites whereas tetragonal zirconia has only Lewis acid sites. Titania has various forms obtained from different preparation methods and these forms exhibit various surface arrangements resulting in different surface reactivity. Active anatase phase has poor stability, poor mechanical strength and low surface area at high temperatures. Kumthekar and Ozkan [63] examined the SCR of NO_x with methane on the Pd/TiO_2 catalyst. They reported that the catalyst can reduce NO.

These metal oxides exhibit superacidity when modified with sulfate, tungstate or molybdate ions. Hino and Arata [64] classified acid strength of these superacids. Table 1 shows their results.

Table 1. Solid superacids and their acid strength [64].

Catalyst (calcination temperature)	Highest acid strength (H_o value)
SO_4/SnO_2 (550 ^oC)	-18.0
SO_4/ZrO_2 (650 ^oC)	-16.1
SO_4/HfO_2 (700 ^oC)	-16.0
SO_4/TiO_2 (525 ^oC)	-14.6
SO_4/Al_2O_3 (650 ^oC)	-14.6
SO_4/Fe_2O_3 (500 ^oC)	-13.0
SO_4/SiO_2 (400 ^oC)	-12.2
WO_3/ZrO_2 (800 ^oC)	-14.6
MoO_3/ZrO_2 (800 ^oC)	-13.3
WO_3/SnO_2 (1000 ^oC)	-13.3
WO_3/TiO_2 (700 ^oC)	-13.1
WO_3/Fe_2O_3 (700 ^oC)	-12.5
B_2O_3/ZrO_2 (650 ^oC)	-12.5

Results indicate that sulfate-modified catalysts possess higher acidity than their tungstated counterparts. However, SO_4^{2-} is unstable at high temperatures under reducing conditions and may result in activity losses. Tungstated metal oxides (WO_3-TiO_2, WO_3-ZrO_2) are structurally more stable than sulfated materials and they exhibited high activity for reaction that requires strong Brønsted acid sites [65]. When WO_3 covers the surface of ZrO_2 as a monolayer, the catalyst shows strong Brønsted and Lewis acidity. It is shown that Pd/ZrO_2 can become highly selective for CH_4-SCR when promoted by tungstate.

It has been observed that thermal stability of titania can be enhanced by the incorporation of zirconia [66, 67]. This property is important because the activation of C-H bond of CH_4 occurs at high temperature. Lu et al. [68] reported that addition of ZrO_2 to TiO_2 may prevent the possible strong metal-support interaction due to migration of TiO_2 onto the metal surface, after reduction at high temperature. Moreover, mixed oxide (TiO_2-ZrO_2) is more acidic with respect to single component oxides. Strong acid sites on the mixed oxides are generated by charge imbalance resulting from heteroatom linkages [69]. Figure 4 shows the structural representation of the situation.

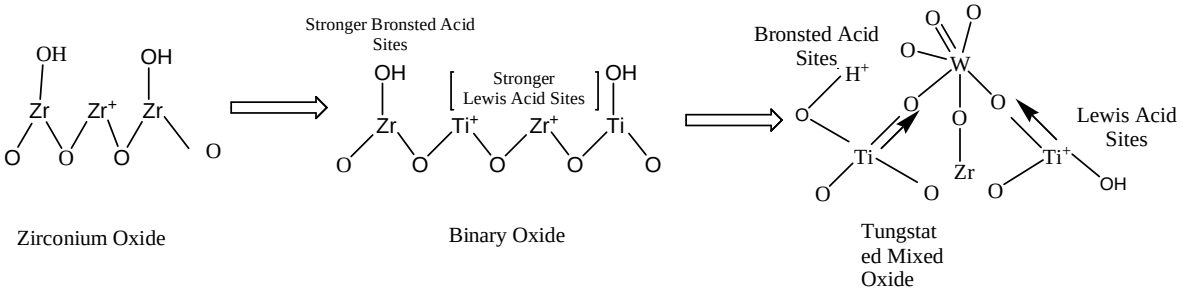

Figure 4. Brønsted and Lewis acid sites on binary and tungstated binary oxides.

On binary oxide surface, there is a charge imbalance based on the generation of Ti-O-Zr bonding [70]. Charge imbalance will create Brønsted and Lewis acid centers. When surface of the mixed oxide is tungstated, tungstate groups will weaken the O-H bond which creates Brønsted acidity, and these groups will also withdraw electron density from unsaturated cationic centers (Ti^{4+} and Zr^{4+}) to form strong electron deficient Lewis acidity. The highest acidity and highest surface area are obtained when the Zr:Ti molar ratio is equal to 1 [71]. It is expected that monolayer coverage of WO_3 on equimolar ratio of TiO_2-ZrO_2 mixed oxide support will exhibit very strong surface acidity.

TiO_2-ZrO_2 can be a valuable support to load Pd for CH_4-SCR reaction in terms of its high acidity, good thermal stability, high surface area (which is necessary for good dispersion of metal) and high mechanical strength. In the course of our work Pd-promoted TiO_2-ZrO_2 catalyst is shown to be SCR-CH_4 inactive. It is reasonable to use tungstated titania-zirconia support to load Pd since the tungstation can create high surface acidity needed for good dispersion of Pd.

1.6. FTIR Spectroscopy and Aim of the Study

It has been established that after NO + O_2 adsorption on CH_4-SCR catalysts, NO_x^-(x = 2, 3) compounds are formed and these species interact with CH_4 to form organic nitro and/or nitrite species that are decomposed via various routes to SCR reaction products. For the search of detailed mechanism of the process, IR spectroscopy gives direct information on the nature of the different surface species. It is the most powerful technique for in-situ characterization of adsorbed NO_x species on catalyst surfaces [72].

The aim of this study is to identify and determine the routes of formation and thermal stability of adsorbed NO_x complexes on the surface of Pd/tungstated titania-zirconia mixed

oxides by means of in-situ FTIR spectroscopy and to investigate the reactivity of adsorbed NO_x species toward methane in order to propose a reaction mechanism.

1.7. Identification of Adsorbed NO_x^- Species by FTIR Spectroscopy

Interpretation of IR spectra of NO_x^- surface species produced under SCR conditions can be quite contradictory due to the fact that the large number of compounds (nitrogen oxo species, hydrogen containing compounds and carbon containing species) may coexist on the surface and some bands from the spectra of different nitrogen-oxo compounds may coincide [72]. Table 2 shows the reported frequencies of adsorbed NO_x species observed on metal oxides [73].

The nitrite anion has a C_{2v} symmetry. $\nu_{as}(NO_2)$ and $\nu_s(NO_2)$ stretches at 1260 cm^{-1} and 1330 cm^{-1}, respectively. Different ways of bonding of nitrite anion to metal cations changes its IR spectrum. Nitro compounds form when NO_2^- coordinated via its N atom and C_{2v} symmetry is preserved. When NO_2^- is coordinated by one or two oxygen atoms, nitrito compounds form. Chelating nitrito species have also C_{2v} symmetry. If free nitrite ion is coordinated simultaneously via an O and its N atom, bridging and bidentate nitro species form.

The free nitrate ion has a D_{3h} symmetry. $\nu_3(NO_2)$ mode is IR active and it vibrates at 1400 cm^{-1} whereas ν_1 mode is Raman active and observed at 1050 cm^{-1}. Surface nitrates have C_{2v} symmetry and they have the ν_3 mode split into two bands and ν_1 mode becomes IR active. Splitting of ν_3 vibration is in the sequence: bridged nitrates > bidentate nitrates > monodentate nitrates. Thermal stability of these species follow the same order [72].

Kanctheva and Ciftlikli [74] analyzed the combination bands of nitrate species and showed that this spectral region can be used for structural identification of bridged and bidentate nitrates. Bridged nitrates produce combination bands at 2845-2800 cm^{-1} [ν(N=O) + $\nu_{as}(NO_2)$] and a pair of bands at 1980-1960 and 1900-1890 cm^{-1} [$\nu_s(NO_2)$ + δ(ONO)]. Bidentate nitrates can be distinguished by the appearance of combination bands in the region of 2600 cm^{-1} [ν(N=O) + $\nu_s(NO_2)$] and a pair of bands at 1755 and 1700 cm^{-1} [$\nu_s(NO_2)$ + δ(ONO)].

Stability factor is important to identify the nature of NO_x adspecies. Weakly adsorbed species can be easily removed by evacuation at ambient temperature and these are noncharged, such as NO, NO_2, N_2O_3 and N_2O_4. Surface nitrosyls and dinitroslys are sometimes very stable. Ionic species (NO_3^-, NO_2^-, NO^+ etc.) are not removed by evacuation at ambient temperature.

Their thermal stability depend on the structure and on the kind of the cation to which they are bonded [72].

Table 2. Frequencies of adsorbed NO_x species observed on metal oxides [73].

NO_x Species	Vibration Modes	Wavenumbers [cm^{-1}]
Free nitrite ion, NO_2^-	$\nu_{as}(NO_2)$	1250
	$\nu_s(NO_2)$	1335
	$\delta(ONO)$	830
Nitro, M-NO_2	$\nu_{as}(NO_2)$	1370-1470
	$\nu_s(NO_2)$	1320-1340
	$\delta(ONO)$	820-850
Nitrito, M-O-NO	$\nu(N=O)$	1400-1485
	$\nu(NO)$	1050-1100
	$\delta(ONO)$	820-840
Chelated nitrito, (M-O_2)=N	$\nu_{as}(NO_2)$	1270-1390
	$\nu_s(NO_2)$	1170-1225
	$\delta(ONO)$	840-860
Bridging nitro, M-O-N(O)-M	$\nu_{as}(NO_2)$	1390-1520
	$\nu_s(NO_2)$	1180-1260
Bidentate nitro 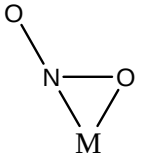	$\nu_{as}(NO_2)$	1390-1520
	$\nu_s(NO_2)$	1180-1260
Free nitrate ion, NO_3^-	$\nu_{as}(NO_2)$	1400
Monodentate nitrate, M-O-NO_2	$\nu_{as}(NO_2)$	1450-1570
	$\nu_s(NO_2)$	1250-1330
	$\nu(NO)$	970-1035
Bidentate nitrate, M-O_2NO	$\nu_{as}(NO_2)$	1200-1310
	$\nu_s(NO_2)$	1003-1040
	$\nu(NO)$	1500-1620

Biridged nitrate, $(M\text{-}O)_2$=NO	$\nu_{as}(NO_2)$	1200-1260
	$\nu_s(NO_2)$	1000-1030
	ν(NO)	1590-1660

2. EXPERIMENTAL

2.1. Sample Preparation

Flow chart 1 shows the preparation steps of the catalysts. TiO_2-ZrO_2 mixed oxide (1:1 mol ratio based on oxides) was prepared by a homogenous coprecipitation of urea at 70°C . By homogenous coprecipitation method, good mixing of oxides (which is important for the generation of strong acid sites due to charge imbalance) and high surface area can be obtained.

Aqueous solutions of $TiCl_4$, $ZrO(NO_3)_2$ and urea were heated together at 110°C under constant reflux and stirring. After 18 hours of heating, pH of the solution increased from 2 to 8 and formation of white precipitate was observed. Urea decomposes to generate in-situ OH^- ions according to the reaction:

$$CO(NH_2)_2 + 3H_2O \rightarrow 2NH_4^+ + 2OH^- + CO_{2(g)} \quad (1)$$

Generation of hydroxide ions favors homogenous coprecipitation of zirconium and titanium hydroxides. After the precipitation, the suspension was aged additionally for 12 hours. The resulting precipitate was collected by suction filtration, washed with deionized water until $AgNO_3$ gave negative test for Cl^- ions. The material was dried at 110°C for 12 hours and calcined at 500°C in air to get mixed oxides.

Oven-dried hydrous titania-zirconia was impregnated with ammonium metatungstate solution by incipient wetness method. The resulting sample was oven-dried at 110°C and calcined at 500°C for 4 hours. Three samples with nominal WO_3 contents of 15 wt %, 20 wt % and 25 wt % were prepared.

To incorporate Pd, required quantity of $Pd(NO_3)_2$ was dissolved in water and powdered oven-dried hydrous tungstated titania-zirconia was added to this solution and excess water was evaporated with continuous stirring. The sample was oven-dried at 383 K and calcined at 500°C for 4 hours. Two catalysts with nominal Pd contens of 0.7 wt % and 1.5 wt % were prepared. The

same method was applied to incorporate Pd to hydrous TiO_2-ZrO_2 and 1.5 wt % Pd on TiO_2-ZrO_2 was obtained.

Catalyst notations used further in the text are shown in Table 3.

Flow chart 1. Preparation routes of the catalysts

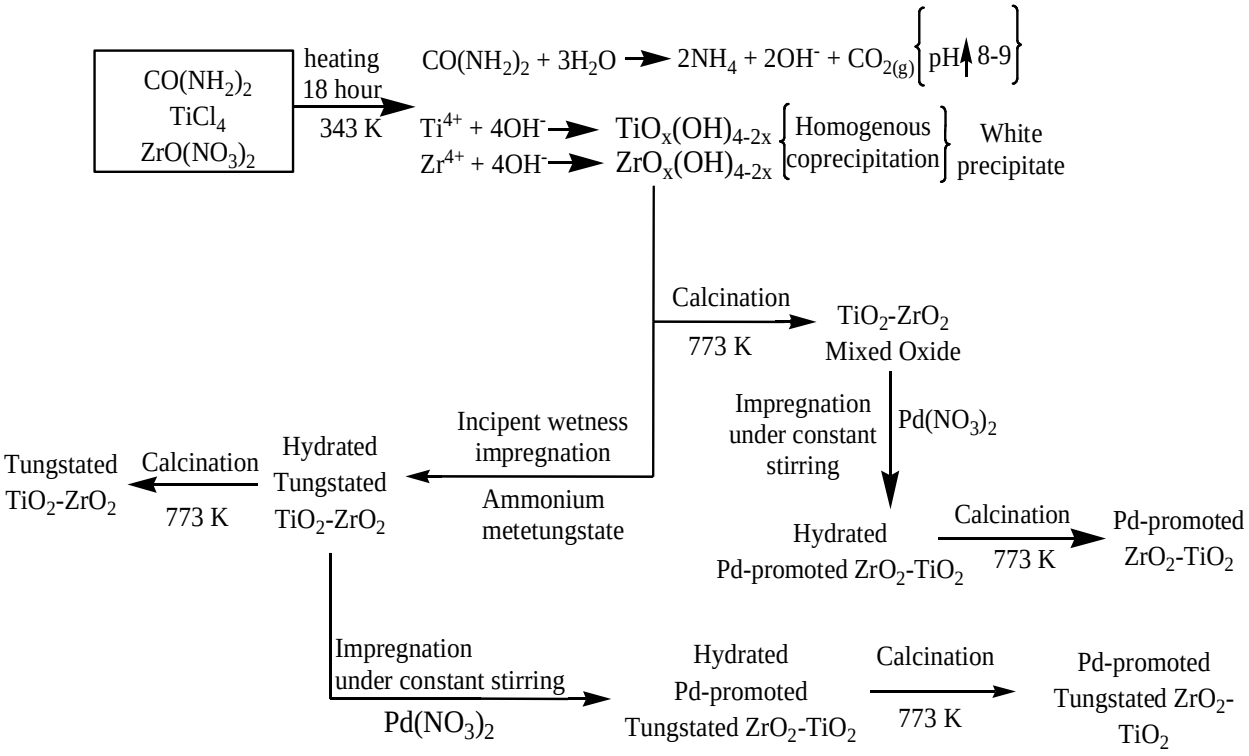

Table 3. Catalysts and notations. All the samples were calcined at 500°C.

Notation	Sample
ZT	(1:1) Titania-Zirconia
1.5Pd/ZT	1.5 wt % Pd promoted Titania-Zirconia
15WZT	15 wt % WO_3 on Titania-Zirconia
20WZT	20 wt % WO_3 on Titania-Zirconia
WZT	25 wt % WO_3 on Titania-Zirconia
0.7Pd/WZT	0.7 wt % Pd promoted 25 wt % WO_3 on Titania-Zirconia
1.5Pd/WZT	1.5 wt % Pd promoted 25 wt % WO_3 on Titania-Zirconia

Pure titania (anatase) and ZrO_2 (monoclinic phase) were prepared by hydrolysis of the corresponding chlorides (pH=9) according to procedure reported in the literature [74, 75].

2.2. Surface Area Measurements, X-ray Diffraction and Diffuse Reflectance UV-Visible Spectroscopy

The BET surface areas of the samples were measured by nitrogen adsorption at 77 K using a MONOSORP apparatus from Quanta chrome. The samples were dehydrated at 573 K for 1 h before the measurements.

XRD analysis performed on a Rigaku Miniflex diffractometer with Ni-filtered Cu Kα radiation under ambient conditions. The scan speed was 2^0/min for the samples studied.

DR-UV-vis spectra were obtained under ambient conditions with fiber optic spectrometer AvaSpec-2048 (Avantes).

2.3. FTIR Spectroscopy

The FTIR spectra were recorded on a BOMEM MB 102 FTIR (Hartman & Braun) spectrometer equipped with a liquid-nitrogen-cooled MCT detector at a resolution of 4 cm^{-1} (128 scans).

2.4. Experimental Setup

A specially designed IR cell (Xenonum Scientific, USA) allows recording of the spectra at ambient and elevated temperatures (Figure 5). The cell has BaF_2 windows. The sample holder of the cell can be moved up and down relative to the light beam, which gives the possibility for the recording the gas phase spectrum. The cell is connected to a vacuum/adsorption apparatus (Figure 6).

2.5. Activation of the Samples

Self-supporting discs (0.025 – 0.035 g/cm^2) were used for the FTIR studies. These specimens were activated by heating for 1 hour in a vacuum at 450^{o}C and in oxygen (100 Torr) at the same temperature followed by evacuation for 1 hour at that temperature.

The spectra of the activated sample that was taken at high temperature and room temperature were used as background references. The high temperature background reference

was used in the subtraction of the spectra taken at high temperatures and similarly the room temperature background reference was used for the spectra registered below 150^{o}C. The spectra of the samples that were subjected to heat treatments at elevated temperatures were recorded at those temperatures.

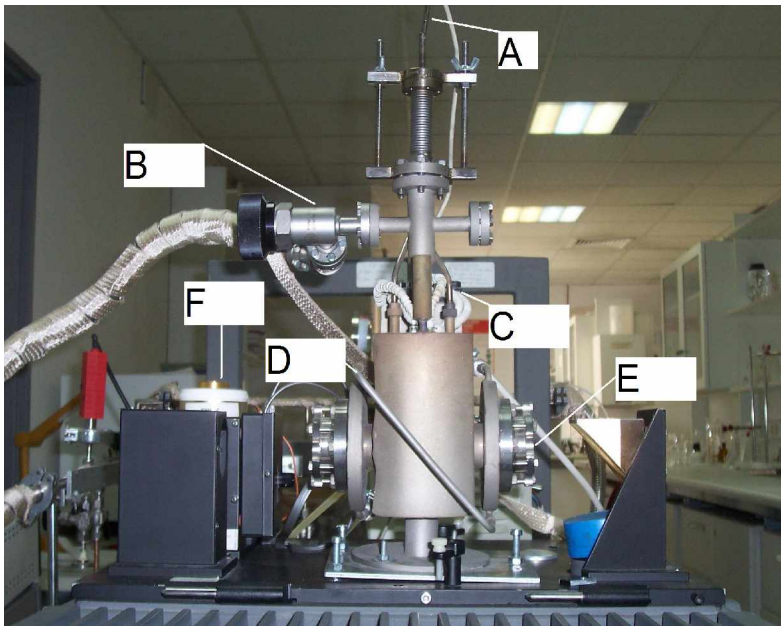

Figure 5. IR cell (A: Thermocouple entrance, B: Vacuum/Adsorption line connection, C: Heating filaments, D: Cooling pipes, E: BaF_2 windows, F: MCT Detector)

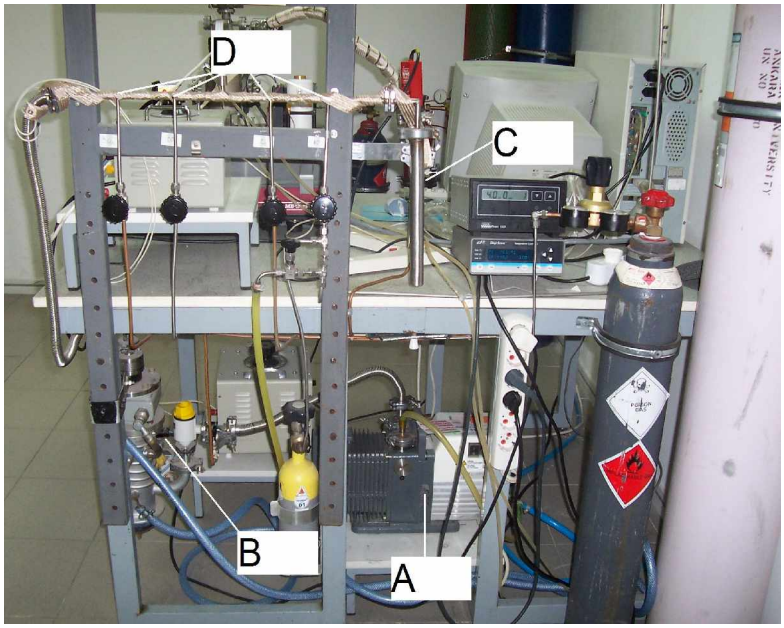

Figure 6. Vacuum/adsorption apparatus (A: Rotary pump, B: Diffusion pump, C: Liquid nitrogen trap, D: Adsorption pipes)

2.6. Adsorption of NO and Co-adsorption with O_2

NO adsorption was performed at room temperature introducing 12 Torr of NO and the evolution of the IR spectra with the time was followed.

Co-adsorption with O_2 was achieved at room temperature introducing a gas mixture (12 Torr) of NO and (6 Torr) of O_2 for a given period of time.

Thermal stability of the adsorbed NO_x species was studied by heating the sample for 15 minutes under vacuum in the temperature range 200°C – 450°C.

2.7. Interaction of CH_4 with the Catalysts

40 Torr of methane was added into the IR cell in order to observe the interaction of CH_4 with the catalyst. Then the closed IR cell was heated from 200°C – 450°C.and the samples were allowed to stay for 15 minutes at each temperature level.

2.8. Interaction of CH_4 with NO_x – precovered catalysts

After the formation of NO_x species by room temperature adsorption of NO and O_2 (1:1) followed by evacuation for 30 minutes, 40 Torr of CH_4 was added. The interaction of methane with the NO_x – precovered catalyst was observed in the temperature range 200°C – 450°C. The interaction time at each temperature level was 15 minutes.

CH_4 and O_2 used were passed through a trap cooled by liquid nitrogen before admission to the IR cell. The purity of NO gas was 99.9 % (Air Products).

2.9. Adsorption of CH_3NO_2

CH_3NO_2 adsorption was performed at room temperature by introducing 1 Torr of CH_3NO_2 in order to observe the interaction of nitromethane with the catalyst.

3. RESULTS AND DISCUSSION

3.1. Characterization of the Samples

3.1.1. BET Surface Area Measurements

Table 4 BET surface areas and tungsten density.

Sample	BET Surface Area	WO_3 (molec/nm^2)	WO_3 coverage monolayer
ZT	118 m^2/g	-	-
WZT	154 m^2/g	3.16	~0.6
1.5Pd/WZT	128 m^2/g	3.80	~0.7

In Table 4 surface areas of the samples are given together with the WO_3 surface density (number of molecules/nm^2). The maximum packing density of planar WO_3 species are taken as 0.21 g. WO_3/100 m^2 [76]. According to this density value, the average cross-section of an adsorbed WO_3 is equal to 0.183 nm^2 and the surface concentration of WO_3 corresponding to the theoretical monolayer is found to be 5.45 WO_3/nm^2. This shows that surface concentrations of WO_3 on WZT and 1.5Pd/WZT samples have nearly 60% and 70% of the monolayer WO_3 coverages, respectively.

3.1.2. X-ray Diffraction

3.1.2.1. Titania-Zirconia Mixed Oxides

Figure 7 shows the XRD pattern of sample ZT calcined at different temperatures. The sample ZT after calcinations at 500°C and 550°C is in amorphous form. Formation of crystalline $ZrTiO_4$ compound at 600°C is observed that can be matched with JCPDS file no. 34-415. Intensity of the lines due to $ZrTiO_4$ increased with increasing calcination temperature. No independent lines due to TiO_2 (rutile or anatase) and ZrO_2 (monolinic, cubic or tetragonal) have been observed.

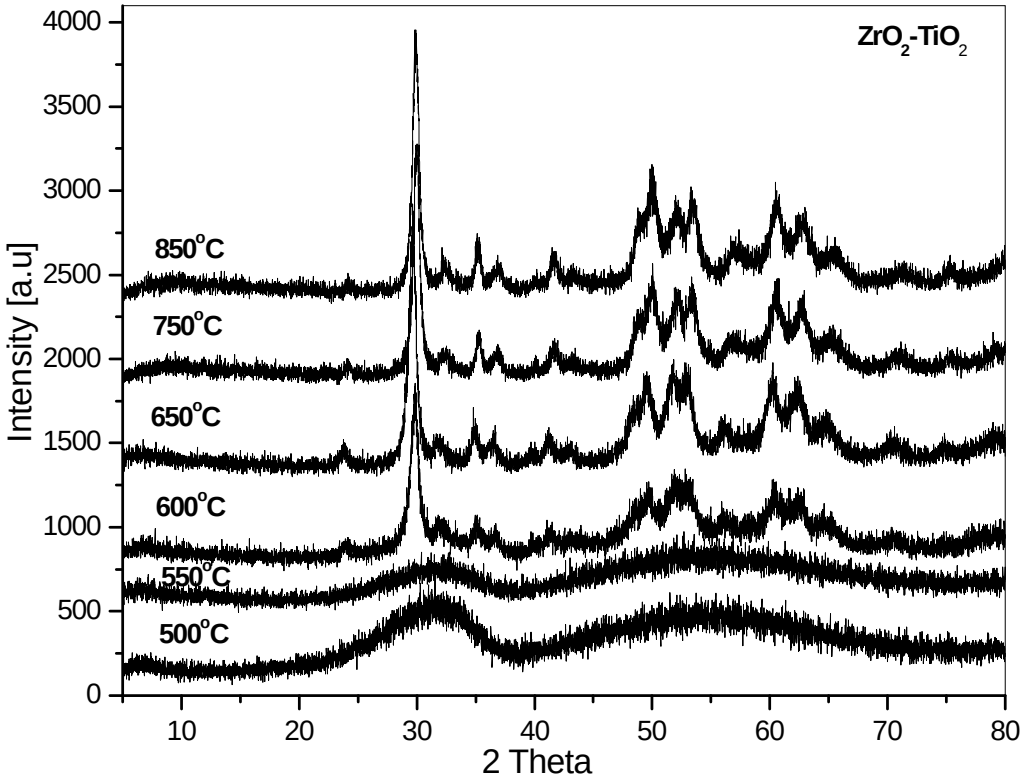

Figure 7. Powder X-ray diffraction patterns of ZT samples calcined at different temperatures.

Crystallite size is calculated using the Scherrer equation [77] (equation 1). The calculations are performed by measuring the broadening of a particular peak in a diffraction pattern associated with a particular planar reflection within the crystal unit cell. It is inversely related to the FWHM (full width at half maximum) of an individual peak. This is due to the periodicity of the individual crystallite domains, in phase, reinforcing the diffraction of the X-Ray beam, resulting in a tall narrow peak. If the crystals are defect free and periodically arranged, the X-ray beam is diffracted to the same angle even through multiple layers of the specimen. If the crystals are randomly arranged or have low degrees of periodicity, the result is a broader peak.

$$\text{Crystallite Size} = K \times \lambda / B \times (\cos \theta_B) \quad (1)$$

where K is the shape factor of the average crystallite (expected shape factor is 0.9). λ is the wavelength (1.54056 Å for Cu $K\alpha_1$), θ_B is the peak position and B is the FWHM of the instrument corrected line profile. Instrumental peak broadening is determined by using Si sample

with 2000 nm crystallite size. In this case, crystal size effect on peak broadening is removed due to large crystallite size of Si and instrumental broadening is found to be 0.1^{o}. The diffraction peak of (111) of the $ZrTiO_4$ phase has 2θ in the range from 29.90^{o} to 30.01^{o}. Deconvolution parameter is built into diffraction lines for FWHM (Full-width at half-maximum) correction to help in assigning the area of the (111) peak with PeakFit^{TM} program. Table 3 shows the crystallite sizes of $ZrTiO_4$ calcined at increasing temperatures, calculated according to the Scherrer equation.

Table 5 Calculated crystallite sizes of $ZrTiO_4$

Calcination Temperature of TiO_2-ZrO_2	Crystallite Size
$600^{o}C$	4.4 nm
$650^{o}C$	4.9 nm
$750^{o}C$	5.2 nm
$850^{o}C$	5.7 nm

The crystallization process initiates with the nucleation and the nuclei grow by diffusion, which depends on temperature, being thus crystallization a thermally activated process. Crystallite size increases with increasing calcination temperatures. At higher temperatures, the oxide diffusion process is accelerated, starting the sintering process. This leads to the augmentation of the particle size.

3.1.2.2. Tungstated Titania-Zirconia

Figure 8 shows XRD patterns of 25 % tungstated ZrO_2-TiO_2 calcined at $500^{o}C$, $550^{o}C$ and $600^{o}C$. The catalysts are found to be XRD amorphous. These results show that tungstation retards the crystallization to higher temperatures. The WO_3 displays its three peaks in medium intensity at 22.99, 23.43 and 24.23 ^{o} (JCPDS file no. 43-1035). Peaks become narrower and higher in intensity as the calcination temperature increases.

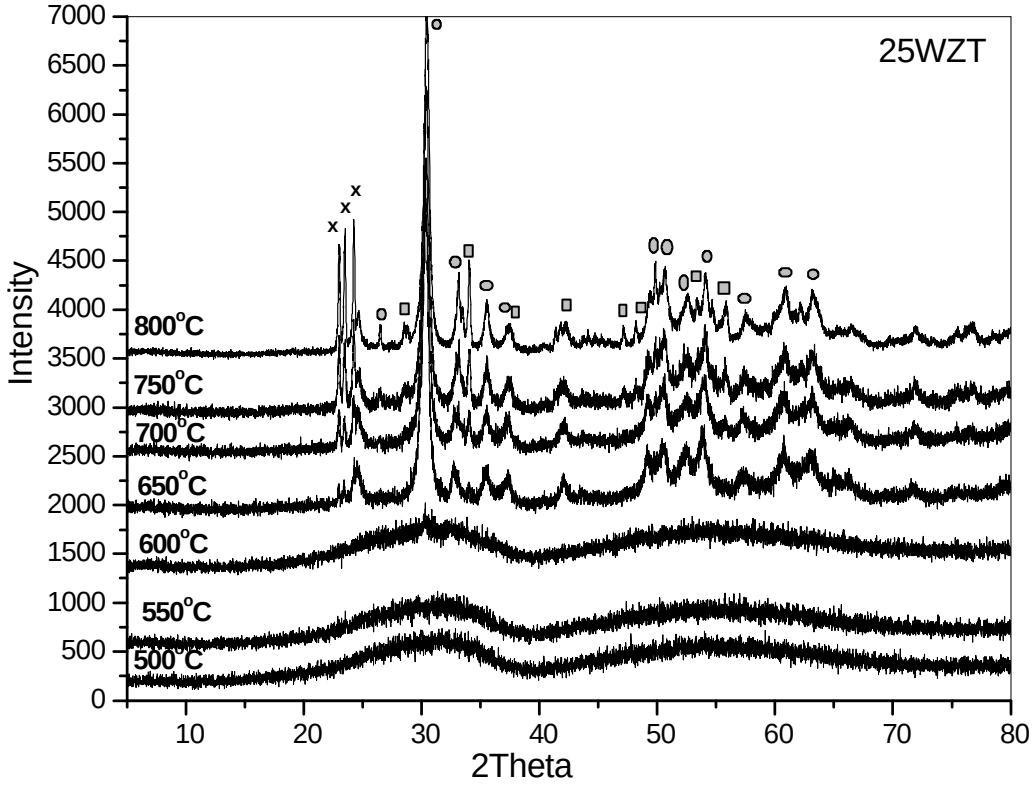

Figure 8. Powder X-ray diffraction patterns of 25WZT samples calcined at different temperatures. Characteristic lines due to (●) $ZrTiO_4$; (■) $Zr(WO_4)_2$; (**x**) WO_3.

In addition to $ZrTiO_4$, $Zr(WO_4)_2$ (JCPDS file no. 31-1500) can be noted. Reddy et al. [70] observed characteristic lines due to $Zr(WO_4)_2$ in their tungstate promoted TiO_2-ZrO_2 catalyst calcined at 800°C. Intensity of lines due to $ZrTiO_4$ and $Zr(WO_4)_2$ increase with increasing calcination temperature up to 800°C.

Table 6. Calculated crystallite sizes of $ZrTiO_4$ phase of WZT

Calcination Temperature of WZT	Crystallite Size
700°C	4.8 nm
750°C	4.9 nm
800°C	5.1 nm

Table 6 shows the crystallite sizes of WZT calcined at increasing temperatures, calculated according to the Scherrer equation. Crystallite sizes are slightly lower than that of ZT samples at corresponding calcinations temperatures. This is due to the fact that the load of WO_x species stabilizes the titania-zirconia structure and prevents sintering of the small crystallites.

3.1.2.3. Pd promoted Tungstated Titania-Zirconia

Figure 9 shows XRD patterns of 1.5 wt % Pd promoted 25 wt % WO_3 on TiO_2-ZrO_2 calcined at 700°C. Diffraction patterns are similar with tungstated sample calcined at 700°C. $ZrTiO_4$, $Zr(WO_4)_2$ and WO_3 phases have been found. PdO(101) and Pd(111) planes have diffraction lines at around 34° and 40°, respectively [78]. Since the amount of PdO and Pd is very low and the diffraction patterns are complex, these phases are difficult to analyze.

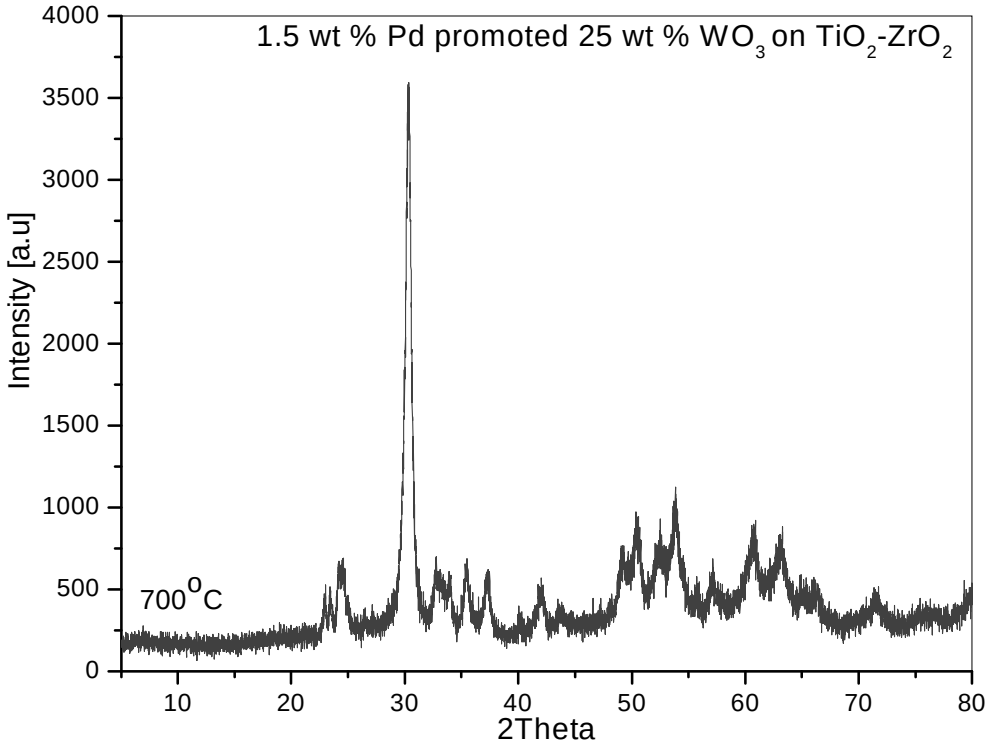

Figure 9. Powder X-ray diffraction pattern of 1.5Pd/WZT samples calcined at 700°C.

3.1.3. Diffuse Reflectance UV-vis Spectra of the Samples

In DR-UV-vis spectroscopy, the position of the absorption edge is sensitive to the bonding between metal oxide and WO_x polyhedra and these data are useful to characterize the average particle size of nanocrystalline insulators and semiconductors [76]. Absorption edge energy for WO_x species is strongly influenced by number of neighboring WO_x polyhedra bonded through W-O-W bonds and by the number of bonds between each polyhedra. In our study, UV-vis absorption edge energies of WO_x compounds on TiO_2-ZrO_2 support are compared with the edge energies of several crystalline standards with known WO_x coordination in order to determine the chemical state of Pd on tungstated TiO_2-ZrO_2.

Optical absorption edge energy is the minimum photon energy required to excite an electron from the top of the valence band (HOMO) to the bottom of conduction band (LUMO). There are 2 types of electronic transitions which are direct and indirect. Photons excite electrons in direct transitions whereas in indirect transitions there are also concerted vibrations and energy from the crystal lattice. In the region near the absorption edge energy, the dependence of absorption coefficient **(**α**)** is given by

$$\alpha \sim (h\nu - E_o)^{\eta} / (h\nu) \qquad (2)$$

where $h\nu$ is energy of incident photon, E_o is optical absorption edge energy and η depends on type of optical absorption caused by photon absorption. Fundamental absorption edge of WO_3 crystallites is caused by indirect electron transitions and a plot of $(\alpha h\nu)^{1/2}$ vs $h\nu$ is linear near the edge for WO_3. This method is used to determine the absorption edge energies. Table 7 shows the edge energies, their corresponding transitions and the electronic structural properties of catalysts studied.

TiO_2-ZrO_2 has an edge energy value of 3.32 eV which is different than pure titania and zirconia. This fact shows that a different matrix has been formed and according to XRD it is found as $ZrTiO_4$ [71].

The absorption spectrum of 25 wt .% WO_3/ZrO_2-TiO_2 sample calcined at 500^oC has an edge energy similar to that in $(NH_4)_{10}H_2W_{12}O_{42}$ (ammonium paratungstate). Ammonium paratungstate has a structure of polyoxotungstate clusters and their WO_x domains of intermediate size contanining octahedra bonded through edges and corners. WO_x domains of intermediate size have unique acid property by forming Brønsted acid centers. Paratungstate-type polytungstate species form an extended network of WO_x domains over which an excess negative charge can be delocalized [79]. The sample 25 wt. %WO_3/ZrO_2-TiO_2 calcined at 800^oC has an edge energy

similar to that in bulk WO_3. This shows that WO_3 crystallites are formed on the surface of mixed oxide support. The XRD data of tungstated samples indicates that the increase in the calcination temperature results in increased sintering rate and particle size which results in loss of surface area. As a result, the average distance between dispersed WO_x octahedra on the TiO_2-ZrO_2 surface decreases and WO_x surface density increases. The dispersed WO_x species will form W-O-W bridging bonds between neighbouring WO_x groups and three dimensional WO_3 crystallites are formed [79]. Structural change in octahedral WO_x species on TiO_2-ZrO_2 surface with increased calcination temperature is shown in the inset of Table 7.

Table 7. Edge energies, their corresponding transitions and the electronic structural properties.

Compound	Absorption Edge Energy	Transition	Property
TiO_2	3.15 eV	O^{2-}--Ti^{4+} O(2p)—Ti(3d)	Semiconductor oxide
ZrO_2	5.0 eV	O^{2-}--Zr^{4+} O(2p)—Zr(4d)	Insulator oxide
TiO_2-ZrO_2 500°C calcined	3.32 eV	O^{2-}---Zr^{4+} O^{2-}---Ti^{4+}	A different matrix from pure titania or zirconia has been formed
Bulk WO_3	2.60 eV	O^{2-}--W^{6+} O(2p)--W(5d)	It contains 6-coordinate $W^{6+}$and WO_x species in an extended 3-D crystalline network of distorted octahedra bonded to 6 neighbouring octahedra.
Na_2WO_4	4.95 eV	O^{2-}--W^{6+} O(2p)--W(5d)	Monomeric tetrahedral tungstate(4-coordinate W^{6+})
$(NH_4)_{10}H_2W_{12}O_{42}$	3.54 eV	O^{2-}--W^{6+} O(2p)--W(5d)	Intermediate value of absorption edge energy. WO_x domains of intermediate size contanining octahedra bonded through edges and corners
25%WO_3/ZrO_2-TiO_2 500°C calcined	3.46 eV	O^{2-}--W^{6+} O(2p)--W(5d)	Tetrahedral monomeric WO_4^{2-} species and microcrystalline WO_3 are not present on tungstated titania-zirconia. Absorption edge enegry more likely matches with ammonium paratungstate which has a structure of polyoxotungstate clusters.
25%WO_3/ZrO_2-TiO_2 800°C calcined	2.68 eV	O^{2-}--W^{6+} O(2p)--W(5d)	Microcrystalline WO_3 species are present.

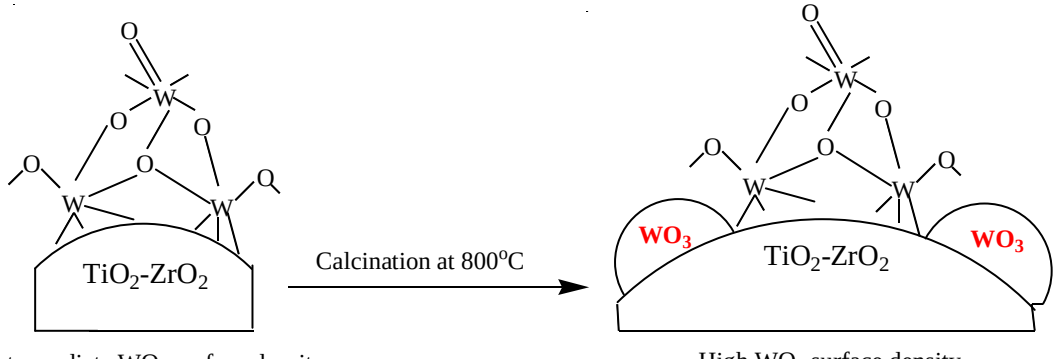

Intermediate WO_x surface density

High WO_x surface density

Structural changes of octahedral WO_x species on TiO_2-ZrO_2 surface with calcination temperature.

Figure 10 shows UV-vis diffuse reflectance spectra of Pd- promoted tungstated samples with increasing Pd content and also Pd promoted mixed oxide samples. The band around 450 nm is attributed to d-d transition of isolated Pd^{2+} ions linked to surface oxygen atoms of the support or small $Pd(O)_n^{2+}$ entities [80]. Shimizu et al. [56] observed in the absorption spectrum of Pd-H-Mor similar band at 460 – 480 nm due to d-d transitions of isolated Pd^{2+} ions coordinated to the cation exchange sites of the zeolite. This leads to the conclusion that tungstated titania-zirconia support is able to stabilize dispersed palladium(II) analogous to the acidic zeolites.

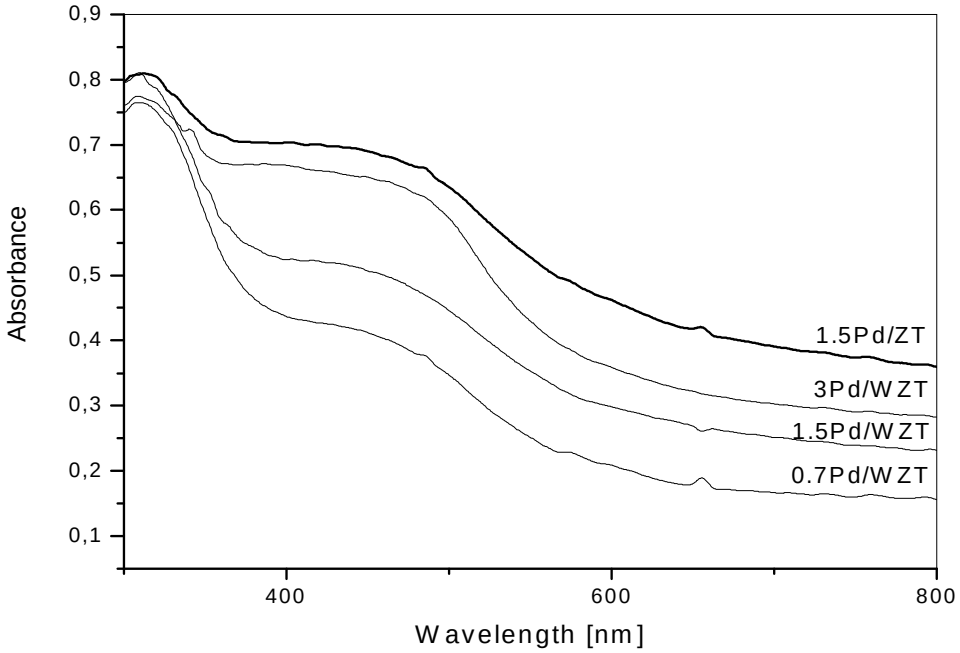

Figure 10. UV-vis diffuse reflectance spectra of the calcined Pd promoted samples.

3.1.4. Discussion of the Catalyst Structure

TiO_2-ZrO_2 mixed oxide (1:1 mol ratio based on oxides) was prepared by a homogenous coprecipitation of urea at 70°C. Formation of crystalline $ZrTiO_4$ compound at a calcination temperature of 600°C is observed. Based on the data of XRD and DR-UV-Vis spectra, very good mixing of oxides has been achieved with high surface area (118 m^2/g) and small crystallite size (4.4 nm). The mixed hydroxide was tungstated with ammonium metatungstate solution.

Tungstation shifts crystallization to higher temperatures. In addition to $ZrTiO_4$, $Zr(WO_4)_2$ and WO_3 phases are observed at high temperatures. 500^oC calcined samples have paratungstate-type polytungstate species forming intermediate WO_x surface densities which can give rise to strong Brønsted acidity. Pd containing samples were prepared by impregnation of ZT and WZT samples with $Pd(NO_3)_2.2H_2O$ solution. Isolated Pd^{2+} ions coordinated to surface oxygen atoms of support indicate the fact that tungstated titania-zirconia support can stabilize dispersed Pd(II) similar to the acidic zeolites. For the FT-IR spectroscopy experiments, 500^oC calcined samples were used since higher temperature calcination leads to formation of WO_3 crystallites which can block the active sites for the SCR-CH_4.

3.1.5. FTIR Spectra of the activated samples

Figure 11 shows the FT-IR spectra of the activated samples together with pure titania and zirconia for comparison. In the spectrum of ZrO_2 in the OH-stretching region (Figure 11B), there are two strong absorptions at 3775 and 3670 cm^{-1} and a broad band between 3600 and 3200 cm^{-1}. According to the literature [81], the band at 3775 cm^{-1} is assigned to terminal OH groups whereas the absorption at 3670 cm^{-1} is attributed to bridged OH groups of monoclinic zirconia. The broad band between 3600 and 3200 cm^{-1} is due to H-bonded tribridged hydroxyls.

The spectrum of TiO_2 displays a pair of bands at 3718 and 3671 cm^{-1} with weak intensity. These absorptions are characteristic of hydroxyl groups of anatase [82].

The spectrum of mixed oxide contains two sharp bands at 3775 and 3671 cm^{-1} corresponding to isolated hydroxyl groups. Population of hydrogen bonded hydroxyls in the 3600 – 2750 cm^{-1} region increases with respect to pure zirconia and titania. This fact indicates that mixed oxide could have higher Brønsted acidity with respect to the pure oxides.

The spectrum of 1.5Pd/ZT catalyst (Figure 11A) in the ν(OH) stretching region is different from that of ZT. The isolated and H-bonded hydroxyl groups disappear from the spectrum. This indicates that Pd^{2+} ions replace protons of the surface hydroxyls during the deposition process.

The spectrum of the WZT sample has sharp bands at 3745 and 3665 cm^{-1}, attributed to isolated OH groups [81]. The broad band between 3515 and 2500 cm^{-1} region indicates the presence of H-bonded hydroxyls. The single band at 2013 cm^{-1} is assigned to the first overtone vibration of fundamental ν(W=O) mode. The fundamental ν(W=O) stretching vibration should be at around 1010 cm^{-1}, however the self absorption of the catalyst makes it difficult to resolve this

band. The presence of single overtone band indicates that WZT sample contains one type of wolframyl groups of well-dispersed uniform WO_x species.

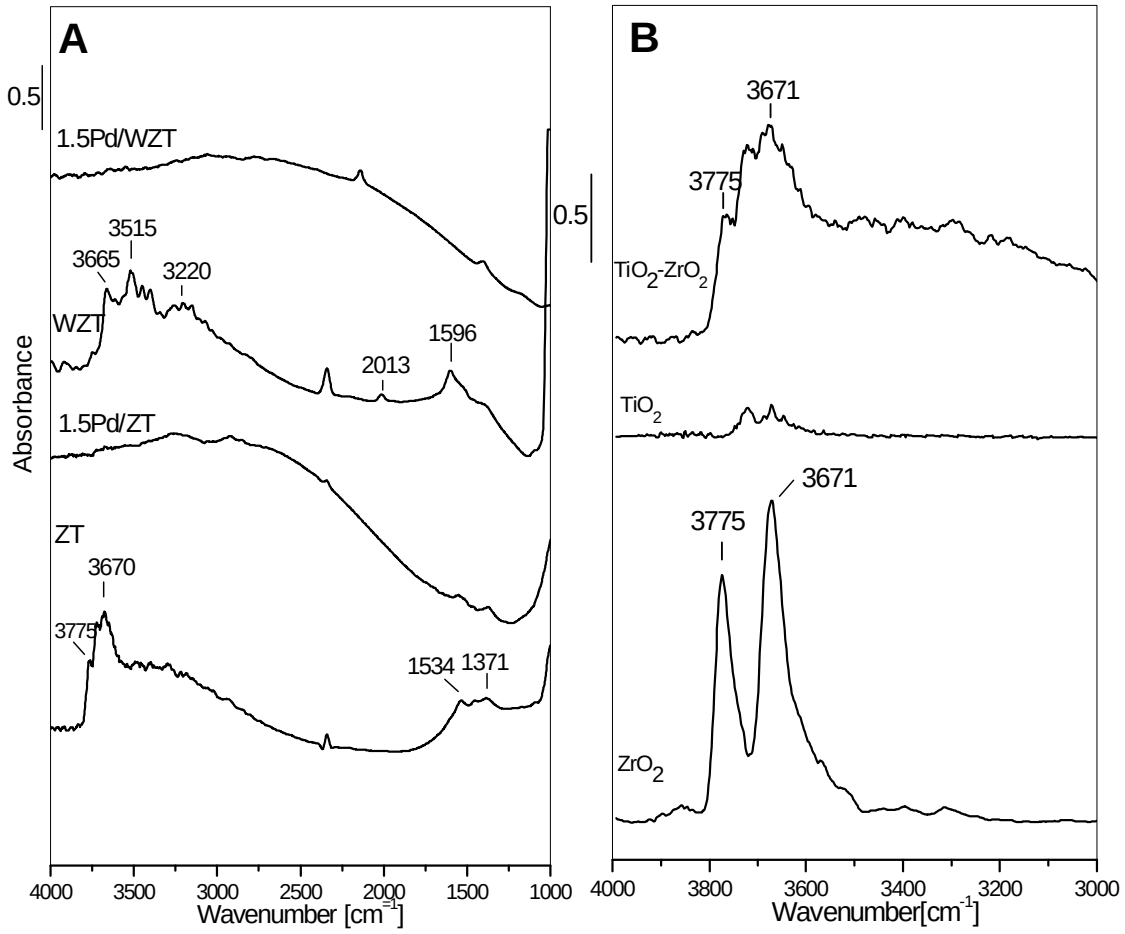

Figure 11. (A) FTIR spectra of activated samples of ZT, WZT and 1.5Pd/WZT in the 4000 -1000 cm^{-1}. (B) Spectra of ZT, TiO_2 and ZrO_2 in the OH-stretching region.

The spectrum of 1.5Pd/WZT catalyst is similar to the spectrum of 1.5Pd/ZT. Isolated hydroxyls are not observed. The overtone vibration of ν(W=O) disappears after the Pd deposition. This behaviour can be explained assuming that Pd^{2+} ions coordinate to the W=O species.

The absorptions at 1596, 1534 and 1371 cm^{-1} (Figure 11A) are due to surface carbonates. Such residual surface species are observed on zirconia and can not be removed by high temperature activation [74].

3.1.6. Adsorption of CO

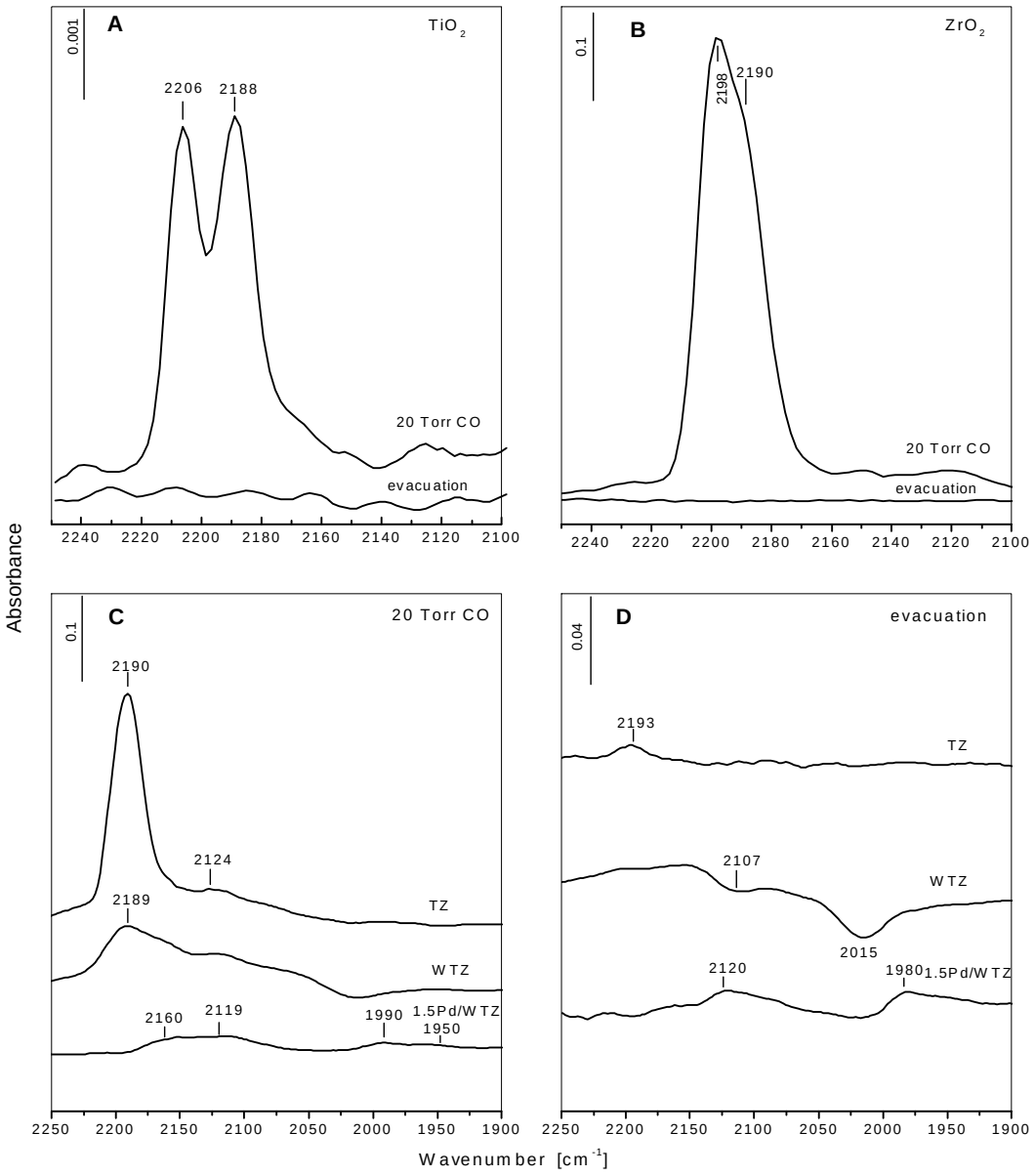

Figure 12. (A) FTIR spectra obtained upon adsorption of CO (20 Torr) for 30 min at room temperature on TiO_2, (B) on ZrO_2, (C) on ZT, WZT and 1.5Pd/WZT, (D) Spectra after evacuation for 30 min at room temperature. The spectrum of the activated sample is used as a background reference. Gas phases are subtracted from spectra.

Figure 12A and Figure 12B show the spectra of adsorbed CO on TiO_2 (anatase) and monoclinic ZrO_2. Two types of coordinatively unsaturated (cus) Ti^{4+} and Zr^{4+} ions are observed on each pure oxide: Ti^{4+}-CO carbonyls at 2206 and 2188 cm^{-1}; Zr^{4+}-CO carbonyls at 2198 and 2190 cm^{-1}. These bands disappear after evacuation of the gas phase at room temperature.

Figure 12C shows adsorption of CO (20 Torr) on activated catalysts and Figure 12D shows the spectra taken after evacuation for 30 minutes at room temperature. The adsorption of CO on the ZT sample at room temperature leads to formation of the band at 2190 cm^{-1}. This frequency is similar to that of Zr^{4+}-CO and Ti^{4+}-CO carbonyls. Since the Zr^{4+} and Ti^{4+} are randomly distributed in the octahedral-like PbO_2-type structure of $ZrTiO_4$, the band at 2190 cm^{-1} is attributed to both types of Zr^{4+}-CO and Ti^{4+}-CO carbonyls. A shoulder at 2124 cm^{-1} of the band at 2190 cm^{-1} (Figure 12C, spectrum ZT) is assigned to Ti^{3+}-CO. High temperature evacuation can reduce Ti^{4+} to Ti^{3+}.

Upon adsorption of CO on WZT sample, two bands at 2189 and 2124 cm^{-1} are observed with the same frequencies as the carbonyls on the ZT. Since CO does not form carbonyl complexes with cus W^{6+} ions [83], the bands at 2189 and 2124 cm^{-1} are attributed to Zr^{4+}/Ti^{4+}-CO and Ti^{3+}-CO carbonyls, respectively. The adsorption of CO causes perturbation of the W=O stretching vibration, that is evident by the negative band of overtone vibration at 2013 cm^{-1}.

The spectrum of CO adsorbed on the 1.5Pd/WZT sample (Figure 12C) indicates that the population of coordinatively unsaturated Ti^{4+}/Zr^{4+} ions decreases considerably after deposition of Pd. Since Pd(II) undergoes reduction by CO at room temperature [84], the bands at 2160 and 2119 cm^{-1} are attributed to Pd^{+}-CO carbonyls in two different environments. The absorption at 2160 cm^{-1} is attributed to CO adsorbed on Pd^{+} sites, which are coordinated to the electrophilic WO_x species. The weak band at 1990 and 1950 cm^{-1} which resist evacuation are assigned to bridged carbonyls adsorbed on Pd^{0} [85].

3.2. NO and NO/O_2 Adsorption

3.2.1. Adsorption of NO

Spectra of NO (10 Torr) adsorbed at room temperature on ZT, WZT, 1.5Pd/ZT and 1.5Pd/WTZ samples for a period of 25 min are shown in Figure 13A. The spectra taken after evacuation for 30 min for each sample are shown in Figure 13B.

In the spectrum of NO adsorbed on ZT, the intense band at 1190 cm^{-1} is assigned to the ν(NO) stretching mode of anionic nitrosyl, NO^- [74]. Ti^{4+} and Zr^{4+} ions are considered to be irreducible under these conditions so anionic nitrosyls are formed by disproportionation of NO on surface O^{2-} sites:

$$3NO + O^{2-} \rightarrow NO_2 + 2NO^- \quad (3)$$

The NO_2 can be adsorbed and it leads to formation of NO_3^- and NO_2^- species. The high frequency component of the ν_3 spectral splitting of bidentate nitrates is observed at 1610 cm^{-1} and its low frequency component is resolved at 1316 cm^{-1} [74]. The weak absorption at 1365 cm^{-1} is attributed to $\nu_{as}(NO_2)$ mode of bidentate nitrite species [72]. The $\nu_s(NO_2)$ mode is covered by the strong NO^- band. The bands at 1682 and 1243 cm^{-1} (which decrease in intensities during the evacuation) are assigned to the ν(N=O) and $\nu_{as}(NO_2)$ modes of bridged NO_3^- species, respectively [74]. The presence of adsorbed NO_x species perturbs the isolated OH groups at 3670 cm^{-1} and gives a positive adsorption on H-bonded hydroxyls (not shown).

The adsorption of NO (10 Torr) on the WZT sample at room temperature makes the spectrum in the 2300-1700 cm^{-1} region more complex than that of the ZT sample (Figure 13A). Assignment of the bands is made taking into account their stability upon evacuation at room temperature (Figure 13B). The broad absorption between 2200 and 2000 cm^{-1} is due to the ν(NO) mode of adsorbed NO^+ species [74, 86, 87]. Therefore, it can be assumed that NO_2 formed by reaction (3) disproportionates with involvement of W^{6+}=O species (negative band at 2014 cm^{-1}).

$$2NO_2 + W^{6+}=O^{2-} \rightarrow {}^-ONO_2\text{-}W^{6+}\text{-}O^{2-}\text{-}NO^+ \quad (4)$$

The small shoulder at 2243 cm^{-1} is assigned to ν(NN) stretching vibration of adsorbed N_2O [74]. Nitrate species formed are of bidentate (1615 and 1216 cm^{-1}) and monodentate type (1570, 1490 and 1300 cm^{-1}). The band at 1930 cm^{-1} is assigned to the mixed nitrato-nitrosyl complex ($ON\text{-}Zr^{4+}\text{-}NO_3^-$) [74]. Upon evacuation the nitrosyl species disappear and the amount of surface nitrates increases.

The spectrum of NO adsorbed on 1.5Pd/ZT displays two bands at 1845 and 1803 cm^{-1} (Figure 13A). They are assigned to NO adsorbed on Pd(II) sites in two different environments. The strong absorption at 1190 cm^{-1}, as in the case of the ZT sample, is assigned to the ν(NO) stretching mode of anionic nitrosyl, NO^- (see reaction (3)). The nitrate species formed are of bidentate (1578 and 1305 cm^{-1}) and monodentate type (1490 and 1305 cm^{-1}). Upon evacuation, most probably the monodentate nitrates transform to bidentates which causes increase in the intensity of the band at 1578 cm^{-1}.

The spectrum of NO adsorbed on 1.5Pd/WZT catalyst at room temperature displays the bands at 1866 and 1819 cm^{-1} which are due to NO adsorbed on two different Pd(II) sites. The

bands between 1690-1200 cm^{-1} correspond to bridged (1672, 1250 cm^{-1}), monodentate (1559, 1320 cm^{-1}) and bidentate nitrates (1620, ~1240).

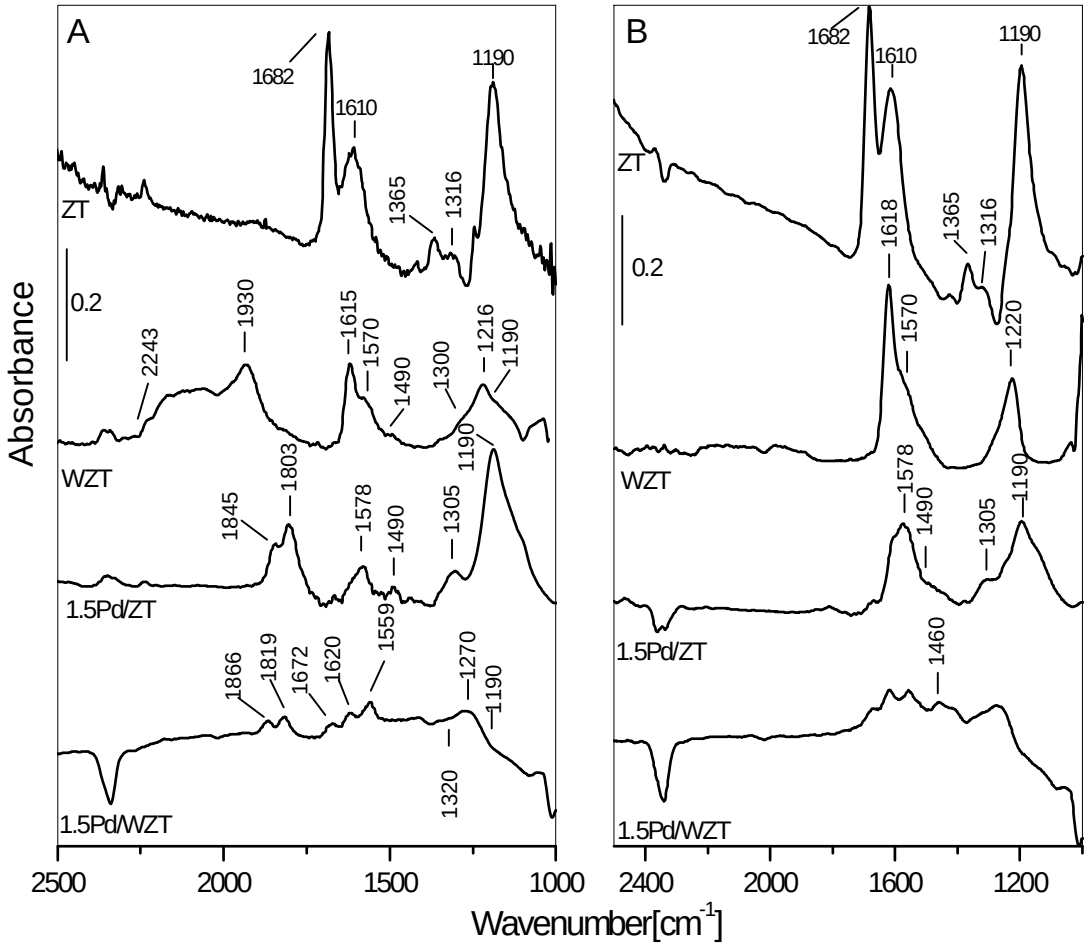

Figure 13. (A) FTIR spectra of NO (10 Torr) adsorbed on ZT, WZT, 1.5Pd/ZT and 1.5Pd/WZT samples at room temperature for 25 min. (B) After evacuation for 30 min at room temperature. The spectrum of the activated sample is used as background reference. Gas phases are subtracted from spectra.

The N_2O band at 2243 cm^{-1} observed in the case of WZT 1.5Pd/ZT and 1.5Pd/WZT samples can form by adsorption of NO on oxygen vacancies [74].

Table 8 summarizes the assignments of the IR bands of the NO_x compounds obtained during the adsorption of NO at room temperature.

Table 8 . Assignments of the FTIR bands observed upon room-temperature adsorption of NO on the samples studied

Sample	NO_x Species	Band Position (cm^{-1})	Mode
ZT	NO_3^- (bidentate nitrate)	1610, 1316	ν(N=O), $\nu_{as}(NO_2)$
	NO^-	1190	ν(NO)
	NO_3^-(bridged nitrate)	1682, 1243	ν(N=O), $\nu_{as}(NO_2)$
	NO_2^-(bidentate nitrite)	1368	ν(N=O)
WZT	N_2O (ads.)	2243	ν(NN)
	NO^+	2200-2000	ν(NO)
	NO_3^- (bidentate nitrate)	1615, 1216	ν_{as}(N=O), ν_s(N=O)
	NO_3^-(monodentate nitrate)	1570-1490, 1300	ν_{as}(N=O), ν_s(N=O)
	ON-Zr^{4+}-NO_3^-	1930	ν(NO)
	NO^-	1190	ν(NO)
1.5Pd/ZT	Pd^{2+}-NO (two types)	1845, 1803	ν(NO)
	NO_3^- (bidentate nitrate)	1578, 1305	ν_{as}(N=O), ν_s(N=O)
	NO_3^- (monodentate nitrate)	1490, 1305	ν_{as}(N=O), ν_s(N=O)
	NO^-	1190	ν(NO)
1.5Pd/WZT	NO^+	2186	ν(NO)
	Pd^{2+}-NO (two types)	1866, 1819	ν(NO)
	N_2O_4(g)	1746, 1264	ν_{as}(NO), ν_s(NO)
	N_2O(g)	2224, 1292	ν(NN), ν(NO)
	NO_3^- (monodentate nitrate)	1559, 1320	ν_{as}(N=O), ν_s(N=O)
	NO_3^- (bridged nitrates)	1672, ~1250	ν(N=O), $\nu_{as}(NO_2)$
	NO_3^- (bidentate nitrates)	1620, ~1240	ν_{as}(N=O), ν_s(N=O)
	NO_2^- (monodentate nitrite)	1460	ν(N=O)
	NO^-	1190	ν(NO)

3.2.2. Coadsorption of NO/O_2

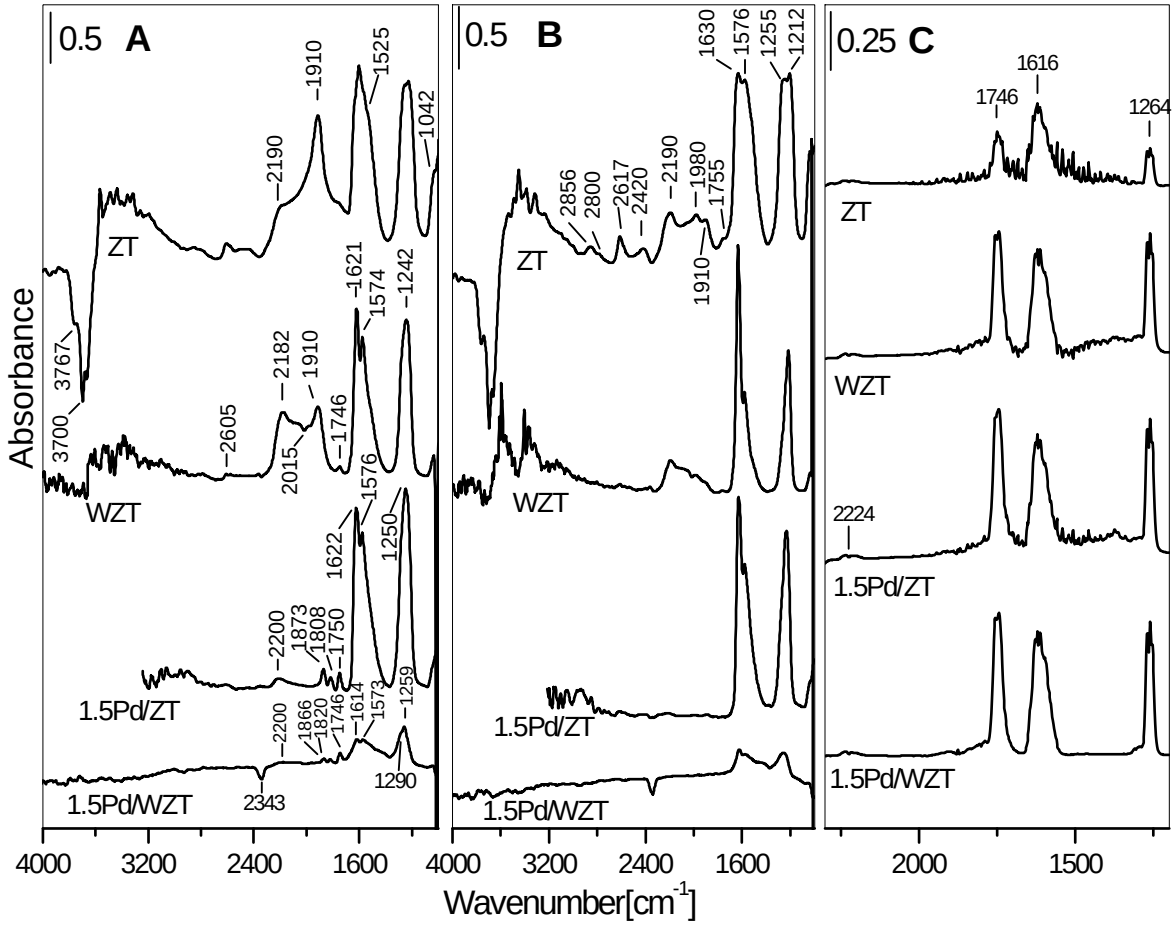

Figure 14. (A) FTIR spectra of NO (10 Torr) adsorbed on ZT, WZT, 1.5Pd/ZT and 1.5Pd/WZT samples at room temperature for 25 min. (B) After evacuation for 30 min at room temperature. (C) Gas phase spectrum of the corresponding spectrum shown on panel A. The spectrum of the activated sample is used as background reference. Gas phases are subtracted from spectra.

Spectra of NO (10 Torr) + O_2 (6 Torr) adsorbed at room temperature on ZT, WZT, 1.5Pd/ZT and 1.5Pd/WTZ samples for a period of 25 min are shown in Figure 14A. The spectra taken after evacuation for 30 min for each sample are shown in Figure 14B. Gas phases spectra taken after addition of NO + O_2 are shown in Figure 14C.

In the gas phase spectrum taken after NO + O_2 adsorption on ZT, formation of NO_2 ($\nu_{as}(NO_2)$ at 1616 cm^{-1}) and N_2O_4 ($\nu_{as}(NO)$ at 1746 cm^{-1} and $\nu_s(NO)$ at 1264 cm^{-1}) is observed.

This causes a significant change in the spectrum of preadsorbed NO. The adsorbed NO^- species (1190 cm^{-1}) disappear and intense bands in the 1700 – 1150 cm^{-1} region appear corresponding to various surface nitrates. Upon evacuation at room temperature, the strong band with a maximum at 1600 cm^{-1} is resolved into two maxima at 1630 and 1576 cm^{-1}. These bands correspond to the ν_3 spectral splitting of surface nitrates [74] : 1630 [ν(N=O)] and 1212 cm^{-1} [ν_{as}(N=O)] and 1576 [ν(N=O)] and 1255 cm^{-1} [ν_{as}(N=O)]. In the spectrum taken after evacuation, weak bands at 2856, 2800, 2617, 2420, 1980, 1910 and 1755 cm^{-1} are detected. These bands are due to combinations of the bands in the fundamental nitrate region and can be used for structural identification [74]. The bands at 2856 and 2800 cm^{-1} and the pair of bands at 1980 and 1910 cm^{-1} reveal the presence of two types of bridged NO_3^- species. The bands at 2617, 2420 and 1755 cm^{-1} belong to bidentate nitrates. The nitrate species give rise to overlapping bands in the fundamental region, which cannot be resolved. However, based on the spectra in the combination region, the bands at 1630 and 1255 cm^{-1} are attributed to bridged nitrates, whereas the bands at 1576 and 1212 cm^{-1} correspond to bidentate nitrates. The ν(N=O) stretching vibration of a second type of bridged nitrate should be positioned at around 1590 cm^{-1} and is not resolved. The shoulder at 1525 cm^{-1} is assigned to the $\nu_{as}(NO_2)$ mode of monodentate nitrates. The latter species do not produce combination bands [74]. The band at 1042 cm^{-1} is due to the $\nu_{as}(NO_2)$ mode of the bidentate and bridged nitrates.

The broad absorption at 2190 cm^{-1}, which looses intensity and is better resolved after evacuation, is attributed to the ν(NO) stretching frequency of adsorbed nitrosonium ion. This indicates that the nitrate species are produced by self-ionization of NO_2/N_2O_4:

$$2NO_2\,(N_2O_4) \rightarrow NO_3^- + NO^+ \qquad (5)$$

In the OH region, the negative bands at 3767 and 3700 cm^{-1} are due to altered terminal groups, which results in appearance of a positive absorption in the 3600 – 3000 cm^{-1} region of hydrogen bonded hydroxyls. These results imply that the surface nitrates can also be formed by disproportionation of NO_2/N_2O_4 with involvement of surface hydroxyls [74, 86, 87]:

$$2OH^- + 3NO_2\,(1.5N_2O_4) \rightarrow 2NO_3^- + NO + H_2O \qquad (6)$$

The sharp band at 1910 cm^{-1}, which disappears upon evacuation is associated with adsorbed N_2O_3. The latter species form usually in mixtures of NO and NO_2 [74]. The residual bands at 1980 and 1910 cm^{-1} observed in the spectrum of ZT after evacuation, (Figure 14B), as explained above, are due to combination band of the bridged nitrate species.

As in the case of the ZT sample, the gas phase spectrum of WZT taken after NO + O_2 adsorption (Figure 14C, spectrum WZT) shows the presence of NO_2 (ν_{as}(NO) at 1620 cm^{-1}) and N_2O_4 (ν_{as}(NO) at 1746 cm^{-1}) due to oxidation of NO and weak absorption at 2224 cm^{-1} belonging

to the ν(NN) mode of N_2O. The weak band at 1746 cm^{-1} (Figure 14A, spectrum WZT) which disappears after evacuation is due to adsorbed N_2O_4. The strong band at 2182 cm^{-1}, which decreases in intensity after the evacuation, is typical of NO^+ species. Adsorbed N_2O_3 gives rise to sharp band at 1910 cm^{-1} which disappears after evacuation (Figure 14B).

The bands at 1621 and 1242 cm^{-1} which resist evacuation, are assigned to ν(N=O) and $\nu_{as}(NO_2)$ modes of bridged nitrates, respectively, whereas the band at 1574 cm^{-1} which decrease in intensity after evacuation, is attributed to monodentate nitrates. Nitrate species can form by self-ionization (reaction 5) and disproportionation (reaction 6) of NO_2/N_2O_4 species. Appearance of positive absorption in the region of hydrogen bonded hydroxyls (3600-3000 cm^{-1}) supports disproportionation process. The weak absorptions at 2800 and 2605 cm^{-1} (Figure 14A, spectrum WZT) are attributed to combination modes of the fundamental nitrate bands.

Promotion of the ZT sample with Pd^{2+} leads to decrease of the amount of the adsorbed NO_3^- species, which is evident from more simple envelop of the bands in the nitrate region (Figure 14A, spectrum 1.5Pd/ZT). The absorption in the 3200-4000 cm^{-1} region is very strong and this region is excluded from the spectra. The gas phase spectra (Figure 14B, spectra ZT and 1.5Pd/ZT) show different equilibrium concentrations of NO_2 and N_2O_4. This difference could be associated with the reduced ability of the 1.Pd/ZT sample to form surface nitrates as a consequence of elimination of active sites for NO_2/N_2O_4 disproportionation after the introduction of Pd. The bands at 1873 and 1808 cm^{-1} correspond to ν(NO) stretching vibrations of two types of Pd^{2+}-NO nitrosyls. Two types of nitrates have been detected with ν_3 spectral splitting at 1622 [ν(N=O)] and 1250 cm^{-1} [ν_{as}(N=O)] and 1576 [ν(N=O)] and 1250 cm^{-1} [ν_{as}(N=O)]. The $\nu_s(NO_2)$ stretching vibrations are at 1043 cm^{-1}. The broad band with a maximum at 2200 cm^{-1} (Figure 14A, spectrum 1.5Pd/ZT) indicates the formation of adsorbed nitrosonium ion.

The spectrum of adsorbed NO/O_2 on 1.5Pd/WZT catalyst indicates the formation of nitrate species which are identified as monodentate (1573 and 1290 cm^{-1}) and bidentate (1614 and 1573 cm^{-1}). (Figure 14A, spectrum 1.5Pd/WZT). The amount of the adsorbed NO_x species is considerably lower with respect to the WZT sample. As in the case of 1.5Pd/ZT sample, there are two types of Pd^{2+}-NO nitrosyls which display the ν(NO) modes at 1866 and 1820 cm^{-1}, respectively. They disappear from spectrum upon evacuation for 30 min at room temperature (Figure 14B, spectrum 1.5Pd/WZT). The negative band at 2015 cm^{-1} indicates the perturbation of W=O species as in the case of NO adsorption. The amount of gaseous NO_x species formed in the presence of the 1.5Pd/WZT catalyst is comparable to that in the case of the WZT and 1.5Pd/ZT samples.

Table 9 summarizes the assignments of the IR bands of the NO + O_2 compounds obtained during the adsorption of NO at room temperature.

Table 9 . Assignments of the FTIR bands observed upon room-temperature coadsorption of NO and O_2 on the samples studied.

Sample	NO_x Species	Band Position (cm^{-1})	Mode
ZT	NO_2(g)	1616	$\nu_{as}(NO_2)$
	N_2O_4(g)	1746, 1264	$\nu_{as}(NO)$, $\nu_s(NO)$
	NO_3^- (bidentate nitrate)	1576,1212,1042	$\nu(N=O)$,$\nu_{as}(NO_2)$, $\nu_s(NO_2)$
	NO_3^- (bidentate nitrate)	2617	$\nu(N=O) + \nu_s(NO_2)$
	NO_3^- (bidentate nitrate)	2420	$2\ \nu_{as}(NO_2)$
	NO_3^- (bidentate nitrate)	1755	$\nu_s(NO_2) + \delta(ONO)$
	NO_3^- (bridged nitrate)	1630,1255,1042	$\nu(N=O)$,$\nu_{as}(NO_2)$,$\nu_s(NO_2)$
	Second type NO_3^- (bridged nitrate)	1590, 1042	$\nu(N=O)$, $\nu_s(NO_2)$
	NO_3^- (bridged nitrate) two types	2856, 2800	$\nu(N=O) + \nu_{as}(NO_2)$
	NO_3^- (bridged nitrate) two types	1980, 1910	$\nu_s(NO_2) + \delta(ONO)$
	NO_3^- (monodentate nitrate)	1525	$\nu_{as}(N=O)$
	NO^+	2190	$\nu(NO)$
	N_2O_3	1910	$\nu(N=O)$
WZT	N_2O (g)	2224	$\nu(NN)$
	NO^+	2182	$\nu(NO)$
	N_2O_4(ads.)	1746	$\nu_{as}(NO)$,
	NO_2(g)	1616	$\nu_{as}(NO_2)$
	NO_3^- (monodentate nitrate)	1574, 1280	$\nu_{as}(N=O)$, $\nu_s(N=O)$
	NO_3^-(bridged nitrate)	1621, 1242	$\nu(N=O)$, $\nu_{as}(NO_2)$
	N_2O_3	1910	$\nu(N=O)$
1.5Pd/ZT	NO^+	2200	$\nu(NO)$
	Pd^{2+}-NO (two types)	1873, 1808	$\nu(NO)$
	NO_3^- (bidentate nitrate) (two types)	1622,1250,1043	$\nu_{as}(N=O)$,$\nu_s(N=O)$,$\nu_s(NO_2)$
		1576,1250,1002	$\nu_{as}(N=O)$,$\nu_s(N=O)$,$\nu_s(NO_2)$
1.5Pd/ZT	NO_2(g)	1616	$\nu_{as}(NO_2)$
	N_2O_4(g)	1746, 1264	$\nu_{as}(NO)$, $\nu_s(NO)$
	N_2O_4(ads)	1746	$\nu_{as}(NO)$
	N_2O(g)	2224	$\nu(NN)$

	NO^+	2200	ν(NO)
	Pd^{2+}-NO (two types)	1866, 1820	ν(NO)
	NO_2(g)	1616	$\nu_{as}(NO_2)$
	N_2O_4(g)	1746, 1264	$\nu_{as}(NO)$, $\nu_s(NO)$
	N_2O_4(ads)	1746	$\nu_{as}(NO)$
1.5Pd/WZT	N_2O(g)	2224, 1292	ν(NN), ν(NO)
	NO_3^- (monodentate nitrate)	1573, 1290	$\nu_{as}(N=O)$, $\nu_s(NO_2)$
	NO_3^- (bidentate nitrates) two types	1614,1259,1043	$\nu_{as}(N=O),\nu_s(N=O),\nu_s(NO_2)$

3.2.3. Summary of the Results on NO and NO/O_2 Adsorption on the Samples Studied

The adsorption of NO at room temperature on the samples studied involves process of disproportionation of NO on surface oxide ions leading to formation of adsorbed anionic nitrosyl, NO^-, and NO_2. The latter also disproportionates giving rise to different kind of surface nitrates. The amount of the adsorbed species varies depending on the composition of the materials, being the smallest in the case of the 1.5Pd/WZT catalyst. Despite of the same palladium content, the intensities of the Pd^{2+}-NO bands is lower on the 1.5Pd/WZT than those on the 1.5Pd/ZT sample. This difference can be explained assuming that, as a result of coordination of the palladium ions to the tungstated species, the amount of coordinatively unsaturated Pd^{2+} sites on the former catalyst has decreased. In addition, the adjacent WO_x species increase the Lewis acidity of the Pd^{2+} ions, which is evident by the higher ν(NO) stretching frequencies of the nitrosyl bands on the tungsten-containing catalyst than those on the tungsten-free sample.

The addition of oxygen to the gaseous NO causes its oxidation to NO_2/N_2O_4. These gases adsorb molecularly on the surface of the samples or undergo self-ionization and disproportionation with the participation of surface hydroxyl groups. The amounts of NO_2 and N_2O_4 in the gas phase reflect the adsorption capacity of the samples. Introduction of WO_x species and Pd^{2+} ions to the zirconia-titania mixed oxide hinders the processes of NO_2/N_2O_4 self-ionization and disproportionation by elimination of the necessary active sites.

3.3. Reactivity of the adsorbed NO_x species toward methane

In order to evaluate the ability of the catalysts containing preadsorbed NO_x species for methane activation, the following experiments were performed:

1. "Blank NO_x" in which the thermal transformation of adsorbed NO_x species is investigated by heating the closed system at various temperatures.
2. "Blank CH_4" experiment involving interaction of the activated catalysts with methane at elevated temperatures.
4. "$NO_x - CH_4$" experiment consisting of interaction of the methane with the catalysts containing preadsorbed NO_x species at various temperatures.

The ability of the catalysts to activate the methane is evaluated by measuring the temperature dependence of consumption of adsorbed NO_x species in the presence of hydrocarbon. In the absence of an interaction between the NO_x species and methane, the surface concentration of the NO_x species detected after cooling to room temperature should be comparable to that obtained in the "blank NO_x experiment".

3.3.1. Blank NO_x Experiment

3.3.1.1. WZT Sample

The preadsorbed NO_x species were obtained by keeping the sample in contact with NO/O_2 gas mixture (10 Torr NO : 6 Torr O_2) for 30 min followed by evacuation for 30 min at room temperature (Figure 15A, spectrum a). Heating the closed IR cell for 15 minutes at 250^{o}C (Figure 15A, spectrum b) results in decrease of the intensities of the bands at 1632-1575 and 1215 cm^{-1} due to bidentate nitrate species. The weak bands at 1440 and 1100 cm^{-1} reveal the formation of monodentate nitrite species at 250^{o}C. Heating at 450^{o}C for 15 minutes (spectrum f) causes complete removal of the adsorbed NO_x species. Gas phase spectra taken at each temperature (Figure 15B, spectrum b-f) contain NO_2 as a decomposition product. After cooling to room temperature (spectrum g) bands due to readsorbed nitrates at 1613, 1498 and 1218 cm^{-1} are detected. Negative absorption at 2014 cm^{-1} due to the overtone of the ν(W=O) modes shows perturbation of the tungstate species.

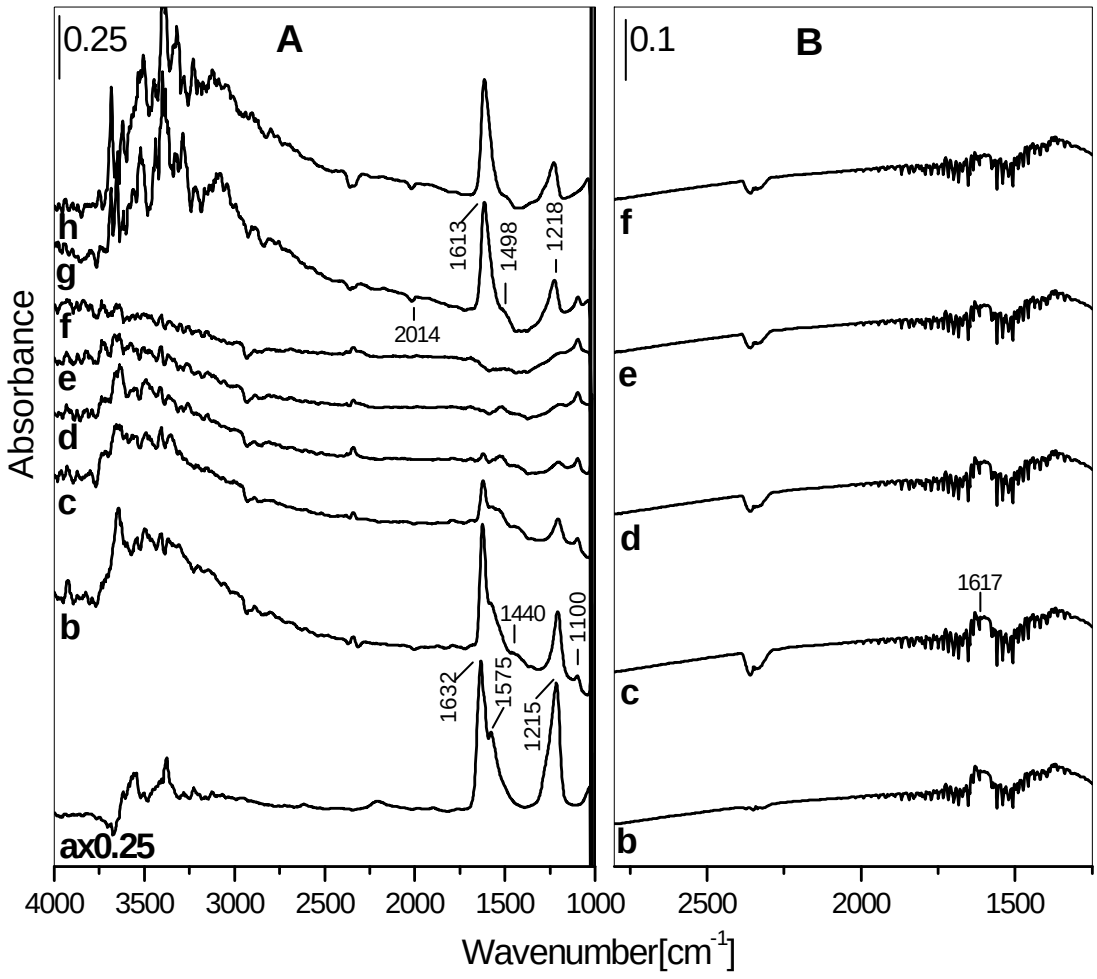

Figure 15. (A) FTIR spectra of WZT sample taken after adsorption of NO/O_2 mixture (10 Torr NO + 6 Torr O_2) at room temperature followed by evacuation for 30 min (a), after heating the closed IR cell for 15 min at 250°C (b), at 300°C (c), at 350°C (d), at 400°C (e), at 450°C (f), then cooling to room temperature (g) and evacuation at room temperature for 30 min (h). The spectrum of the activated sample is used as background reference. Gas phases are subtracted from spectra. Spectra a is divided by 4 to display the bands with small intensity in the frame. (B) Gas phase spectrum of the corresponding spectrum shown on panel A.

3.3.1.2 1.5Pd/ZT Sample

Heating the closed IR cell for 15 minutes in the 200-450^{o}C (Figure 16A, spectrum b-g) results in gradual decrease of the bands at 1627-1578, 1230 and 1040-1000 cm^{-1} due to the nitrate species. The new bands at 1438 and 1088 cm^{-1} detected at 200^{o}C and 300^{o}C, respectively, indicate the formation of nitrito species. The weak bands in the 1650-1000 cm^{-1} region detected at 450^{o}C indicate that some amount of adsorbed nitrato-nitrito species is still present. When the cell is cooled to room temperature (Figure 16A, spectrum h), the decomposition products of NO_x are readsorbed to generate nitrato-nitrito species and NO adsorbed on palladium sites (broad absorption at 1820-1700 cm^{-1} in spectrum h). The weak bands at 1776 and 1732 cm^{-1} detected after room temperature evacuation (spectrum i) correspond to NO adsorbed on Pd^{o} [88]. These results indicate that during the decomposition of the nitrate species at high temperatures, NO is formed. The latter is oxidized by the Pd^{2+} ions to NO_2, which readsorbs at room temperature giving rise mainly to nitrate species. Due to the low partial pressures of the NO and NO_2, they were not detected in the gas phase spectrum.

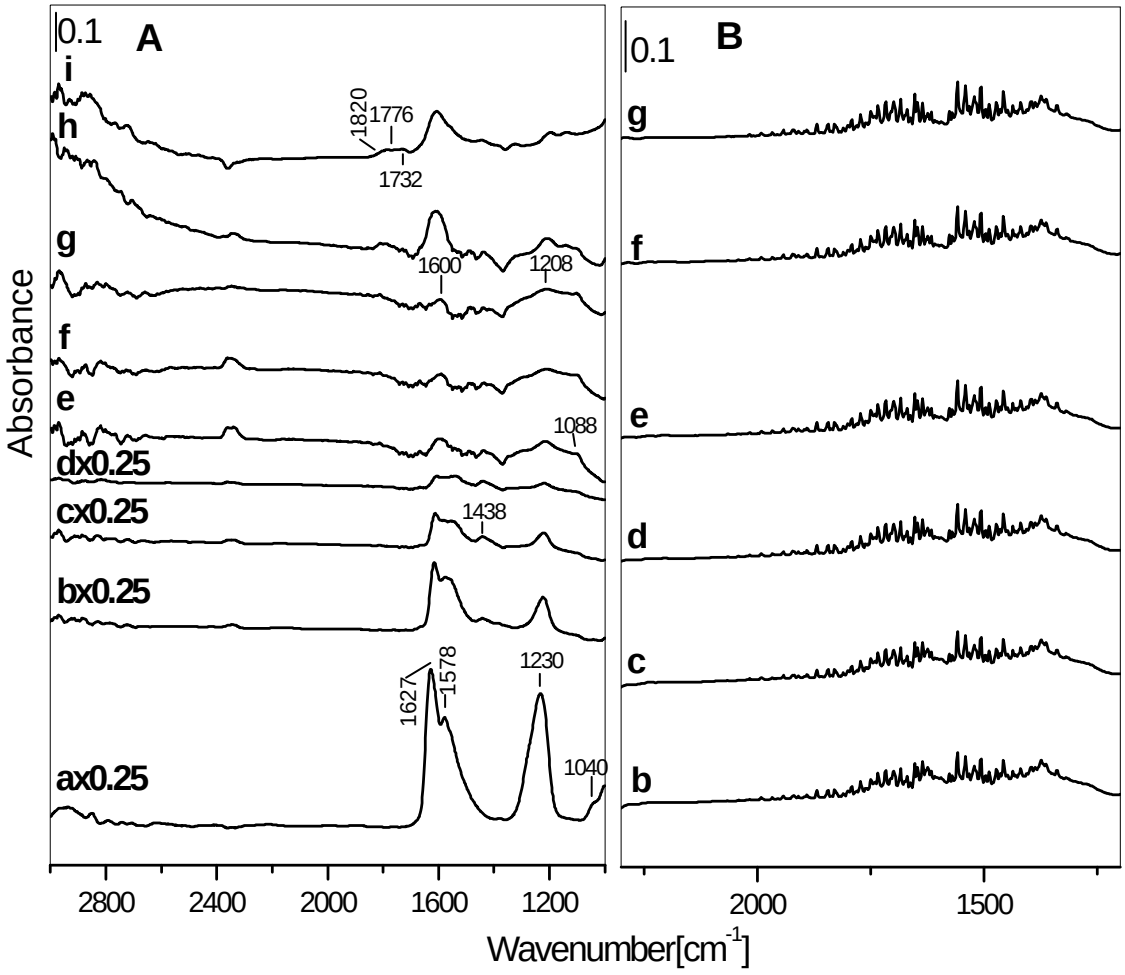

Figure 16. (A) FTIR spectra of 1.5Pd/ZT sample taken after adsorption of NO/O_2 mixture (10 Torr NO + 6 Torr O_2) at room temperature followed by evacuation for 30 min (a), after heating the closed IR cell for 15 min at 200°C (b), at 250°C (c), at 300°C (d), at 350°C (e), at 400°C (f), at 450°C (g), then cooling to room temperature (h) and evacuation at room temperature for 30 min (i). The spectrum of the activated sample is used as background reference. Gas phases are subtracted from spectra. Spectra a,b,c and d are divided by 4 to display the bands with small intensity in the frame. (B) Gas phase spectrum of the corresponding spectrum shown on panel A.

3.3.1.3 1.5Pd/WZT Sample

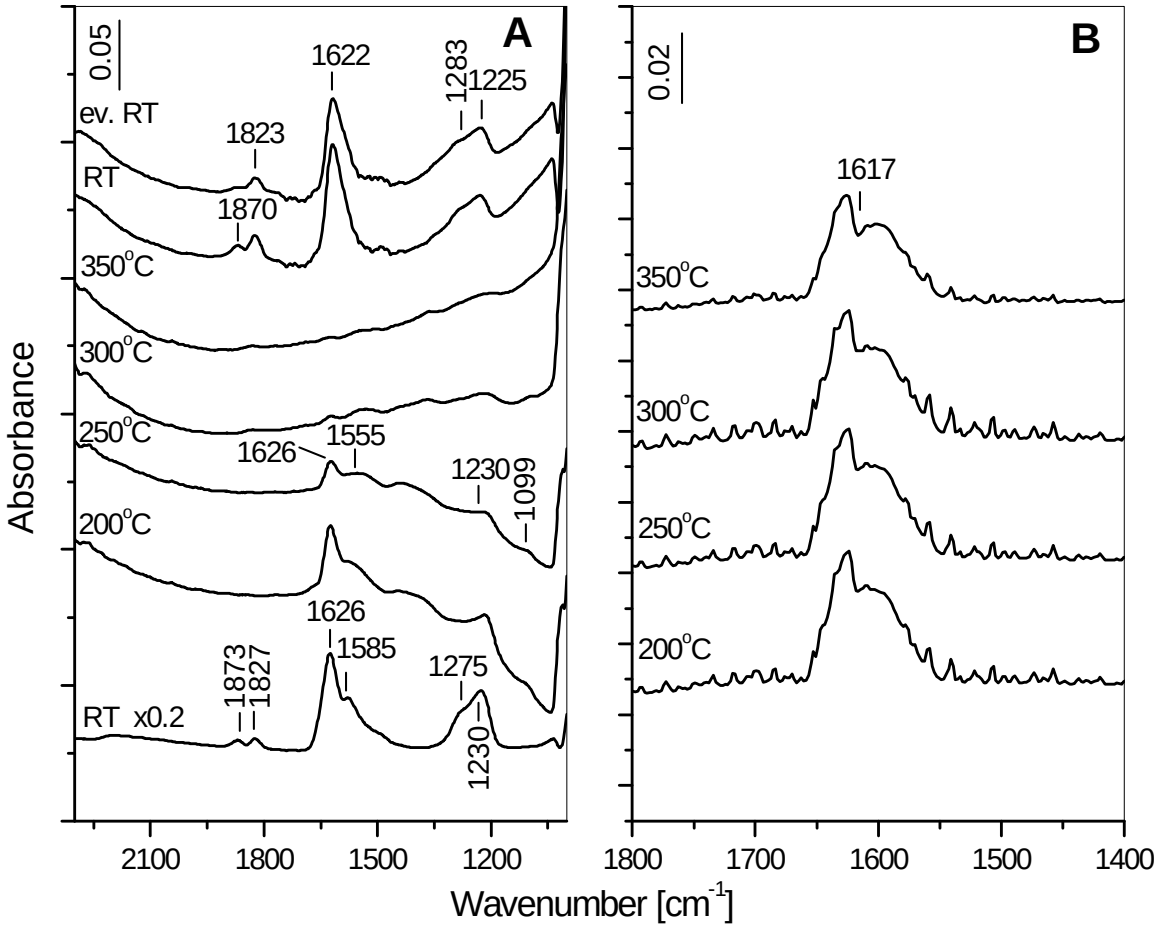

Figure 17. (A) FTIR spectra of 1.5Pd/ZT sample taken after adsorption of NO/O_2 mixture (10 Torr NO + 6 Torr O_2) at room temperature followed by evacuation for 30 min, after heating the closed IR cell for 15 min at 200°C-350°C then cooling to room temperature and evacuation at room temperature. The spectrum of the activated sample is used as background reference. Gas phases are subtracted from spectra. Room temperature spectrum is divided by 5 to display the bands with small intensity in the frame. (B) Gas phase spectrum of the corresponding spectrum shown on panel A.

The results of heating the activated 1.5Pd/WZT sample under NO/O_2 atmosphere are shown in Figure 17. At 200°C, the Pd^{2+}–NO nitrosyls disappear and the amount of the adsorbed nitrate species (1626, 1585, 1275 and 1230 cm^{-1}) decreases significantly. This is accompanied by

appearance of a broad absorption in the 1500 – 1300 cm^{-1} region and weak band at 1099 cm^{-1}. These bands are characteristic of monodentate nitrito (NO_2^-) species [72]. The gas phase spectrum shows formation of NO_2, which is present in the 200 – 450^oC temperature range (the spectra above 350^oC are not shown). This indicates that transformation to nitrite species and decomposition of the nitrates has occurred. The increase in the temperature causes gradual decrease in the intensity of the absorption bands and at 350^oC the nitrate and nitrite species leave the surface. The spectrum taken after cooling to room temperature is identical to the starting one although the intensities of the absorption bands are lower.

3.3.2. Blank CH_4 Experiment

3.3.2.1. 1.5Pd/ZT Sample

Figure 18 shows the FTIR spectra of 1.5Pd/ZT catalyst taken after addition of methane and heating the closed IR cell at various temperatures and cooling to room temperature followed by evacuation for 30 min. The spectra in the OH stretching region are of poor quality and not shown. The weak band at 1300 cm^{-1} present in all of the spectra shown is due to the methane in the gas phase. Heating the closed IR cell at 200^oC leads to appearance of absorption in the carbonate region (spectrum a). The band at 1617 cm^{-1} can be due to both bending mode of adsorbed water and $\nu_{as}(CO_2)$ vibration of hydrogen carbonate, [δ(OH) at 1219 cm^{-1}]. The bands at 1540 and 1452 cm^{-1} are due to bidentate and monodentate carbonates, respectively. The weak band at 1891 cm^{-1} detected at 250^oC is attributed to tribridging CO adsorbed on metallic palladium [84]. This indicates that Pd(II) undergoes reduction. The adsorbed water and hydrogen carbonate disappear from the spectrum taken at 350^oC and the carbonate species decompose after the heating at 450^oC. In the spectrum obtained after cooling to room temperature (spectrum g), the bands corresponding to the species already described are detected with increased intensities. The bands at 2083 and 1970 cm^{-1} correspond to linear Pd^+-CO and bridging Pd^0-CO species [85].

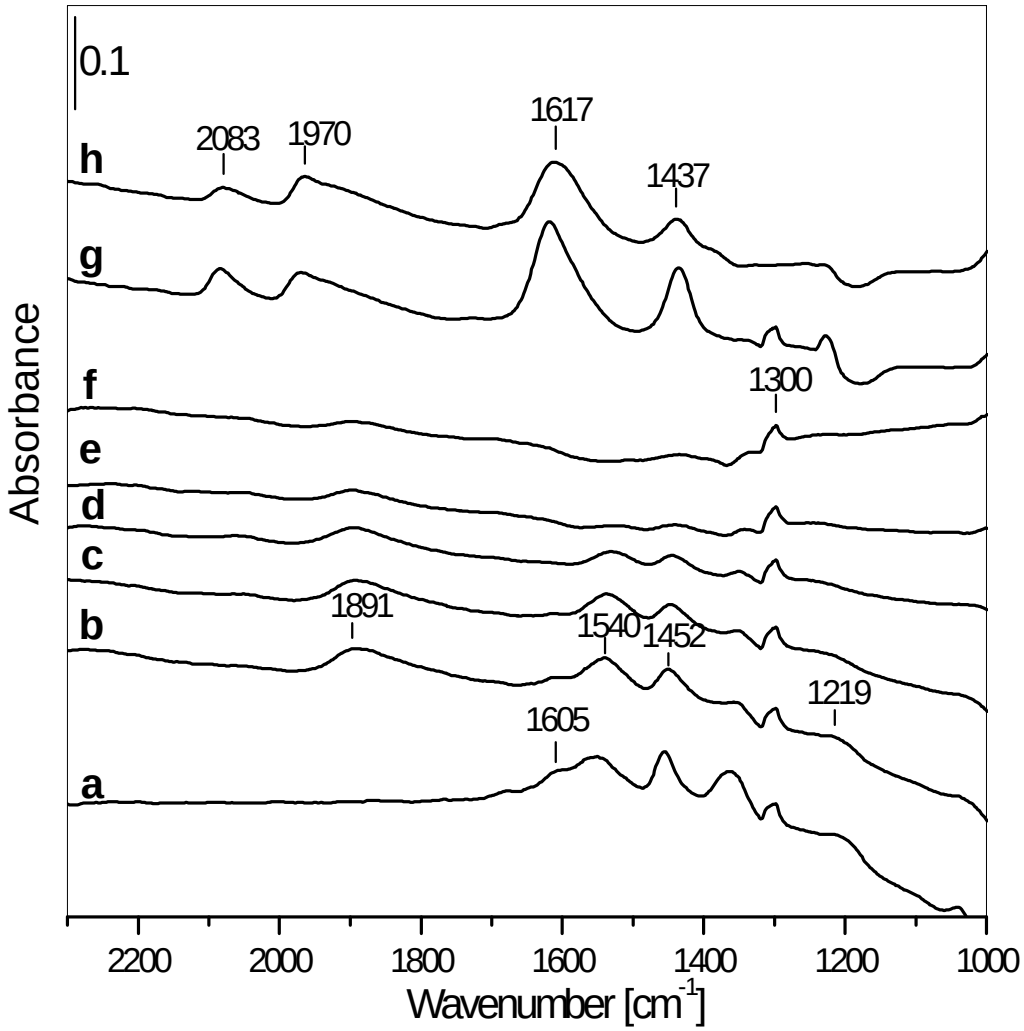

Figure 18. FTIR spectra of 1.5Pd/ZT sample taken after addition of methane (40 Torr) at room temperature and after heating the closed IR cell for 15 min at 200°C (a), at 250°C (b), at 300°C (c), 350°C (d), 400°C (e), 450°C (f) then cooling to room temperature (g), and evacuation at room temperature for 30 min (h). The spectrum of the activated sample is used as background reference.

3.3.2.2. WZT and 1.5Pd/WZT Samples

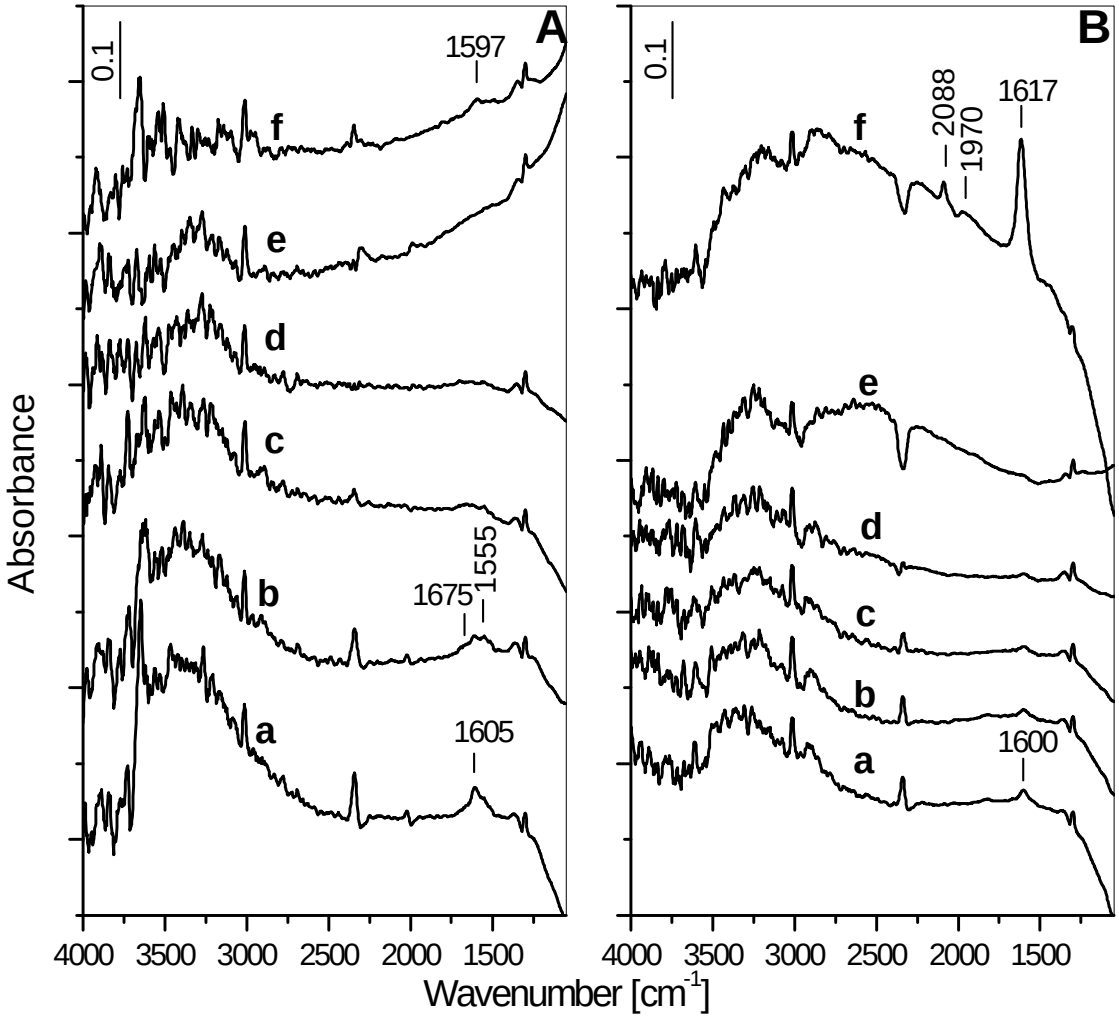

Figure 19. (A) FTIR spectra of WZT and (B) 1.5Pd/WZT samples taken after addition of methane (40 Torr) at room temperature and after heating the closed IR cell for 15 min at 200°C (a), at 250°C (b), at 300°C (c), 350°C (d), 400°C (e) then cooling to room temperature (f). The spectrum of the activated sample is used as background reference.

The spectra obtained during the interaction of the methane with the WZT and 1.5Pd/WZT samples at temperatures ranging from 200 to 400°C are shown in Figure 19. The positive absorption in the OH stretching region and the weak band at 1600 – 1605 cm^{-1} due to adsorbed water indicate that both samples are able to oxidize the hydrocarbon already at 200°C. Some amount of adsorbed carbonate species (weak bands at 1675 and 1555 cm^{-1}) are detected on the

WZT sample, which desorb from the surface at 300 – 350°C. Judging from the intensities of the water bands detected after cooling to room temperature, it seems that the oxidation of methane occurs in larger extent on the palladium-containing sample. As in the case of the 1.5Pd/WZT catalyst, the bands at 2083 and 1970 cm^{-1} correspond to linear Pd^{+}-CO and bridged Pd^{0}-CO species [85].

Figure 20 compares the spectra of WZT, 1.5Pd/ZT and 1.5Pd/WZT taken from blank CH_4 experiment after cooling of the closed IR cell to room temperature. The carbonate species prevail on the 1.5Pd/ZT sample. This can be associated with both large extent of CH_4 oxidation and formation of stable carbonate species on the surface of the basic 1.5Pd/ZT oxide. Some oxidation of CH_4 takes place also on the WZT sample. The activity of the 1.5Pd/WZT catalyst seems to be lower than that of the WO_x – free sample. This could be associated with the dispersion of the Pd^{2+} ions, being better in the case of the tungstated support.

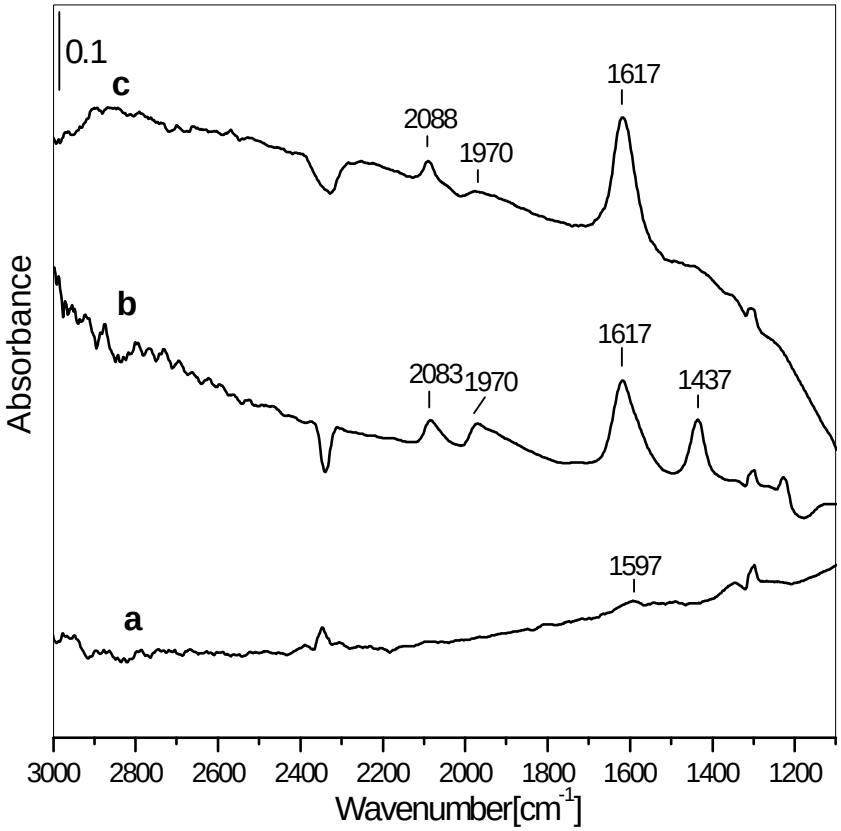

Figure 20. FTIR spectra of taken from "Blank CH_4" experiment after cooling the closed IR cell to room temperature for WZT sample (a), for 1.5Pd/ZT sample (b) and for the 1.5Pd/WZT sample (c).

3.3.3. Interaction of Preadsorbed NO_x species with Methane

3.3.3.1. WZT Sample

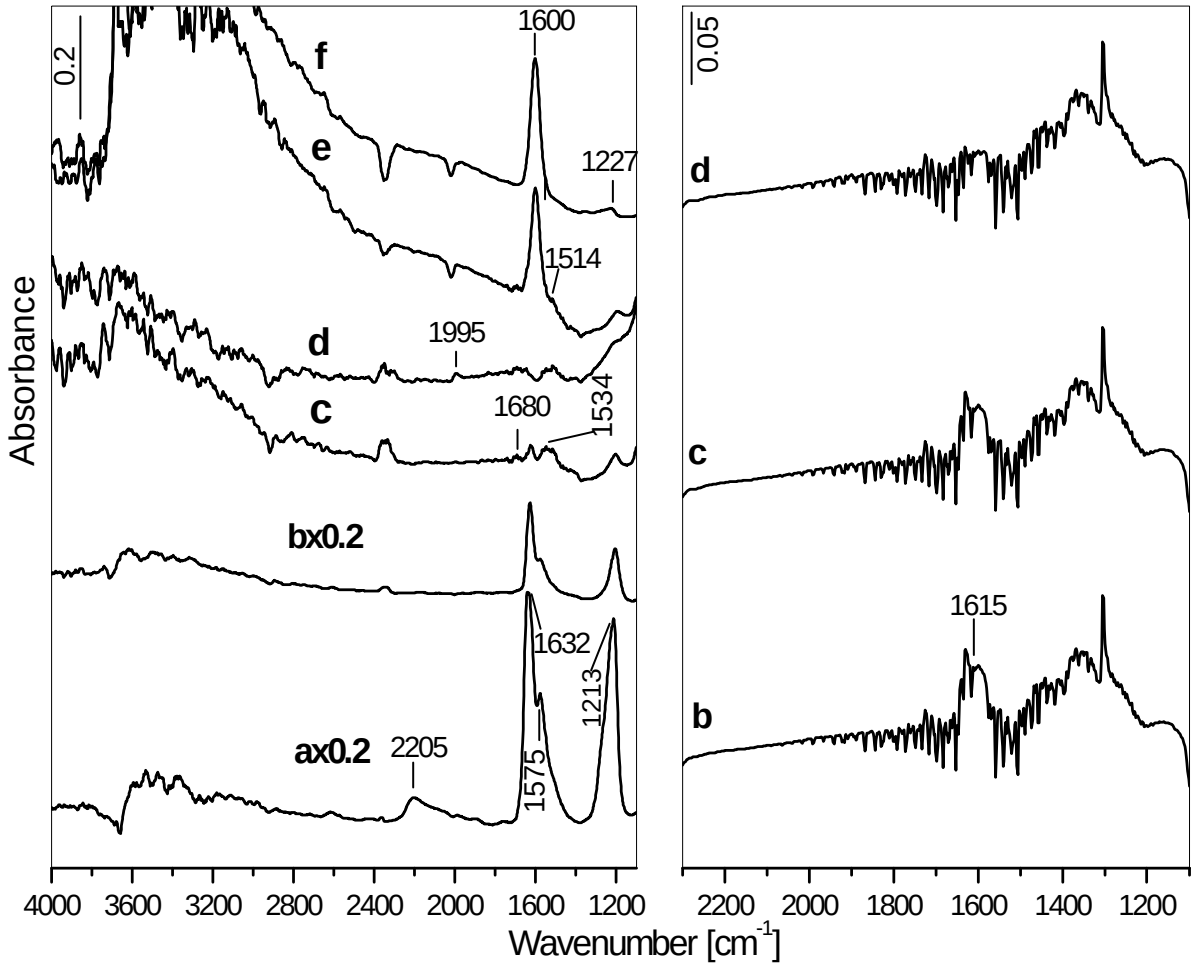

Figure 21. (A) FTIR spectra of the WZT catalyst taken after adsorption of NO/O_2 mixture (10 Torr NO + 6 Torr O_2) at RT followed by evacuation for 30 min and addition of 40 Torr of CH_4 (a), after heating the closed IR cell for 15 min at 250°C (b), at 350°C (c), at 450°C (d) and cooling to room temperature (e) then evacuation of the gas phase at RT (f). Spectra a and b are divided by 5 to display the bands with small intensity in the frame. The spectrum of activated sample is used as a background reference. Gas phases are subtracted from spectra. (B) Gas phase spectrum of the corresponding spectrum shown on panel A.

Figure 21A shows the FTIR spectra of the WZT catalyst obtained after introduction of NO/O_2 mixture (10 Torr NO + 6 Torr O_2) for 30 min followed by evacuation at room temperature for 30 min. To the catalyst treated in this way, 40 Torr of methane was added (spectrum a) and the closed IR cell was heated at various temperatures (spectrum b to d). Figure 21B shows the gas phase spectra corresponding to each spectrum shown in panel A. Heating the sample at 250^{o}C leads to decrease in the intensity of the nitrate bands at 1632, 1575 and 1213 cm^{-1} and disappearance of the band at 2205 cm^{-1} due to NO^+. Formation of small amount of NO_2 is detected in the gas phase. NO_2 production continues up to 450^{o}C (Figure 22B, spectrum d). Heating the IR cell at 350^{o}C causes desorption of nitrates and appearance of absorption in the region of H-bonded hydroxyls. Formation of new bands at 1680 and 1534 cm^{-1} is detected. Similar bands are observed in the blank CH_4 experiment with the same sample (Figure 19). These observations indicate that at 350^{o}C oxidation of CH_4 has started. In the case of NO_x-free WZT sample, the oxidation of the hydrocarbon is detected to take place already at 250^{o}C. This process on the NO_x-precovered sample becomes noticeable at higher temperature (350^{o}C). This difference shows that the nitrate species formed at room temperature on the surface of the WZT sample block the active sites for methane oxidation. The spectrum taken after cooling to room temperature (Figure 22A, spectrum g) contains strong bands due to adsorbed water (1600 cm^{-1} and strong absorption in the OH stretching region) and carbonate species (1514 cm^{-1}). The weak absorption at 1227 cm^{-1} (that resists evacuation) indicates presence of some amount of adsorbed nitrate species which contribute to the intensity of the band at 1600 cm^{-1}.

Figure 22 compares the results of the "Blank CH_4" (spectrum a), "NO_x-CH_4" (spectrum b) and "Blank NO_x" (spectrum c) experiments after the final evacuation at room temperature. In the absence of CH_4, relatively intense nitrate bands at 1617, 1505 and 1227 cm^{-1} are present in spectrum c. The strong absorption in the OH stretching region is attributed to adsorbed water molecules produced by recombination of isolated hydroxyls. The bending $\delta(H_2O)$ mode is superimposed of the nitrate band at 1617 cm^{-1}. Compared to the blank NO_x experiment, the amount of the nitrate species left unconsumed during the NO_x-CH_4 interaction (spectrum b) is significantly lower. This result indicates that the active sites on the surface of the WZT sample (W^{6+} ions) are needed for the activation of CH_4. The activated hydrocarbon can react with the gaseous NO_2 produced during the thermal decomposition of the adsorbed nitrates. Judging from the intensities of the bands due to the produced water (spectrum a and b), it can be concluded that the extent of CH_4 oxidation is larger in the presence of pre-adsorbed NO_x species.

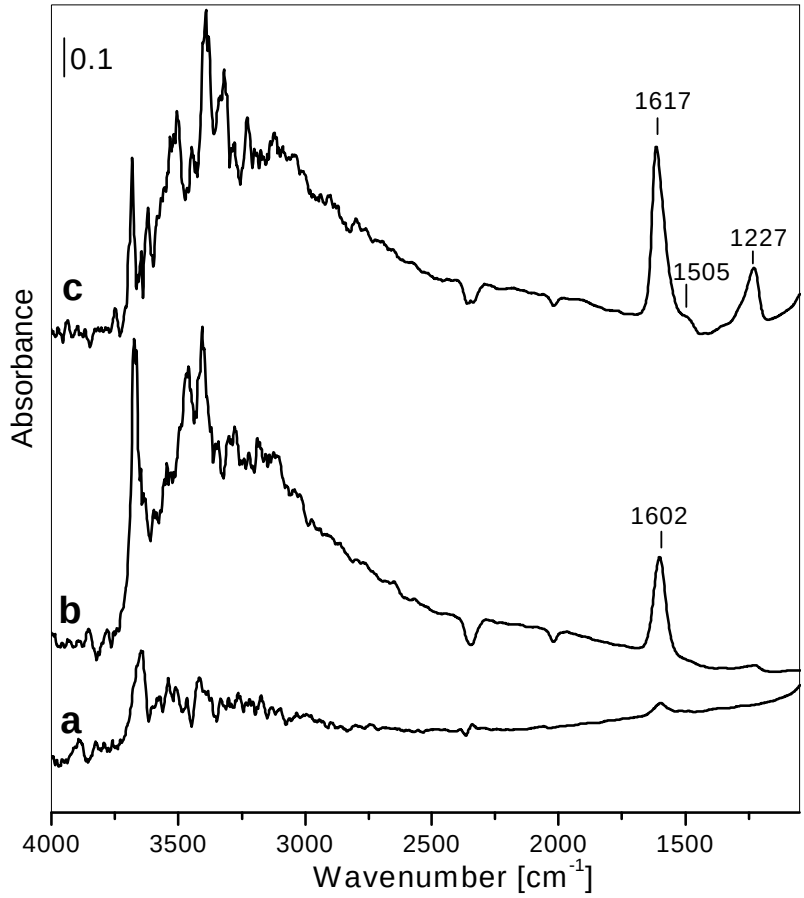

Figure 22. FTIR spectra of the WZT catalyst taken from the "Blank CH_4" (a), the interaction of the preadsorbed NO_x with CH_4 (b) and the "Blank NO_x" (c) experiments after the evacuation at room temperature. The spectrum of activated sample is used as a background reference. Gas phases are subtracted from spectra.

3.3.3.2. 1.5Pd/ZT Sample

Figure 23 shows the results of NO_x-CH_4 experiment in the presence of the 1.5Pd/ZT sample. Heating the sample at 250°C (Figure 23A, spectrum b) causes disappearance of the NO^+ species (2206 cm^{-1}) and Pd^{2+}-NO nitrosyls (1885 and 1817 cm^{-1}) and decrease in the intensities of the bands at 1627, 1578, 1240 and 1040-1000 cm^{-1} due to nitrate species. No NO_2 formation has been detected in gas phase. At 350°C (spectrum d), the nitrates completely desorb from the surface and the weak absorptions at 1565, 1437 and 1100 cm^{-1} are detected indicating formation of surface carbonates. In the "Blank CH_4" experiment (see section 3.3.2.1), formation of these

species takes place already at 200°C. This indicates that, as in the case of the WZT sample, the nitrate species block the sites for methane activation.

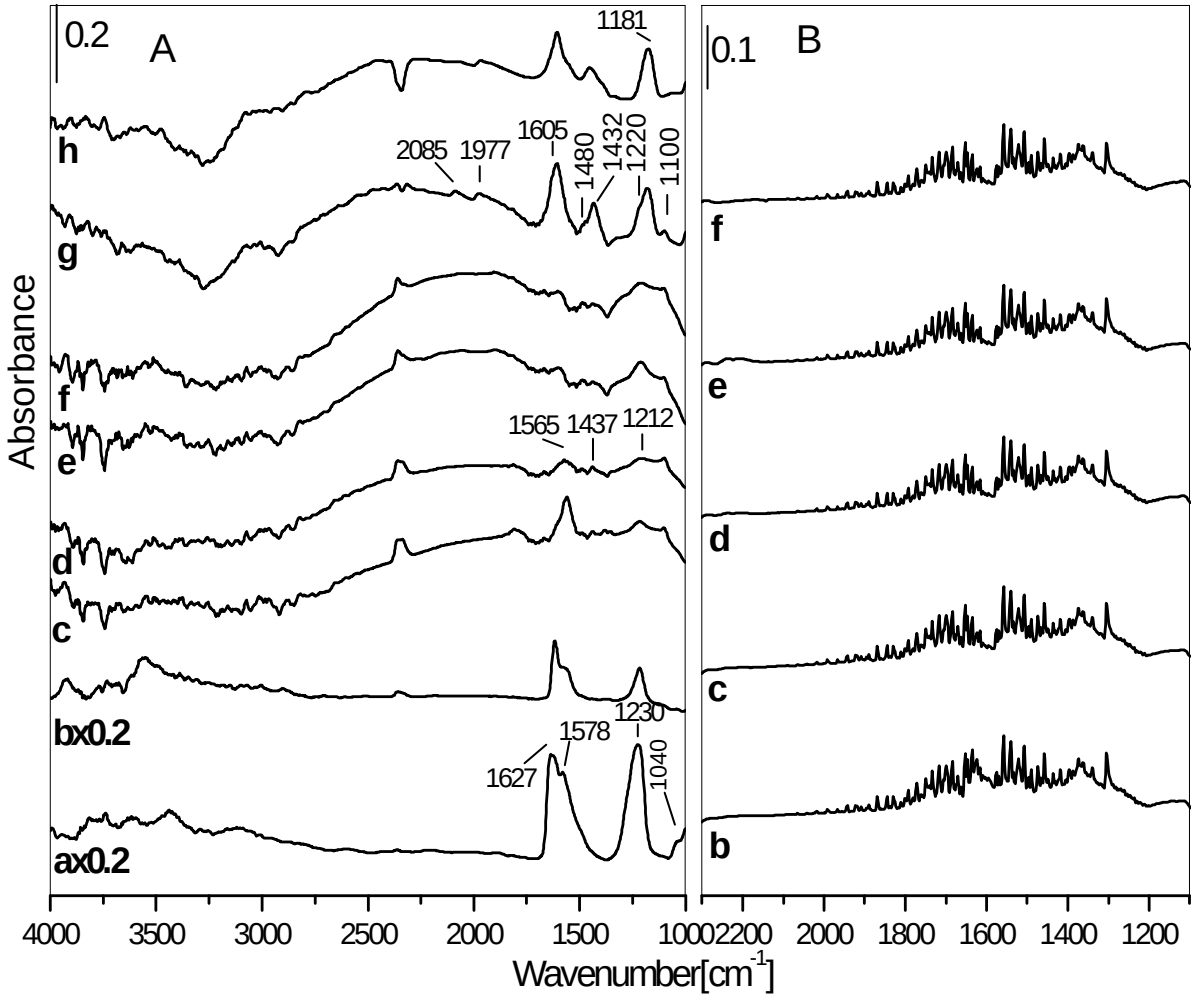

Figure 23. (A) FTIR spectra of the 1.5Pd/ZT catalyst taken after adsorption of NO/O_2 mixture (10 Torr NO + 6 Torr O_2) at RT followed by evacuation for 30 min and addition of 40 Torr of CH_4 (a), after heating the closed IR cell for 15 min at 250°C (b), at 300°C (c), at 350°C (d) at 400°C (e), at 450°C (f) and cooling to room temperature (g) then evacuation of the gas phase at RT (h). Spectra a and b are divided by 5 to display the bands with small intensity in the frame. The spectrum of activated sample is used as a background reference. Gas phases are subtracted from spectra. (B) Gas phase spectrum of the corresponding spectrum shown on panel A.

The spectra g and h obtained after cooling to room temperature contain adsorbed NO_x and carbonate species. The bands at 2081 and 1970 cm^{-1} correspond to CO adsorbed on Pd^o (linear and bridged carbonyls, respectively) [85]. Figure 24 summarizes the results of the "CH_4" and "NO_x blank" and "CH_4-NO_x" experiments. It can be concluded that the pre-adsorbed NO_x species do not affect considerably the degree of CH_4 oxidation. The reason for this is that the main product of decomposition of the NO_x species adsorbed on 1.5Pd/ZT sample is NO, which does not react with the activated methane.

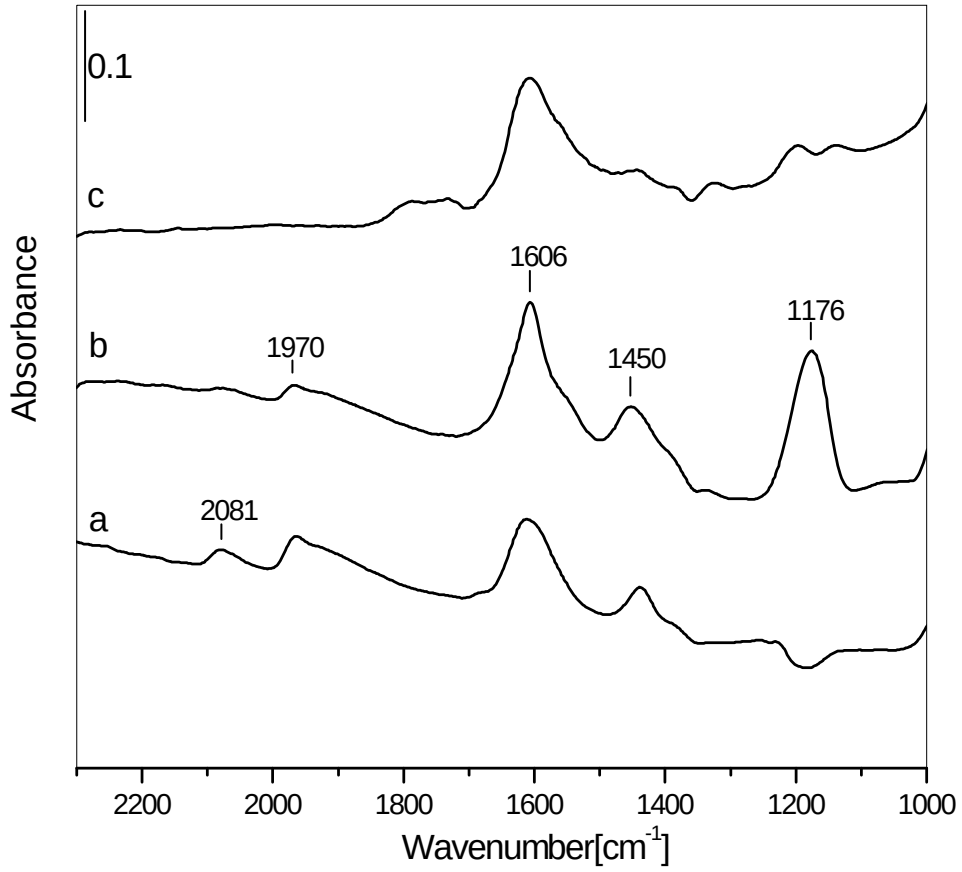

Figure 24. FTIR spectra of the 1.5Pd/ZT catalyst taken from the "Blank CH_4" (a), the interaction of the preadsorbed NO_x with CH_4 (b) and the "Blank NO_x" (c) experiments after the final evacuation at room temperature. The spectrum of activated sample is used as a background reference.

3.3.3.3. 1.5Pd/WZT Sample

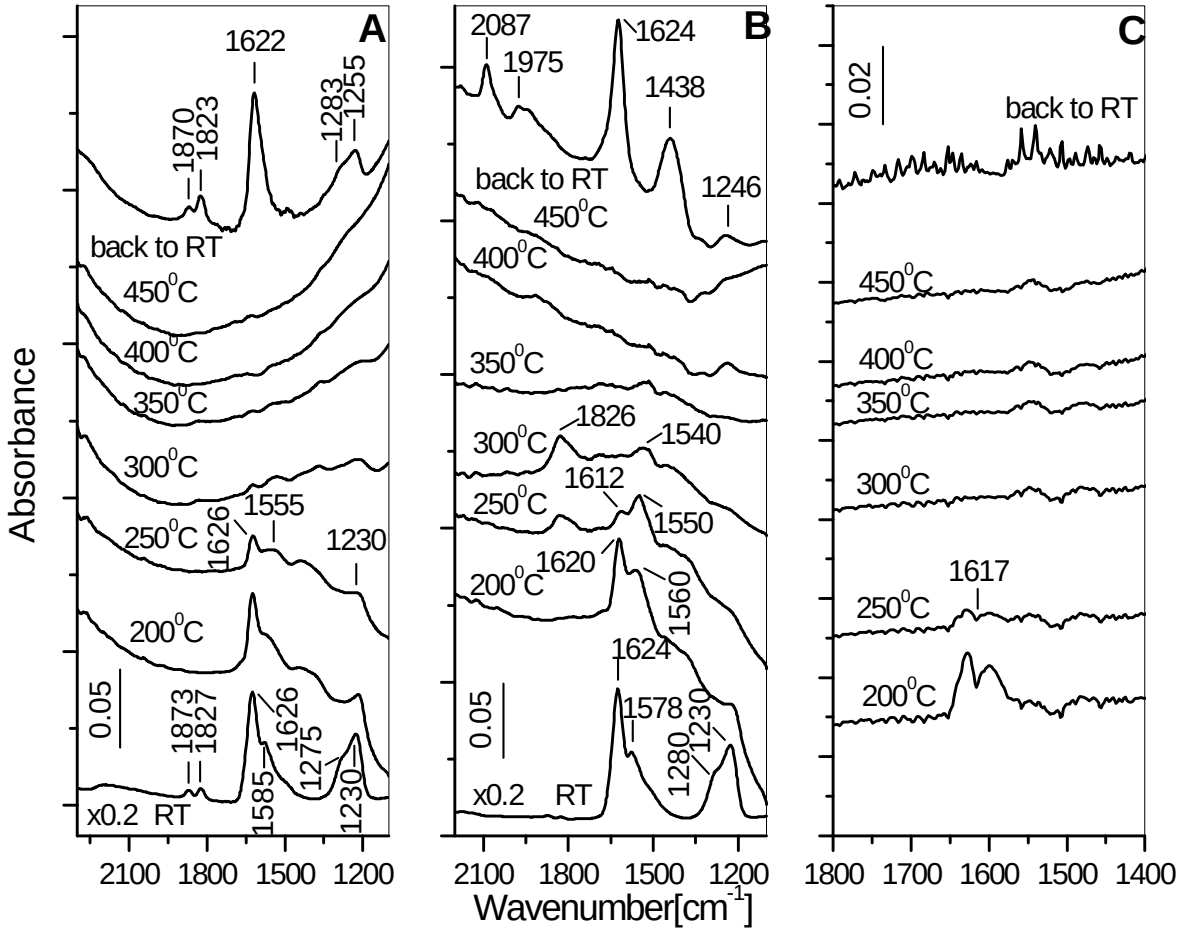

Figure 25. (A) FTIR spectra of the "Blank NO_x" experiment of 1.5Pd/WZT catalyst. (B) FTIR spectra of the 1.5Pd/WZT catalyst taken after adsorption of NO/O_2 mixture (10 Torr NO + 6 Torr O_2) at RT followed by evacuation for 30 min and addition of 40 Torr of CH_4 (a), after heating the closed IR cell for 15 min at temperatures 200°C-450°C and cooling to room temperature followed by evacuation of the gas phase. (C) Gas phase spectrum of the corresponding spectrum shown on panel B. Room temperature spectra of panel A and B are divided by 5 to display the bands with small intensity in the frame.

In order to propose clear interpretation of the results on the reactivity of the NO_x species adsorbed on the 1.5Pd/WZT catalyst, the spectra of the blank NO_x experiment are compared with

those obtained in the CH_4-NO_x experiment (Figure 25). As explained in Section 3.3.1.3, the nitrate species decompose to NO_2 and this process is completed at 350^{o}C.

The spectrum in the 1700 – 1100 cm^{-1} region taken at 250^{o}C in the presence of methane (panel B) has different shape from that at the same temperature shown in panel A. The positions of the bands at 1612 and 1550 cm^{-1} are close to those detected in the "Blank NO_x" experiment. However, the relative intensities of the bands are different. It can be assumed that the bands at 1612 and 1550 cm^{-1} correspond to new species that cannot be formed in absence of methane. The gas phase spectra obtained in the NO_x-CH_4 experiment (panel C) show that the thermal decomposition of the nitrates at 200^{o}C leads also to production of NO_2. The amount of NO_2 decreases significantly at 250^{o}C and no NO_2 is observed at higher temperatures. This result indicates that NO_2 is consumed interacting with the methane. It is reasonable to propose that the product of this process is nitromethane. Therefore the band at 1550 cm^{-1} is assigned to the $\nu_{as}(NO_2)$ mode of CH_3NO_2. The bending CH_3 and $\nu_s(NO_2)$ modes of the free molecule are of low intensity [89-92] and are observed in the spectra detected at 250^{o}C as a broad, weak absorption between 1480 and 1300 cm^{-1}. Judging from the relative intensities of the bands in the 1700 – 1500 cm^{-1} region obtained at 200^{o}C in the "Blank NO_x" and "NO_x-CH_4" experiments, it can be concluded that adsorbed nitromethane is present on the catalyst surface already at 200^{0}C. At 250^{o}C, Pd^+–NO nitrosyls appear in the spectrum recognized by the band at 1826 cm^{-1} [89-93]. No such species are observed during the "Blank NO_x" experiment. Therefore, it is concluded that the Pd^+–NO species are produced as a result of the decomposition of nitromethane to NO and compound(s) characterized by the weak absorption at 1540 cm^{-1}. This conclusion is supported by the fact that the intensity of the nitromethane band at 1550 cm^{-1} decreases as the nitrosyl band at 1826 cm^{-1} grows with simultaneous appearance of the species at 1540 cm^{-1}. The decomposition of nitromethane is discussed in details in the next section. Here, it should be noted only that, this process takes place with the intermediacy of the species characterized by the absorption band at 1612 cm^{-1}.

The maximum intensity of the Pd^+–NO species is observed at 300^{o}C. Further increase in the temperature leads to disappearance of the nitrosyls and decrease in the intensity of the band at 1540 cm^{-1}. Rising of the temperature to 400 and 450^{o}C, results in complete disappearance of all of the absorption bands. The spectrum obtained after cooling to room temperature contains bands corresponding to Pd^0–CO carbonyls (2087 and 1975 cm^{-1} [85]), hydrogen carbonates (1624, 1438 and 1246 cm^{-1} [94]) and water (1624 cm^{-1}). In contrast to the blank NO_x experiment, no adsorbed NO is detected under these conditions. This suggests that NO has been reduced to

molecular nitrogen most probably through a reaction with the decomposition product(s) of nitromethane at 1540 cm^{-1}.

Figure 26 compares the results of the "Blank CH_4" (spectrum a), "NO_x-CH_4" (spectrum b) and "Blank NO_x" (spectrum c) experiments after cooling the closed IR cell to room temperature. The NO_x precovered catalyst ensures complete oxidation of the hydrocarbon as a result of the reduction of the adsorbed NO_x species to molecular nitrogen.

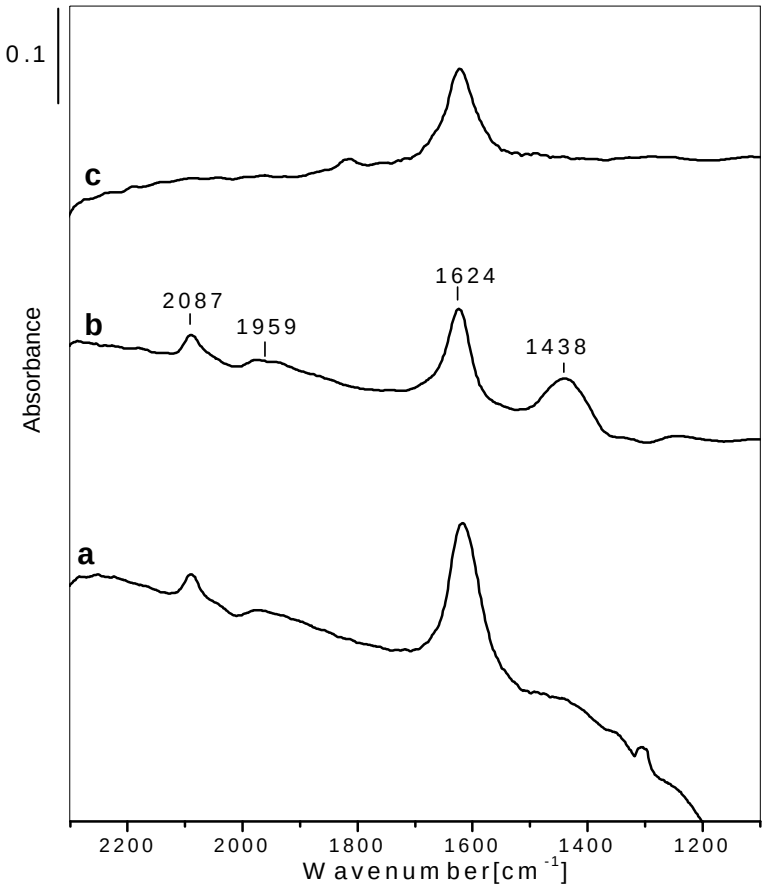

Figure 26. FTIR spectra of the 1.5Pd/WZT catalyst taken from the "Blank CH_4" (a), the interaction of the preadsorbed NO_x with CH_4 (b) and the "Blank NO_x" (c) experiments after the cooling IR cell to room temperature. The spectrum of activated sample is used as a background reference. Gas phases are subtracted from spectra.

The experimental results show that nitromethane is a primary intermediate product of the CH_4-SCR on over 1.5Pd/WZT catalyst. To get deeper insight into the reaction scheme, the routes of transformation of authentic nitromethane have been studied.

Figure 27 shows the FT-IR spectra of the WZT sample taken after introduction of nitromethane vapor (1.5 Torr) at room temperature and heating of the closed system for 15 min at various temperatures. The spectrum detected at room temperature is characterized by bands attributable to molecularly adsorbed nitromethane [89-93]: $\nu_a(NO_2)$ at 1561 cm^{-1}, $\nu_s(NO_2)$ at 1420 cm^{-1}, $\delta_a(CH_3)$ and $\delta_s(CH_3)$ at 1395 and 1376 cm^{-1}, respectively. The band at 1248 cm^{-1} corresponds to the first overtone of the bending NO_2 modes, whereas the absorption at 1100 cm^{-1} is due to the rocking CH_3 vibration.

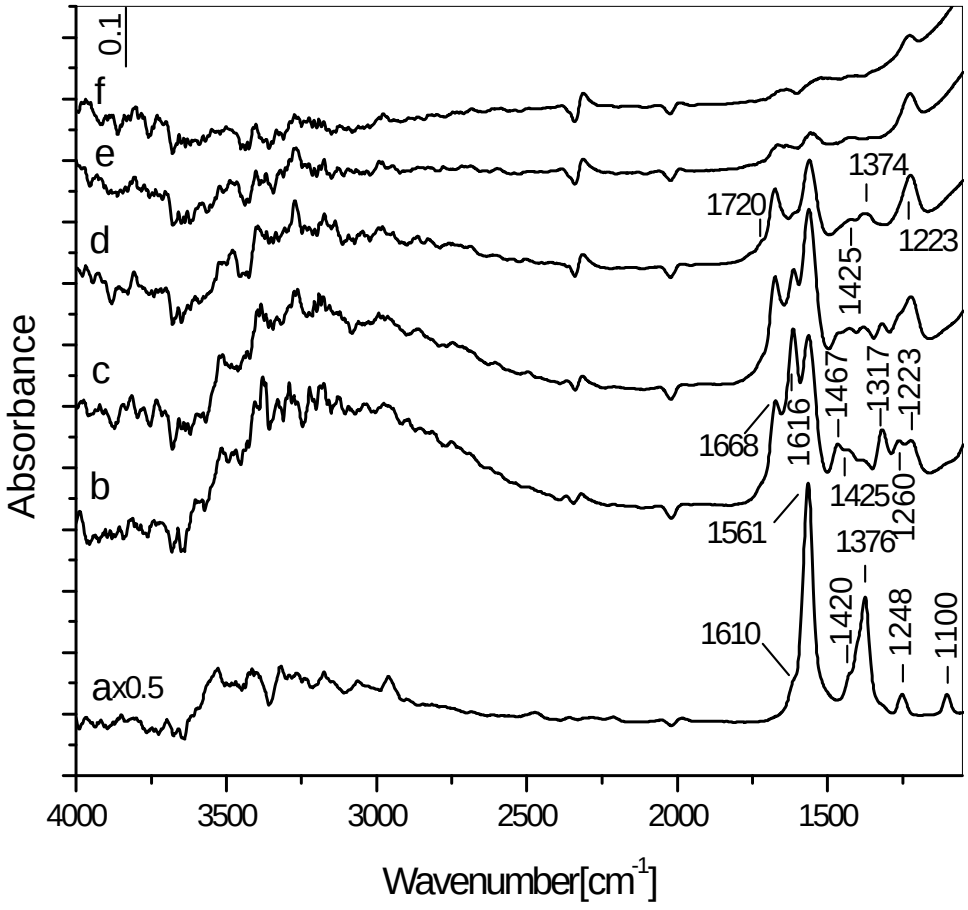

Figure 27. (A) FTIR spectra of WZT sample taken after adsorption of CH_3NO_2 (1.5 Torr) at room temperature (a) followed by heating the closed IR cell for 15 min at 150 ^oC (b), at 200^oC (c), at 250^oC (d), at 300^oC (e), and at 350^oC (f). Spectrum a is divided by 2.

The shoulder at about 1610 cm^{-1} is attributed to the $\nu_a(NO_2)$ mode of the isomer of nitromethane, cis-methyl nitrite [95]. The surface concentration of the latter compound increases significantly after heating at 150°C giving rise to a distinct band with maximum at 1616 cm^{-1}. The band at 1668 cm^{-1} is characteristic of the $\nu_a(NO_2)$ mode of trans-CH_3ONO [95]. Obviously, the conformers of methyl nitrite are formed at the expense of the adsorbed nitromethane. This is evident by the lowering of the intensity of the band at 1561 cm^{-1} during the heating at 150°C. The weak bands at 1467, 1425, 1380, 1317, 1260 and 1223 cm^{-1} are attributed to bending vibrations of the CH_3 and overtones of the bending modes of the NO_2 groups of the nitromethane and its isomers. Further increase in the temperature shows that the adsorbed cis-isomer has lower thermal stability than those of nitromethane and trans-CH_3ONO: it disappears from the spectrum at 350°C. At the same temperature, the surface concentrations of nitromethane and the trans-isomer decrease significantly. The spectra taken in the 250 – 350°C temperature range allow attributing the band at 1223 cm^{-1} to the trans-CH_3NO_2.

The spectra obtained between 150 and 250°C contain weak unresolved absorption at about 1720 cm^{-1}. This band is assigned to the ν(C=O) mode of adsorbed trans-formohydroxamic acid (HC(O)NH(OH)) [96]. Formation of this compound from nitromethane has been proposed in several studies [58, 93, 97, 98]. This process is assumed to take place through interconversion between nitromethane and aci-nitromethane [58]:

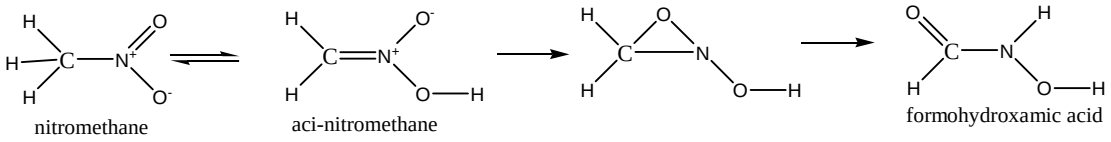

(7)

Since the spectra of the WZT sample contain bands that can be assigned to adsorbed nitromethane and products of its intramolecular transformations, it can be concluded that upon heating, the nitromethane does not undergoe decomposition.

In the case of the 1.5Pd/WZT sample, the pressure of nitromethane vapor added to the cell was 0.74 Torr. The spectra detected upon heating of the closed system from room temperature to 350°C are shown in Figure 28. The nitromethane adsorbed at room temperature produces spectrum similar to that detected in the case of the WZT support. The band at 1655 cm^{-1} assigned to the $\nu_a(NO_2)$ mode of trans-CH_3ONO indicates that isomerization of the nitromethane takes place already at room temperature. The increase in the temperature to 150°C leads to enhancement of the intensity of the band at 1655 cm^{-1} at the expense of the nitromethane band at

1568 cm^{-1}. A shoulder at about 1720 cm^{-1} corresponding to adsorbed trans-formohydroxamic acid and weak absorption at 2195 cm^{-1} are detected. At 200°C, these bands appear with increased intensity. At the same time the band at 1655 cm^{-1} broadens and poorly resolved shoulder at about 1670 cm^{-1} is observed as well. The band at 1670 cm^{-1} could be assigned to the ν(C=O) mode of adsorbed cis-formohydroxamic acid (HC(O)NH(OH)) [96].

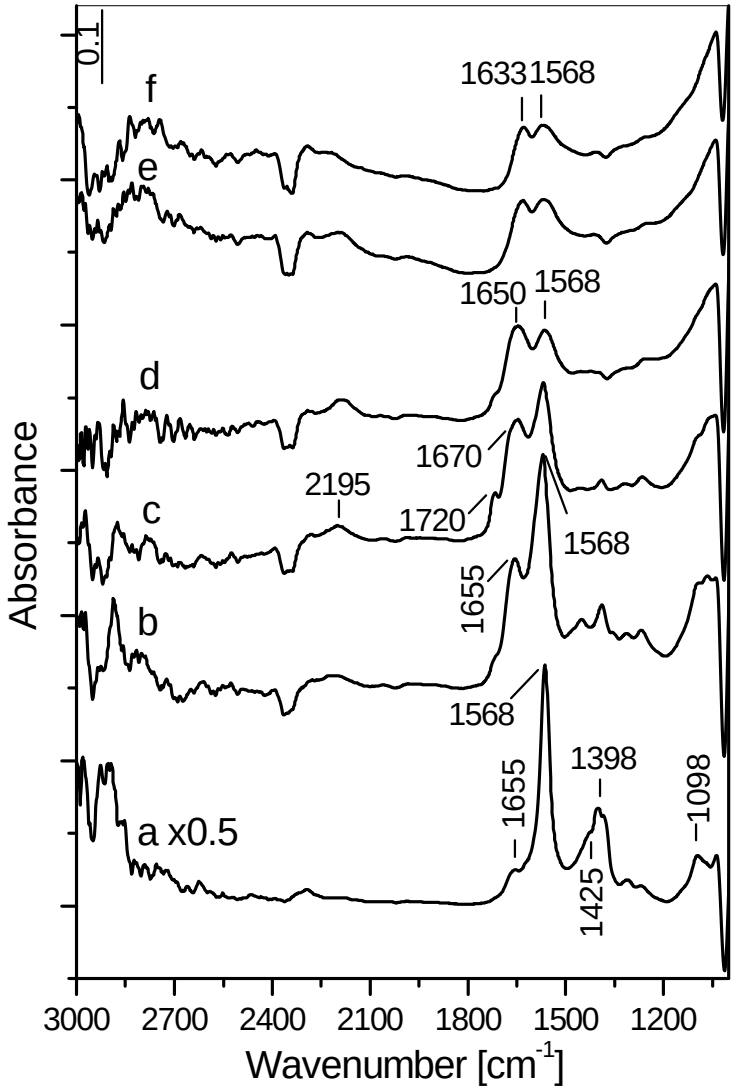

Figure 28. FTIR spectra of 1.5Pd/WZT sample taken after adsorption of CH_3NO_2 (1.5 Torr) at room temperature (a) followed by heating the closed IR cell for 15 min at 150 °C (b), at 200°C (c), at 250°C (d), at 300°C (e), and at 350°C (f). Spectrum a is divided by 2.

By analogy with the results of Solymosi and Bansagi [99] on adsorption of HNCO on Cu-ZSM-5, the weak band at 2195 cm^{-1} is attributed to Pd^{2+}–NCO. The isocyanate species may form by dehydration of the formohydroxamic acid [58]:

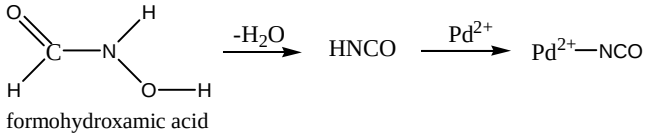

formohydroxamic acid (8)

The adsorbed acid disappears from the spectrum at 300°C and the isocyanate species are removed at 350°C. The spectra taken under these conditions contain bands at 1568 and 1634 cm^{-1} which can be assigned to adsorbed nitromethane and its trans isomer, respectively. The broad absorption in the 2900 – 2750 cm^{-1} suggests formation of formate species and formic acid with ν(C=O) modes superimposed to the $\nu_a(NO_2)$ bands. The differences in the amounts and thermal stability of the species obtained at 350°C on both materials supports also this conclusion.

The experimental results indicate that the modification of the WZT sample with palladium leads to variety of intermolecular transformations of nitromethane. Compared to the WZT support, the Pd-containing sample is able to stabilize larger amounts of formohydroxamic acid. In the presence of the 1.5Pd/WZT catalyst, this compound decomposes to isocyanate and most probably formic acid and formate species, whereas in the case of the WZT support it desorbs from the surface at 300°C. Although there is no particular requirement for the participation of transition metals in the intermolecular rearrangements and decomposition of the adsorbed nitromethane (see reactions 7 and 8), it can be proposed that these processes may take place by the assistance of the Pd^{2+} ions. Another important difference between both samples is that no cis-CH_3ONO adsorbed on the 1.5Pd/WZT catalyst has been detected.

The spectra of authentic CH_3NO_2 adsorbed on the 1.5Pd/WZT catalyst in the 150 -350°C temperature range display different features from those obtained in the CH_4-NO_x experiment (Figure 25). As described above, the band at 1550 cm^{-1} in the spectrum taken at 250°C (Figure 25B) is assigned to the $\nu_{as}(NO_2)$ mode of CH_3NO_2 formed in situ as a result of the interaction between the methane and NO_2. This band is accompanied by a weaker absorption at 1612 cm^{-1}. The most likely candidate, which can be assigned to this band, is the cis-CH_3ONO. This compound starts to decompose at 250°C leading to formation of Pd^{+}–NO species. This is in a strong contrast with the processes observed during the high-temperature adsorption of authentic nitromethane. In the latter case, no cis-CH_3ONO and Pd^{+}–NO species are detected. This

difference suggests that the nitromethane formed in situ follows different decomposition route involving intermediacy of cis-methyl nitrite. The products of thermal transformation of authentic nitromethane are trans-formohydroxamic acid and isocyanate species. They have relatively low thermal stability and their surface concentrations are the highest between 200 and 300^{o}C. These temperatures are below the temperature at which the adsorbed NO is reduced (350^{o}C, see Figure 25). Therefore, it is concluded that the formohydroxamic acid and isocyanate species (if formed during the CH_4-NO_x experiment) have no significance for the reduction of the adsorbed NO. It should be pointed out that Park et al. [91] and Beloshapkin et al. [100] reported formation of NO adsorbed on cobalt sites during the interaction of nitrometane with Co-ZSM-5 at 280 – 300^{o}C.

3. 4. Summary of the Results on the Reactivity of Adsorbed NO_x Species toward Methane

The experimental results show that the NO_x species formed at room temperature on the WZT and 1.5Pd/ZT samples suppress the oxidation of the methane, whereas in the case of the 1.5Pd/WZT catalyst the surface nitrates initiate the formation of nitromethane. Most probably, this process starts at 200^{o}C (see Figure 25). According to the "Blank CH_4" experiment, at the same temperature the 1.5Pd/WZT sample is able to activate the hydrocarbon (Figure 19). Kato et al. [101] proposed that NO_x adsorbed on the Pd/H-ZSM-5 catalyst is unreactive toward methane and the C–H bond dissociation of methane is exerted by palladium. In general, the activation of methane can involve homolytic or heterolytic cleavage of the C−H bond and at present there is no agreement on the correct mechanism. According to Burch et al. [102], PdO-containing catalysts activate methane heterolytically with formation of CH_3^- and OH^- groups. In this process strong Lewis acid-base pairs are involved [103]. Valyon et al. [104] pointed out that, if the CH_3^- groups cannot be stabilized by the oxide, $\bullet CH_3$ radicals can be produced. In this study, no experimental evidence for formation of metal-alkyl species has been found. Therefore, it is assumed that in the process of methane activation $\bullet CH_3$ radicals are formed, which react with the NO_2 evolved during the thermal decomposition of the nitrate species:

$$\bullet CH_3 + NO_2 \rightarrow CH_3NO_2 \qquad (9)$$

The nitromethane rearranges unimolecularly to cis-methyl nitrite:

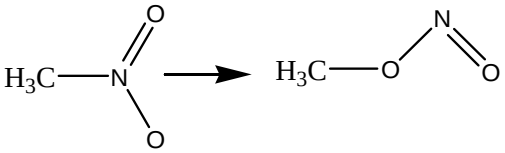

(10)

The latter compound gives rise to the band at 1612 cm^{-1} corresponding to the $\nu_{as}(NO_2)$ mode (Figure 25B). This is followed by a redox step, in which Pd^{2+} ions are involved:

$$CH_3ONO + Pd^{2+}–O^{2-} \rightarrow Pd^{+}–NO + H_2C=O + OH^{-} \quad (11)$$

Formation of Pd^{+}–NO nitrosyls is detected at 250°C by the appearance of the band at 1826 cm^{-1}. This band increases in intensity at 300°C with simultaneous disappearance of the adsorbed methyl nitrite. The absorption at 1540 cm^{-1} detected under these conditions can be due either to adsorbed nitromethane or to decomposition product of the methyl nitrite. At 350°C the adsorbed NO disappears, which is accompanied by a decrease in the intensity of the band at 1540 cm^{-1}. Since the thermal stability of Pd^{+}–NO nitrosyls is high [105, see also Figure 25], it can be concluded that a reaction between the adsorbed NO and the compound characterized by the band at 1540 cm^{-1} has occurred. Possible candidate for the latter absorption is the formate species. It is well known that formaldehyde is unstable on oxide surfaces at high temperatures and can easily convert into formate species (formic acid) [94] either by oxidation:

$$H_2C=O + Pd^{2+}–O^{2-} (W^{6+}=O^{2-}) \rightarrow HCOOH + Pd^{0} (W^{4+}) \quad (12)$$

or Canizzaro-type disproportionation:

$$2H_2C=O + O^{2-} \rightarrow CH_3O^{-} + HCOO^{-} \quad (13)$$

It should be pointed out that participation of the Pd^{2+} ions in more than one redox process is unlikely. Therefore, the formation of formate ions characterized by $\nu_{as}(CO_2)$ at 1540 cm^{-1} is visualized by the involvement of the WO_x species or surface O^{2-} ions. The formic acid (formate ion) produced reduces the adsorbed NO to molecular nitrogen according to the reaction:

$$HCOO^{-} + NO \rightarrow HCO_3^{-} + 0.5N_2 \quad (14)$$

The occurrence of this process is confirmed by the absence of adsorbed NO in the spectrum taken after cooling to room temperature. This spectrum contains bands corresponding to hydrogen carbonates and reduced Pd species. The latter can arise by interaction of the Pd^{+} ions with CO, which is a byproduct under the anaerobic conditions employed.

Scheme 15 summarizes the proposed mechanism for interaction of methane with the surface of NO_x-precovered 1.5Pd/WZT catalyst. The species given in parentheses have not been detected experimentally.

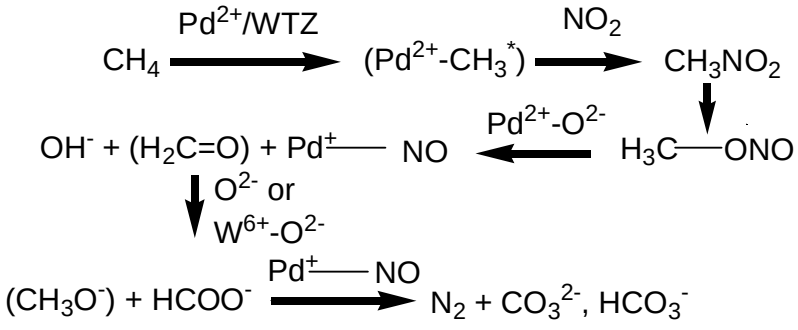

(15)

This reaction scheme differs from the mechanisms proposed for CH_4-SCR of NO in the presence of Pd-containing oxide systems. In these mechanistic studies, adsorbed cyanides [55,56], isocyanates [56] and ammonia [56, 57] have been considered as important intermediates leading to the products of the reaction, molecular nitrogen and carbon oxides. The formation of these compounds has been deduced from assumptions based on the possible routes of transformation of nitrosomethane [55] or interaction between adsorbed NO and CH_x species [56, 57]. In this study, we did not detect ammonia, cyanide or isocyanide species, which could be expected to form under the anaerobic conditions of our experiments. To our knowledge no report has succeeded in presenting IR evidence on in situ formation of nitromethane on Pd-containing $DeNO_x$ catalysts.

4. CONCLUSIONS

- The structure and surface properties of zirconia-titania (mole ratio ZrO_2: TiO_2 = 1:1, denoted as ZT), WO_3-modified ZT (25 wt % of WO_3, denoted as WZT) and palladium (II)-promoted (1.5 wt % of Pd) zirconia-titania (1.5Pd/ZT) and tungstated zirconia-titania (1.5Pd/WZT) are studied by XRD, DR-UV-vis spectroscopy and FT-IR spectroscopy of adsorbed CO and NO. The interaction of methane with NO_x species formed by room-temperature adsorption of NO/O_2 mixture on the samples is investigated using in situ FT-IR spectroscopy. Zirconia-titania was prepared by a homogenous coprecipitation of urea at 70°C. This material is in amorphous form up to calcination temperature of 550°C. At 600°C, formation of crystalline $ZrTiO_4$ is observed. XRD, DR-UV-Vis and BET data show that very good mixing of the oxides has been achieved with a high surface area (118 m^2/g) and small crystallite size (4.4 nm). Modification of the ZT sample with WO_3 is performed impregnating the hydrated mixed ZT oxide with aqueous solution of ammonium metatungstate. The WZT sample has paratungstate-type WO_x species with intermediate domain size and crystallization temperature higher than that of the WO_x-free mixed oxide. The crystalline WZT sample contains WO_3, $ZrTiO_4$ and $Zr(WO_4)_2$. According to the DR-UV-Vis spectra, the Pd-promoted WZT samples (prepared by impregnation with $Pd(NO_3)_2.2H_2O$ aqueous solution) contain isolated Pd^{2+} ions.
- The spectrum of CO adsorbed on the ZT sample reveals the presence of coordinatively unsaturated (cus) Zr^{4+} and Ti^{4+} sites. Their amount decreases considerably after the modification of the sample with WO_3. Promotion with Pd(II) results in complete disappearance of the exposed Ti^{4+} and Zr^{4+} ions, removal of the surface hydroxyls and decrease in the intensity of the W=O terminal bonds. The adsorption of CO and NO on the 1.5Pd/ZT and 1.5Pd/WZT samples indicates presence of palladium ions in two different environments. The amount of cus Pd^{2+} ions deposited on the WZT sample decreases relative to that on the ZT support. This is a consequence of the coordination of some Pd^{2+} ions to the WO_x species. The adjacent tungstates increase the Lewis acidity of the Pd^{2+} ions, which is evident by the higher ν(NO) stretching frequencies of the nitrosyl bands on the tungsten-containing catalyst than those on the tungsten-free sample.
- The adsorption of NO at room temperature on the samples studied involves process of disproportionation of NO on surface oxide ions leading to formation of adsorbed anionic nitrosyl, NO^-, and NO_2. The latter also disproportionates giving rise to different kind of

surface nitrates. The amount of the adsorbed species varies depending on the composition of the materials, being the smallest in the case of the 1.5Pd/WZT catalyst.

- The addition of molecular oxygen to the NO causes its oxidation to NO_2/N_2O_4. These gases adsorb molecularly on the surface of the samples and undergo self-ionization and disproportionation with the participation of surface hydroxyl groups. The amounts of NO_2 and N_2O_4 in the gas phase reflect the adsorption capacity of the samples. Introduction of WO_x species and Pd^{2+} ions to the titania-zirconia mixed oxide hinders the processes of NO_2/N_2O_4 self-ionization and disproportionation by elimination of the necessary active sites.
- The oxidation of methane in absence of molecular oxygen takes place on WZT, 1.5Pd/ZT and 1.5Pd/WZT catalysts already at 200^oC. Carbonates, hydrogen carbonates and adsorbed CO are the oxidation products. The experimental results on the reactivity of the adsorbed NO_x species toward methane show that the nitrates formed on the WZT and 1.5Pd/ZT samples suppress the oxidation of methane, whereas on 1.5Pd/WZT sample they initiate the formation of nitromethane. This process starts at 200^0C with direct activation of the hydrocarbon on the catalyst leading to formation of CH_3 radicals. The latter species interact with the NO_2 evolved during the thermal decomposition of the surface nitrates.
- Mechanism for the reduction of NO over the 1.5Pd/WZT catalyst is proposed, which involves a step of thermal decomposition of the nitromethane to adsorbed NO and partially oxidized hydrocarbons (methoxy and/or formate species) through the intermediacy of cis-methyl nitrite. The reduction of the adsorbed NO by the partially oxidized hydrocarbons leads to the products of the CH_4-SCR, molecular nitrogen and carbon oxides.
- The identity of the nitromethane formed in situ is confirmed by the spectra of authentic nitromethane adsorbed on the WZT and 1.5Pd/WZT samples. The authentic nitromethane and the nitromethane formed in situ on the 1.5Pd/WZT catalyst follow different decomposition routes. This difference arises from the fact that under in situ conditions, nitromethane and cis-methyl nitrite are stabilized on the surface of the 1.5Pd/WZT catalyst, whereas the adsorption of the authentic reagent results in adsorbed nitromethane and its trans isomer. The products of thermal transformation of nitromethane are trans-formohydroxamic acid and isocyanate species. The latter compounds have relatively low thermal stability and cannot be of significance for the reduction of adsorbed NO.

5. REFERENCES

1. G. Ertl, H. Knözinger, J. Weitkamp, Environmental Catalysis, Weinheim ; New York Wiley-VCH, (1999).

2. V. I. Pârvulescu, P. Grange, B. Delmon, Cat. Today, 4, (1998), 233.

3. G.L. Manney, L. Froidevaux, J.W. Waters, R.W. Zurek, W.G. Read, L.S. Elson, J.B. Kumer, J.L. Mergenthaler, A.E. Roche, A. O'Nelll, R.S. Harwood, I. MacKenzie, R. Swinbank, Nature, 370, (1994), 429.

4. N. Armor. Appl. Catal. B 1 (1992), 221.

5. Emissions of Greenhouse Gases in the United States: 1987-1992. DOE/EIA Report # 0573, US Government Printing Office. Washington, DC, October, (1994).

6. http://www.remtechnology.com/applications/lean_con2.htm

7. http://www.che.lsu.edu/COURSES/4205/2000/Dawag/

8. M. Shelef, Chem. Rev., 95, (1995), 209.

9. M.D. Amiridis, T. Zhang, R.J. Farrauto, Appl. Catal. B, 10, (1996), 203.

10. R.M. Heck and R.J. Farrauto, Catalytic Air Pollution Control: Commercial Technology, Van Nostrand Reinhold, New York (1995).

11. http://www.traxcorp.com/scroperations.html

12. J. N. Armor, Catal. Today, 26, (1995), 99.

13. T. Salvese, S. Roesch, P.A. Sermon and P. Kaur, Top. Catal.16, 381, (2001), 1.

14. Air Pollution Engineering Manual, AP-42, U.S. Environmental Protection Agency.

15. M.D. Fokema and J.Y. Ying. Catal. Rev. 43, (2001), 1.

16. Y. Li and J.N. Armor. Appl. Catal. B 1, (1992), L31.

17. Iwamoto, M., Yahiro, H., Shundo, S., Yu-u, Y., Mizuno, N., Shokubai, 32, (1990), 430.

18. Iwamoto, M., Proc. Meeting of Catalytic Technology for Removal of Nitrogen Monoxide, Tokyo, (1990), 1.

19. Held, W. and Koenig, A., Ger. Offen., DE 3642018, (1987).

20. Held, W., Koenig, A., Richter, T., and Puppe, L., SAE Paper, (1990), 900496.

21. Y. J. Li, J. N. Armor, Appl. Catal. 3, (1993), 55-60.

22. C. Yokoyama, M. Misono, Chem. Lett. (1992), 1669-1672.

23. Y. Li and J.N. Armor. J. Catal.,145, (1992), 1-9.

24. Y. Nishizaka, M. Misono, Chem. Lett. (1993), 1295-1298.

25. K.C. Kharas, H.J. Robota and D.J. Liu, Appl. Catal. B, 2, (1993), 225.

26. K.C. Kharas et al., ACS Symp. Ser., 552, (1994), 215.

27. V.A. Bell. J.S. Feeley, M. Deeba and R.J. Farauto, Catal. Lett., 29, (1994), 15.

28. Zhang, X., Walters, A. B., Vannice, M. A., J. Catal. 146, (1994), 568.

29. Zhang, X.,Walters,A. B., Vannice, M. A., Appl. Catal. B Environ. 7, (1996), 321.

30. Xie, S., Ballinger, T. H., Rosynek, M. P., and Lunsford, J. H., Stud. Surf. Catal. 101, (1996), 711. [11th International Congress on Catalysis]

31. M.D. Fokema, J.Y. Ying, Appl. Catal. B, 18, (1998), 71-77.

32. V.N. Stathopoulos, C.N. Costa, P.J. Pomonis, A.M. Efstathiou, Top. Catal., 16/17, (2001), 231-235.

33. U.S. Ozkan, M.W. Kumthekar, G. Karakas, Catal. Today, 40, (1998), 3-14.

34. J. Mitome, G. Karakas, K.A. Bryan, U.S. Ozkan, Catal. Today, 42, (1998), 3-11.

35. M. Inaba, Y. Kintaichi, M. Haneda, H. Hamada, Catal. Lett., 39, (1996), 269-275.

36. C.J. Loughran and D.E. Resasco. Appl. Catal. B., 7, (1995), 113.

37. M. Misono, Y. Nishizaka, M. Kawamoto and H. Kato, Progress in zeolite and microporous materials. Stud. Surf. Sci. Catal. 105, (1997), 1501.

38. C. Descorme, P. Gelin, M. Primet, C. Lecouyer, J. Saint-Just, in: L. Bonneviot (Ed.), Zeolites: A Refined Tool for Designing Catalytic Sites, Elsevier, (1995), 287.

39. Nishizaka, M. Misono, Chem. Lett., (1994), 2237.

40. Y.H. Chin, D. E. Resasco, in: Catalysis, vol. 14, Roy. Soc. Chem., London (1999).

41. Y. Li, P.J. Battavio and J.N. Armor. J. Catal. 142, (1993), 561.

42. E. Kikuchi, M. Ogura and I. Terasaki. J. Catal., 161, (1996), 465.

43. Y. Li and J.N. Armor. Appl. Catal. B., 5, (1995), L257.

44. M.C. Campa, D. Pietrogiacomi, S. Tuti, G. Ferraris and V. Indovina. Appl. Catal. B., 18, (1998), 151.

45. X. Wang, T. Zhang, X. Sun, W. Guan, D. Liang and L. Lin. Appl. Catal. B., 24, (2000),169.

46. K. Yogo, M. Ihara, I. Terasaki and E. Kikuchi. Catal. Lett. 17, (1993), 303.

47. Y. Nishizaka, M. Misono, Chem. Lett., (1994), 1295.

48. H. Ohtsuka and T. Tabata. Appl. Catal. B., 26, (2000), 275.

49. M. Iwamoto and H. Yahiro. Catal. Today, 22, (1994), 5.

50. Y. Li and J.N. Armor. J. Catal. 150, (1994), 376.

51. Y. Li, T.L. Slager and J.N. Armor. J. Catal. 150, (1994), 388.

52. D.B. Lukyanov, G. Still, J.L. d'Itri and W.K. Hall. J. Catal. 153, (1995), 265.

53. T. Beutel, B.J. Adelman, G.D. Lei and W.M.H. Scachtler. Catal. Lett., 32, (1995), 83.

54. X. Wang, H.-Y. Chen and W.M.H. Sachtler, J. Catal., 197, (2001), 281.

55. Lisa J. Lobree, Adam W. Aylor, Jeffrey A. Reimer, and Alexis T. Bell1, J. Cat. 181, (1999), 189.

56. K. Shimizu, F. Okada, Y. Nakamura, A. Satsuma, T. Hattori, J. Catal. , 195, (2000), 151.

57. Junko M.Watson and Umit S. Ozkan Journal of Catalysis 210, (2002), 295.

58. Andrew D. Cowan, Noel W. Cant, Brian S. Haynes, and Peter F. Nelsonz, J. Cat., 176, (1998), 329.

59. S. Xie, M.P. Rosynek, J. H. Lunsford, Catal. Lett., 43, (1997), 1-5.

60. M. Inaba, Y. Kintaichi, M. Haneda and H. Hamada. Nippon Kagaku Kaishi, 7, (2000), 467.

61. N. Li, A. Wang, L.Li, X. Wang, L. Ren, T. Zhang App. Cat. B. 50, (2004), 1-7.

62. Y. Zhao, W. Li, M. Zhang, K. Tao, Catal. Comm., 3, (2002), 239-245.

63. M. Watson., U. S. Ozkan, J. Cat., 171, (1997), 45–53.

64. K. Arata, H. Matsuhashi, M. Hino, H. Nakamura, Cat. Tod., 81, (2003), 17-30.

65. M. Hino, K. Arata, J. Chem. Soc., Chem. Commun., (1987), 1259.

66. P.D.L. Marcer, J.G. Van Oman, E.B.M. Doesburg, A. Burggraaf, J.R.H. Ross, Appl. Catal. A: Gen., 471, (1991), 363.

67. I. Wang, W.F. Cheng, R.J. Shiau, J.C. Wu, C.S. Chung, J. Catal., 83, (1983), 428.

68. C.-M. Lu, Y.-M. Lin, I. Wang, Appl. Catal. A., 198, (2000), 223.

69. K. Tanabe, T. Sumiyoshi, K. Shibata, T. Kiyoura, J. Kitagawa, Bull. Chem. Soc. Jpn., 47, (1974), 1064.

70. B. M. Reddy, P.M. Sreekanth, Y. Yamada, Q. Xu, T. Kobayashi, Appl. Catal. A., 228, (2002), 269.

71. J. A. Anderson, C. Fergusson, I.R. Ramos, A.G. Ruiz, J. Catal., 192, (2000), 344.

72. K. I. Hadjiivanov, Catal. Rev. – Sci. Eng., 42, 1&2, (2000), 71-144.

73. S.-J. Huang, A. B. Walters, and M. A. Vannice1 J. Cat., 192, (2000), 29–47.

74. M. Kantcheva, E. Z. Ciftlikli, J. Phys. Chem. B, 106 (15), (2002), 3941.

75. K. Hadjiivanov, D. Klissurski, A. Davydov, J. Catal., 116, (1989), 498.

76. D.G. Barton, M. Shtein, R.D. Wilson, S.L. Soled, E. Iglesia, J. Phys. Chem. B, 103, (1999), 630-640.

77. H.P. Klug, L.E. Alexander, X-ray Diffraction Procedures, Wiley, New York, (1974).

78. Y.Ozawa, Y. Tochihara, M. Nagai, S.Omi, Chem. Eng. Science 58, 3-6, (2003), 671-677.

79. D. Barton, S.L. Soled, G.D.Meitzner, G. A. Fuentes,E. Iglesia, J. Catalysis, 181, (1999), 57.

80. Rakai, A., Tessier, D., Bozon-Verduraz F. New J. Chem., 16, (1992), 869.

81. Jung, K.T., Bell, A.T. J. Mol. Catal. A., 163, (2000), 27.

82. M. Kantcheva, M. U. Kucukkal, S. Suzer, J. Cat., 190, (2000), 144.

83. Scheithauer, M., Cheung, T.-K., Jentoft, R. E., Grasselli, R. K., Gates, B. C.; Knözinger, H. J. Catal., 180, (1998), 1.

84. Vijayanand, P., Chakarova, K., Hadjiivanov, K., Likinskas, P., Knözinger, H. Phys. Chem. Chem Phys., 5, (2003), 4040.

85. Adam W. Aylor, Lisa J. Lobree, Jeffrey A. Reimer, and Alexis T. Bell, J. Cat., 172, (1997), 453.

86. Kantcheva, M. M,, Bushev, V.P., Hadjiivanov, K. I. J. Chem. Soc., Faraday Trans., 88, (1992), 3087.

87. Hadjiivanov, K., Bushev, V., Kantcheva, M., Klissurski, D., Langmuir, 10, (1994), 464.

88. K. Almusaiteer, S. S. C. Chuang, J. Catal., 184, (1999), 189.

89. C. L. Levoguer, R.M. Nix, J. Chem. Soc., Faraday Trans. 93, (1997), 1813.

90. J. R. Hill, D. S. Moore, S. C. Schmidt, C. B. Storm, J. Phys. Chem. 95, (1991), 3037.

91. S. –K. Park, L. Kevan, PCCP, 3, (2001), 3247.

92. M. Yamaguchi, J. Chem. Soc. Faraday Trans., 93, (1997), 3581.

93. Y. H. Yeom, B. Wen, W. M. H. Sachtler, E. Weitz, J. Phys. Chem. B., 108, (2004), 5386.

94. G. Busca, V. Lorenzelli, Mater. Chem., 7, (1982), 89-126.

95. M. Bodenbinder, S. Elic, H. Willner, J. Phys. Chem., 98, (1994), 6441.

96. M. Saldyka, Z. Mielke, Chem. Phys. Lett., 371, (2003), 713.

97. E. A. Lombardo, G. A. Sill, J.L. d'Itri, W. K. Hall, J. Cat., 173, (1998), 440.

98. N. W. Cant, D. C. Chambers, A. D. Cowan, I. O. Y. Liu, A. Satsuma, Top. Cat., 10, (2000), 13.

99. F. Solymosi, T. Bansagi, J. Catal., 75, (1995), 156.

100. S. A. Beloshapkin, E.A. Paukshtis, V.A. Sadykov, J. Mol. Cat. A., 158, (2000), 355.

101. H. Kato, C. Yokoyama, M. Misono, Catal. Today, 45, (1998), 93.

102. R. Burch-. D. J. Crittle, M. J. Hayes, Cat. Tod., 47, (1999), 229.

103. V. R. Choudhary, V. H. Rane, J. Catal., 130, (1991), 411.

104. Valyon, J., Engelhardt, J., Kallő, D., and Hagedüs, M., Catal. Lett. 82, (2002), 29.

105. M. Kantcheva, I. Cayirtepe, Langmuir (submitted).